

---

STUDY OF THE EFFECTIVE POTENTIAL ENERGY IN A SEGMENTED LINEAR  
PAUL TRAP

---

## Internship Report

---

*Author :*  
Oner Faruk ODEMIS

*Internship Supervisor :*  
Katrin Erath-DULITZ

From June 24<sup>th</sup> to September 20<sup>th</sup> 2024

# Contents

|          |  |           |
|----------|--|-----------|
| <b>1</b> | <b>Introduction</b>  | <b>5</b>  |
| <b>2</b> | <b>The linear Paul trap and previous studies</b>   | <b>5</b>  |
| 2.1      | The linear Paul trap . . . . .   | 5         |
| 2.2      | Previous studies . . . . .   | 6         |
| <b>3</b> | <b>Theoretical background</b>  | <b>6</b>  |
| 3.1      | Theoretical background of the first method . . . . .   | 6         |
| 3.2      | Theoretical background of the second method . . . . .  | 10        |
| <b>4</b> | <b>Using SIMION and Python for plotting 2D contour graphs</b>                                      | <b>12</b> |
| 4.1      | SIMION . . . . .   | 12        |
| 4.1.1    | SIMION Overview . . . . .  | 12        |
| 4.1.2    | Working with SIMION for $V(R)$ . . . . .   | 12        |
| 4.1.3    | Working with SIMION for $V^*(R)$ . . . . .   | 13        |
| 4.2      | Python . . . . .   | 14        |
| 4.2.1    | Calculation of $V(R)$ . . . . .  | 14        |
| 4.2.2    | Calculation of $V^*(R)$ . . . . .  | 14        |
| 4.2.3    | Plotting the graph of position and effective potential energy ( $V(R)$ ) . . . . .                 | 14        |
| 4.2.4    | Plotting the graph of position, DC potential and effective potential energy ( $(V^*(R))$ . . . . . | 18        |
| <b>5</b> | <b>Results</b>   | <b>23</b> |
| 5.1      | Results for $V(R)$ . . . . .   | 23        |
| 5.2      | Results for $V^*(R)$ . . . . .   | 25        |
| <b>6</b> | <b>Mathieu Equations and Stability Diagram</b>   | <b>28</b> |
| 6.1      | Theoretical background of Mathieu equations . . . . .  | 28        |
| 6.2      | Stability Diagram . . . . .  | 30        |
| 6.3      | Longitudinal frequency . . . . .   | 32        |
| 6.3.1    | Calculation of longitudinal frequency analytically . . . . .                                       | 32        |
| 6.3.2    | Calculation of longitudinal frequency numerically . . . . .  | 33        |
| 6.3.3    | Calculation of $\kappa$ with numerical methods . . . . .   | 34        |
| 6.4      | Radial frequency . . . . .   | 36        |
| 6.4.1    | Calculation of radial frequency analytically . . . . .   | 36        |
| 6.4.2    | Calculation of radial frequency numerically . . . . .  | 37        |
| 6.4.3    | A novel approach to analytical calculation of radial frequency . . . . .                           | 39        |
| <b>7</b> | <b>An alternative design for linear Paul trap</b>  | <b>40</b> |

|          |   |           |
|----------|---|-----------|
| 7.1      | Designing the ion trap model in SolidWorks . . . . .  | 40        |
| 7.2      | Difficulties . . . . .  | 42        |
| 7.2.1    | Grid cell size . . . . .  | 42        |
| 7.2.2    | Importing Solidworks design into SIMION . . . . .   | 42        |
| 7.3      | Calculation of $V^*(R)$ . . . . .   | 43        |
| 7.4      | Result graphs . . . . .   | 45        |
| 7.5      | Calculation of longitudinal and radial frequency . . . . .  | 52        |
| 7.5.1    | Calculation of longitudinal frequency numerically . . . . .   | 52        |
| 7.5.2    | Calculation of $\kappa$ with numerical methods . . . . .  | 54        |
| 7.6      | Calculation of radial frequency . . . . .   | 55        |
| 7.6.1    | Calculation of radial frequency analytically . . . . .  | 55        |
| 7.6.2    | Calculation of radial frequency numerically . . . . .   | 55        |
| <b>8</b> | <b>A trap design for trapping both positive and negative ions simultaneously</b>                              | <b>56</b> |
| 8.1      | Designing the ion trap model in Solidworks . . . . .  | 57        |
| 8.2      | Determination of parameters used in the design of the ion trap . . . . .                                      | 60        |
| 8.2.1    | RF electrode length ( $L_{RF}$ ) . . . . .  | 61        |
| 8.2.2    | Distance between two washers ( $dx$ ) . . . . .   | 61        |
| 8.2.3    | Distance between inner radius and outer radius of washer ( $dy$ ) . . . . .                                   | 62        |
| 8.2.4    | Distance from the center of the trap to the inner radius of the washer on the ZY axis ( $R$ ) . . . . .       | 63        |
| 8.2.5    | Conclusion . . . . .  | 65        |
| 8.3      | Determination of the configuration of the DC voltage applied to the DC electrodes (washers) . . . . .         | 66        |
| 8.3.1    | DC voltage applied to the central washer (Electrode07) . . . . .  | 66        |
| 8.3.2    | DC voltage applied to the washers between the end and central washers (Electrode06 and Electrode08) . . . . . | 68        |
| 8.3.3    | DC voltage applied to the end washers (Electrode05 and Electrode09) . . . . .                                 | 69        |
| 8.3.4    | Conclusion . . . . .  | 70        |
| 8.4      | Difficulties . . . . .  | 71        |
| 8.4.1    | Slow reading of data depending on grid cell size . . . . .  | 71        |
| 8.5      | Calculation of $V^*(R)$ . . . . .   | 71        |
| 8.6      | Result graphs . . . . .   | 73        |
| 8.6.1    | $x = \max(x/2)$ . . . . .   | 73        |
| 8.6.2    | $x = \max(x/2) \pm \Delta x/2$ . . . . .  | 79        |
| 8.6.3    | $x = \max(x/2) \pm \Delta x$ . . . . .  | 82        |
| <b>9</b> | <b>Using SIMION for ion trajectory simulations</b>  | <b>86</b> |
| 9.1      | General overview . . . . .  | 86        |
| 9.2      | Lua code for ion trajectory simulation . . . . .  | 87        |
| 9.3      | Simulation parameters . . . . .   | 87        |

|                     |  |            |
|---------------------|--|------------|
| 9.4                 | Comparison between effective potential energy graphs and SIMION simulation results . . . . . | 88         |
| 9.4.1               | $U_{RF,max} = 300V$ and $U_{DC} = 5V$ . . . . .  | 89         |
| 9.4.2               | $U_{RF,max} = 300V$ and $U_{DC} = 10V$ . . . . .   | 91         |
| 9.4.3               | $U_{RF,max} = 300V$ and $U_{DC} = 25V$ . . . . .   | 93         |
| <b>10</b>           | <b>Conclusion</b>  | <b>95</b>  |
| <b>Appendix A</b>   |  | <b>97</b>  |
| <b>A Components</b> |  | <b>97</b>  |
| A.1                 | The alternative design for three segmented linear Paul trap . . . . .                        | 97         |
| A.2                 | The trap design for trapping both positive and negative ions simultaneously . . . . .        | 99         |
| <b>Appendix B</b>   |  | <b>100</b> |
| <b>B Codes</b>      |  | <b>100</b> |
| B.1                 | Lua code . . . . .   | 100        |

# 1 Introduction

During the third year of my undergraduate degree, I was required to complete a compulsory 15-day internship. Seeking to gain more exposure and experience, I applied for a three-month internship at Professor Dulitz's laboratory. Upon acceptance, I had the opportunity to work on linear Paul trap experiments, specifically focusing on data imaging, under the guidance of my supervisor, Katrin Erath Dulitz. This report details the work done during the my internship, including experimental setup, theoretical background, the use of SIMION and Python for experiment, and results.

Most of my work was done with Python and SIMION. **SIMION** is a software package used primarily to calculate electric fields and trajectories of charged particles within those fields, given an electrode configuration with voltages and particle initial conditions, including optional RF (quasi-static), magnetic field, and collision effects [1].

## 2 The linear Paul trap and previous studies

### 2.1 The linear Paul trap

The primary focus of this experiment is to understand chemical reactions within a regime dominated by quantum effects, which is facilitated through advanced laser cooling and trapping techniques. One such technique involves the use of a linear Paul trap, a device designed to confine charged particles using electric fields. The linear Paul trap functions by applying a combination of radio frequency (RF) and direct current (DC) voltages, thereby creating a dynamic potential well that effectively traps ions. The LPT is based on a quadrupole design, with four cylindrical rods each separated lengthwise into a number of electrode segments [5]. We used a design employed in the present work involves three separate electrode segments per rod, with each of the four rods being identical in geometric design.

The main objective of my work is to image the effective potential energy using a linear Paul trap design, as described by A. Gingell [5] and illustrated in Solidworks by B. Breitmeier [2]. Effective potential energy is defined as the potential energy of a system considering both the static potential energy and the contributions from dynamic interactions such as forces acting on particles in the field. By generating and analyzing these effective potential energy graphs, we aim to gain a deeper understanding of ion behavior within the trap. This detailed examination will provide insights into the dynamics of ions under various trapping conditions.

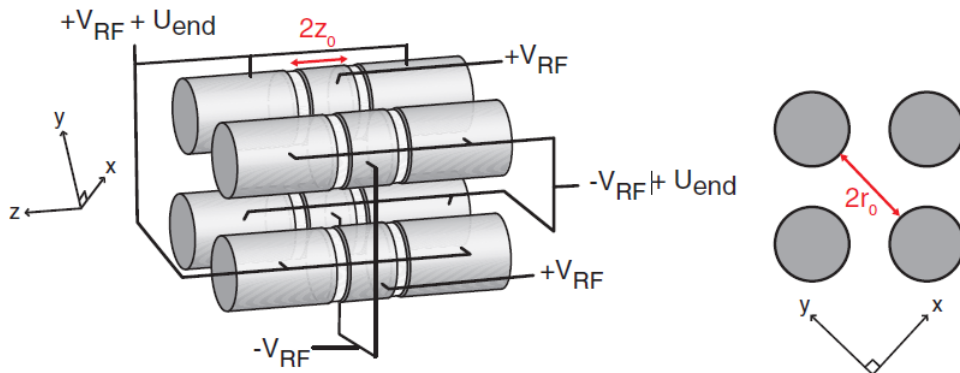


Figure 1: The design of the linear Paul trap, including the voltage configuration for ion trapping. This figure is taken from Ref. [5].  $V_{RF}$  is the RF voltage varies with time, while  $U_{end}$  is the constant DC voltage.

## 2.2 Previous studies

Several key studies provided the foundation for this project :

1. **Simulation of the simultaneous trapping of positively and negatively charged ions in a linear quadrupole trap** by Beke Leonie Breitmeier [2]. This thesis is crucial for current project and further work.
2. **Nondestructive inelastic recoil spectroscopy of a single molecular ion: A versatile tool toward precision action spectroscopy** by Geistlinger (2021) [3]. This article provides valuable methodologies relevant to our experiments.
3. **A sub-4 Kelvin radio frequency linear multipole wire trap** by Calvin (2023) [4]. This paper introduces advanced trapping techniques that are beneficial for our study.
4. **Applications of Coulomb Crystals in Cold Chemistry** by Gingell (2010) [5]. Specifically Appendix 2.2.2 is very important for effective potential energy calculations in a linear Paul trap.

## 3 Theoretical background

I applied two different methods to calculate the effective potential energy. The effective potential energy obtained from the first method is denoted as  $V(R)$ , while the effective potential energy derived from the second method is represented as  $V^*(R)$ .

### 3.1 Theoretical background of the first method

As illustrated in Figure 1, we applied both RF and DC voltages to the electrodes for ion trapping in the first method. Following A. Gingell's design, we utilized the same voltage values. The specific voltages applied to the electrodes are detailed below :

$U_{DC}$  : DC voltage [V]

$U_{RF}(t)$  : RF voltage [V]

- Electrode01:  $U_{RF}(t) + U_{DC}$
- Electrode02:  $-U_{RF}(t) + U_{DC}$
- Electrode03:  $U_{RF}(t) + U_{DC}$
- Electrode04:  $-U_{RF}(t) + U_{DC}$
- Electrode05:  $U_{RF}(t) + U_{DC}$
- Electrode06:  $-U_{RF}(t) + U_{DC}$
- Electrode07:  $-U_{RF}(t) + U_{DC}$
- Electrode08:  $U_{RF}(t) + U_{DC}$
- Electrode09:  $-U_{RF}(t)$
- Electrode10:  $U_{RF}(t)$
- Electrode11:  $-U_{RF}(t)$
- Electrode12:  $U_{RF}(t)$

In Figure 2, you can also see the more detailed numbering of the electrodes.

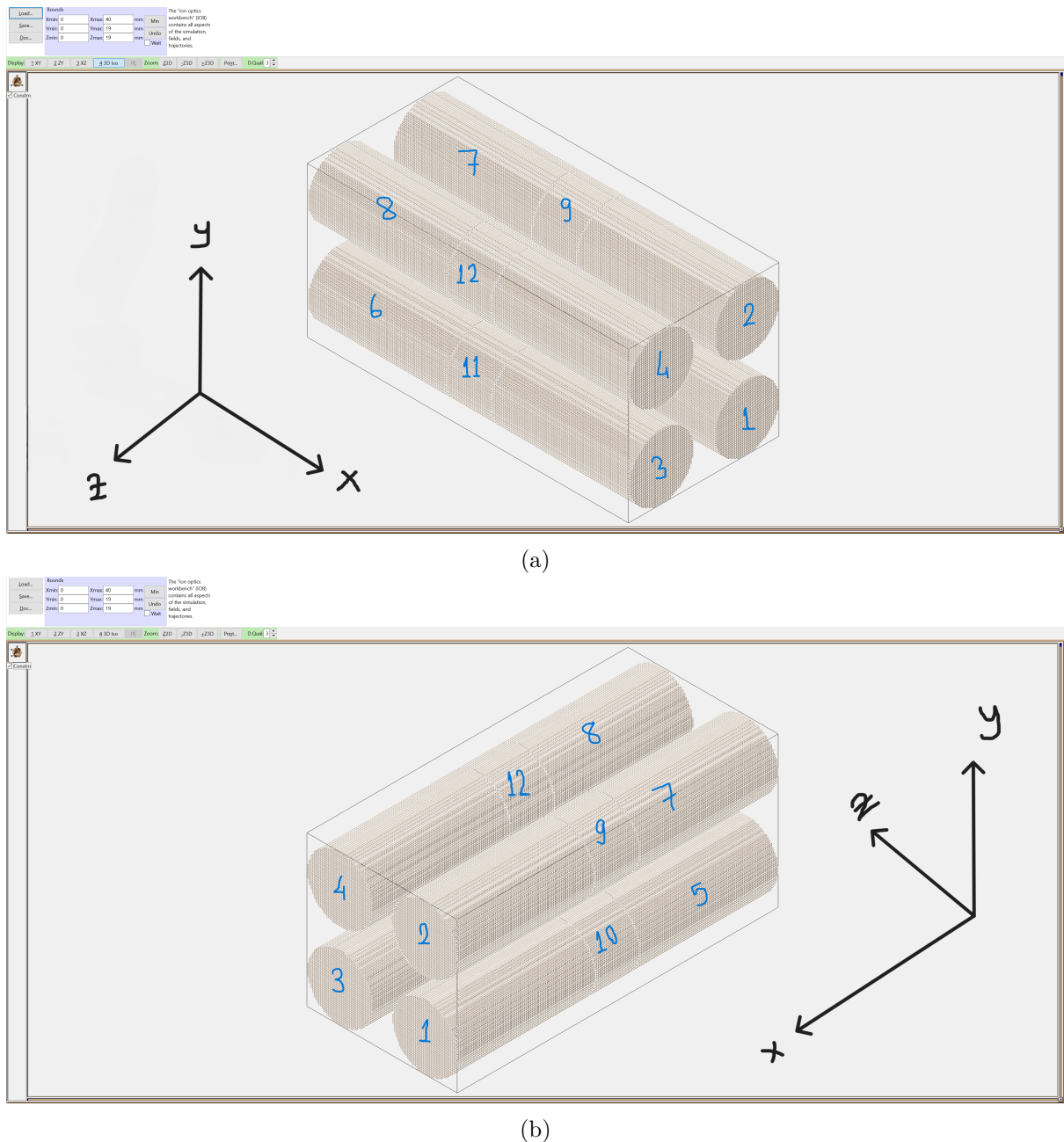


Figure 2: Detailed numbering of the electrodes.

Also for calculation of effective potential energy, we have to describe some terms :

- $U_{RF_{max}}$  : Maximum RF voltage [V]
- $f$  : Frequency of RF voltage [1/s]
- $\Omega$  : Angular frequency of RF voltage [1/s]

We determined  $U_{DC}$ ,  $U_{RF_{max}}$  and  $f$  ourselves . We can also calculate  $\Omega$  by using following formula :

$$\Omega = 2\pi f \quad (1)$$

The values determined for parameters  $U_{DC}$ ,  $U_{RF_{max}}$ , and  $f$  are presented in Table 1. After establishing these values using the stability diagram show in [2], we calculated  $\Omega$  using equation (1). The resulting value is also shown in Table 1.

|                |                 |
|----------------|-----------------|
| $U_{DC}$       | 200.00 V        |
| $U_{RF_{max}}$ | 600.00 V        |
| $f$            | 3850000.00 1/s  |
| $\Omega$       | 24190263.43 1/s |

Table 1

We also can calculate  $U_{RF}(t)$  by using following formula :

$$U_{RF}(t) [\text{V}] = U_{RF_{max}} \cdot \sin(\Omega t) \quad (2)$$

Since it was not possible to receive continuous data, we took 30 equal points in a full time period. This can be more clearly observed in Figure 3. I calculated the  $U_{RF}(t)$  in these points by using equation (2).

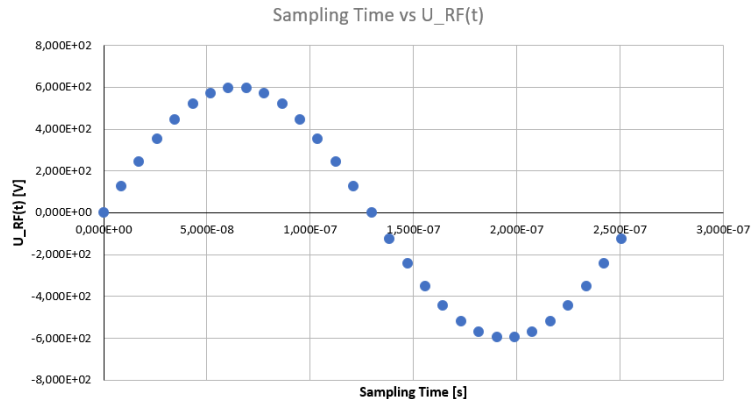


Figure 3: Sampling time and  $U_{RF}(t)$

Then I calculated  $U_{\text{RF}}(t)$  in these sampling times by using equation (2). I imported the RF and DC voltages at one sampling time after the other into SIMION and calculated the electric field values at each position. This process will be explained in more detail in Section 4. Finally, I calculated the effective potential energy using the following formula :

$$V(R) = \frac{Q^2 E_0^2}{4m\Omega^2} \quad (3)$$

$V$  : Effective potential energy [J]

$R$  : Position [m]

$Q$  : Electric charge of the ion [C]

$E_0$  : Time-averaged magnitude of electric field [V/m]

$m$  : Mass of ion [kg]

$\Omega$  : Angular frequency of RF [1/s]

### 3.2 Theoretical background of the second method

This method is used to calculate the effective potential energy ( $V(R)$ ), as detailed in Alex Ginnell's thesis [5]. In this approach,  $E_0$  is determined using only the radiofrequency voltage. This differs from the previous method, where  $E_0$  is derived by summing the RF and DC components. Unlike the first method, the second method does not involve applying a time-varying RF voltage. Instead, I used  $U_{RF_{max}}$  as the RF voltage. Consequently, there is no need to consider the time-dependent processes required in the previous method. Additionally, all values determined and calculated in Table 1 remain consistent with this method.

Initially, I applied only a constant DC voltage to some of the electrodes. The specific voltages applied to these electrodes are detailed below :

- Electrode01:  $U_{DC}$
- Electrode02:  $U_{DC}$
- Electrode03:  $U_{DC}$
- Electrode04:  $U_{DC}$
- Electrode05:  $U_{DC}$
- Electrode06:  $U_{DC}$
- Electrode07:  $U_{DC}$
- Electrode08:  $U_{DC}$
- Electrode09: 0
- Electrode10: 0
- Electrode11: 0
- Electrode12: 0

Secondly, I applied  $U_{RF_{max}}$  to the electrodes. The specific voltages applied to each electrode are detailed below :

- Electrode01:  $U_{RF_{max}}$
- Electrode02:  $-U_{RF_{max}}$
- Electrode03:  $U_{RF_{max}}$
- Electrode04:  $-U_{RF_{max}}$
- Electrode05:  $U_{RF_{max}}$
- Electrode06:  $-U_{RF_{max}}$
- Electrode07:  $-U_{RF_{max}}$
- Electrode08:  $U_{RF_{max}}$
- Electrode09:  $-U_{RF_{max}}$
- Electrode10:  $U_{RF_{max}}$

- Electrode11:  $-U_{\text{RF}_{\max}}$
- Electrode12:  $U_{\text{RF}_{\max}}$

I imported  $U_{\text{DC}}$  voltage into SIMION and calculated the potential values at each position. Next, I imported the  $U_{\text{RF}_{\max}}$  into SIMION and calculated electric field values at each position. This process will be explained in more detail in Section 4. Finally, I calculated the effective potential energy using the following formula [5] :

$$V^*(R) = \frac{Q^2 E_0^2}{4m\Omega^2} + Q\Phi_s \quad (4)$$

$V^*$  : Effective potential energy [J]

$R$  : Position [m]

$Q$  : Electric charge of the ion [C]

$E_0$  : Magnitude of electric field values of  $U_{\text{RF}_{\max}}$  [V/m]

$m$  : Mass of ion [kg]

$\Omega$  : Angular frequency of RF [1/s]

$\Phi_s$  : Potential values of constant DC [V]

Additionally, I separated the contributions to the effective potential energy arising from  $U_{\text{RF}_{\max}}$  voltage and the DC voltage. This division will facilitate a more detailed and insightful analysis in the subsequent stages.

$$V_{\text{RF}}^*(R) = \frac{Q^2 E_0^2}{4m\Omega^2}$$

$$V_{\text{DC}}^*(R) = Q\Phi_s$$

$$V^*(R) = V_{\text{RF}}^*(R) + V_{\text{DC}}^*(R)$$

$V_{\text{RF}}^*(R)$  : Contribution from  $U_{\text{RF}_{\max}}$  voltage to effective potential energy

$V_{\text{DC}}^*(R)$  : Contribution from DC voltage values to effective potential energy

## 4 Using SIMION and Python for plotting 2D contour graphs

### 4.1 SIMION

#### 4.1.1 SIMION Overview

SIMION [1] is a comprehensive software package designed for the simulation and analysis of ion optics in mass spectrometry and related fields. It enables users to adjust the voltage of electrodes, design experimental setups, export voltage and electric field measurements, assign properties to ions, and simulate their behavior within these setups. "By approximating voltages at points between electrodes and considering the linear properties of the Laplace equation, SIMION calculates electrostatic fields. Additionally, for particle trajectory calculations, SIMION uses a Runge-Kutta method, which is an iterative approach similar to the Euler method. This method calculates the new trajectory for each specified time step, enabling accurate particle path simulations." [2] Since we simulate ions before setting up the SIMION experimental setup, it has a very important place in terms of predicting the errors that may be made before the experiment and understanding whether the logic of the experimental setup we have established is correct.

#### 4.1.2 Working with SIMION for $V(R)$

I imported the DC and RF voltage values to the electrodes into SIMION for each sampling times and converted the electric field values due to the electrodes in the environment into a .patxt file via SL Tools. Since we determined 30 sampling times, we created 30 .patxt files containing location-dependent electric field data. The file contains electric field and position data, as illustrated in Figure 4.

```
 5.1.32DE-08-electric-field.pat - Editor
Date: Burkholder Format: ASCII Hilfe
# ASCII text representation of a SIMION PA file.
begin_header
    npx 2
    symmetry planar
    max_voltage 1000000
    nx 40
    ny 188
    nz 188
    mirror_x 0
    mirror_y 0
    mirror_z 0
    field_type electrostatic
    ng 10
    dx_nm 0.1
    dy_nm 0.1
    dz_nm 0.1
    fast_adjustable 0
    data_format x y z is_electrode field_x field_y field_z
end_header
begin_data
    0 0 0 9.47920852228345e-010 5.2159381165943e-010 4.806679498869926e-010
    0 0 0 1.37481492567501e-009 5.6362411369211e-009 4.67936204264175e-010
    0 0 0 2.7496283101822e-009 5.98687758733022e-009 4.30803800745021e-010
    0 0 0 3.96482465541359e-009 4.24566520525143e-010 3.835793904727252e-010
    0 0 0 5.57892045182612e-009 3.144577931317989e-010 2.74440826259081e-010
    0 0 0 6.691948232880748e-009 2.308792275926998e-010 2.02362571144765e-010
    0 0 0 6.65919594412399e-009 1.53477234924161e-010 1.18689058313671e-010
    0 0 0 7.65919594412399e-009 1.53477234924161e-010 1.18689058313671e-010
    0 0 0 9.47920852228345e-010 5.2159381165943e-010 -5.26865716765081e-011 -7.912683905424745e-011
    0 0 0 1.37481492567501e-009 5.6362411369211e-009 -1.69393382052979e-010 -1.91676080388644e-010
    0 0 0 2.7496283101822e-009 5.98687758733022e-009 -4.251877377844e-010 -4.35647982149232e-010
    0 0 0 3.96482465541359e-009 4.24566520525143e-010 -2.12871427085925e-009 -5.645688361255452e-010
    0 0 0 5.57892045182612e-009 3.144577931317989e-010 -6.96476109967567e-010 -6.96218194231756e-010
    0 0 0 6.691948232880748e-009 2.308792275926998e-010 -9.39573252791509e-010 -9.66792867846227e-010
    0 0 0 6.65919594412399e-009 1.53477234924161e-010 -1.18689058313671e-010 -1.18689058313671e-010
    0 0 0 7.65919594412399e-009 1.53477234924161e-010 -1.18689058313671e-010 -1.18689058313671e-010
    0 0 0 9.47920852228345e-010 5.2159381165943e-010 -1.42267708724380e-009 -1.393573252791509e-009
    0 0 0 1.37481492567501e-009 5.6362411369211e-009 -1.124817572417669e-009 -1.18486868978665e-009
    0 0 0 2.7496283101822e-009 5.98687758733022e-009 -1.024400788915156e-009 -1.888111080888059e-009
    0 0 0 3.96482465541359e-009 4.24566520525143e-010 -2.12871427085925e-009 -2.084334882781868e-009
    0 0 0 5.57892045182612e-009 3.144577931317989e-010 -2.393772776655415e-009 -2.383522785915384e-009
    0 0 0 6.691948232880748e-009 2.308792275926998e-010 -2.50971427085925e-009 -2.496476109967567e-009
    0 0 0 6.65919594412399e-009 1.53477234924161e-010 -2.879592652470805e-009 -2.837623469515356e-009
    0 0 0 7.65919594412399e-009 1.53477234924161e-010 -3.196419213939955e-009 -3.1657236831312e-009
    0 0 0 9.47920852228345e-010 5.2159381165943e-010 -3.58967790415301e-009 -3.56887758733022e-009
    0 0 0 1.37481492567501e-009 5.6362411369211e-009 -4.01553755844944e-009 -3.98689790415301e-009
    0 0 0 2.7496283101822e-009 5.98687758733022e-009 -4.5192791731968e-009 -4.49699655216244e-009
    0 0 0 3.96482465541359e-009 4.24566520525143e-010 -5.1711785058604e-009 -5.1111785058604e-009
    0 0 0 5.57892045182612e-009 3.144577931317989e-010 -5.789592652470805e-009 -5.736823469515356e-009
    0 0 0 6.691948232880748e-009 2.308792275926998e-010 -6.412871427085925e-009 -6.35647982149232e-010
    0 0 0 6.65919594412399e-009 1.53477234924161e-010 -7.084334882781868e-009 -7.02362571144765e-010
    0 0 0 7.65919594412399e-009 1.53477234924161e-010 -7.756476109967567e-009 -7.6952867846227e-010
    0 0 0 9.47920852228345e-010 5.2159381165943e-010 -8.42267708724380e-009 -8.283522785915384e-009
    0 0 0 1.37481492567501e-009 5.6362411369211e-009 -9.093573252791509e-009 -8.952362571144765e-009
    0 0 0 2.7496283101822e-009 5.98687758733022e-009 -9.76440826259081e-009 -9.62318194231756e-009
    0 0 0 3.96482465541359e-009 4.24566520525143e-010 -1.0479584471751e-009 -1.0357236831312e-009
    0 0 0 5.57892045182612e-009 3.144577931317989e-010 -1.124817572417669e-009 -1.113657236831312e-009
    0 0 0 6.691948232880748e-009 2.308792275926998e-010 -1.204400788915156e-009 -1.192362571144765e-009
    0 0 0 6.65919594412399e-009 1.53477234924161e-010 -1.2871427085925e-009 -1.27588775844944e-009
    0 0 0 7.65919594412399e-009 1.53477234924161e-010 -1.36476109967567e-009 -1.353522785915384e-009
    0 0 0 9.47920852228345e-010 5.2159381165943e-010 -1.4412871427085925e-009 -1.43093573252791509e-009
    0 0 0 1.37481492567501e-009 5.6362411369211e-009 -1.5193382052979e-009 -1.508038868978665e-009
    0 0 0 2.7496283101822e-009 5.98687758733022e-009 -1.594400788915156e-009 -1.583111080888059e-009
    0 0 0 3.96482465541359e-009 4.24566520525143e-010 -1.6711785058604e-009 -1.66087758733022e-009
    0 0 0 5.57892045182612e-009 3.144577931317989e-010 -1.74792867846227e-009 -1.736657236831312e-009
    0 0 0 6.691948232880748e-009 2.308792275926998e-010 -1.824334882781868e-009 -1.813362571144765e-009
    0 0 0 6.65919594412399e-009 1.53477234924161e-010 -1.9011785058604e-009 -1.89087758733022e-009
    0 0 0 7.65919594412399e-009 1.53477234924161e-010 -1.97892867846227e-009 -1.96857236831312e-009
    0 0 0 9.47920852228345e-010 5.2159381165943e-010 -2.05571427085925e-009 -2.045476109967567e-009
    0 0 0 1.37481492567501e-009 5.6362411369211e-009 -2.132871427085925e-009 -2.122562571144765e-009
    0 0 0 2.7496283101822e-009 5.98687758733022e-009 -2.2099400788915156e-009 -2.19963775844944e-009
    0 0 0 3.96482465541359e-009 4.24566520525143e-010 -2.2876522785915384e-009 -2.2773434882781868e-009
    0 0 0 5.57892045182612e-009 3.144577931317989e-010 -2.365322785915384e-009 -2.355011785058604e-009
    0 0 0 6.691948232880748e-009 2.308792275926998e-010 -2.44267708724380e-009 -2.432362571144765e-009
    0 0 0 6.65919594412399e-009 1.53477234924161e-010 -2.5193382052979e-009 -2.509038868978665e-009
    0 0 0 7.65919594412399e-009 1.53477234924161e-010 -2.69689790415301e-009 -2.68657236831312e-009
    0 0 0 9.47920852228345e-010 5.2159381165943e-010 -2.773775844944e-009 -2.763476109967567e-009
    0 0 0 1.37481492567501e-009 5.6362411369211e-009 -2.85064471751e-009 -2.84033573252791509e-009
    0 0 0 2.7496283101822e-009 5.98687758733022e-009 -2.9273434882781868e-009 -2.9170362571144765e-009
    0 0 0 3.96482465541359e-009 4.24566520525143e-010 -2.99400788915156e-009 -2.983703522785915384e-009
    0 0 0 5.57892045182612e-009 3.144577931317989e-010 -3.061694199134407e-009 -3.0513817785915384e-009
    0 0 0 6.691948232880748e-009 2.308792275926998e-010 -3.128464515367266e-009 -3.11815236831312e-009
    0 0 0 6.65919594412399e-009 1.53477234924161e-010 -3.195232785915384e-009 -3.1849206476109967567e-009
    0 0 0 7.65919594412399e-009 1.53477234924161e-010 -3.262000444744536e-009 -3.2516873175844944e-009
    0 0 0 9.47920852228345e-010 5.2159381165943e-010 -3.328775844944e-009 -3.318464515367266e-009
    0 0 0 1.37481492567501e-009 5.6362411369211e-009 -3.3955522785915384e-009 -3.385236831312e-009
    0 0 0 2.7496283101822e-009 5.98687758733022e-009 -3.4623234882781868e-009 -3.4520103522785915384e-009
    0 0 0 3.96482465541359e-009 4.24566520525143e-010 -3.5290901775844944e-009 -3.51877744645367266e-009
    0 0 0 5.57892045182612e-009 3.144577931317989e-010 -3.5958578447445367266e-009 -3.585544645367266e-009
    0 0 0 6.691948232880748e-009 2.308792275926998e-010 -3.66262522344944e-009 -3.65231210344944e-009
    0 0 0 6.65919594412399e-009 1.53477234924161e-010 -3.7293928447445367266e-009 -3.7190797125844944e-009
    0 0 0 7.65919594412399e-009 1.53477234924161e-010 -3.7961605223445367266e-009 -3.7858473910844944e-009
    0 0 0 9.47920852228345e-010 5.2159381165943e-010 -3.8629282003445367266e-009 -3.8526151790844944e-009
    0 0 0 1.37481492567501e-009 5.6362411369211e-009 -3.9296958775844944e-009 -3.9193827462667266e-009
    0 0 0 2.7496283101822e-009 5.98687758733022e-009 -3.99646355522785915384e-009 -3.9861504240844944e-009
    0 0 0 3.96482465541359e-009 4.24566520525143e-010 -4.0632312329844944e-009 -4.0529181017844944e-009
    0 0 0 5.57892045182612e-009 3.144577931317989e-010 -4.1300089107445367266e-009 -4.11968578447445367266e-009
    0 0 0 6.691948232880748e-009 2.308792275926998e-010 -4.19678565844944e-009 -4.186464337125844944e-009
    0 0 0 6.65919594412399e-009 1.53477234924161e-010 -4.263462326125844944e-009 -4.25314909480844944e-009
    0 0 0 7.65919594412399e-009 1.53477234924161e-010 -4.33014011390844944e-009 -4.319826882781868e-009
    0 0 0 9.47920852228345e-010 5.2159381165943e-010 -4.39684785160844944e-009 -4.3865346522785915384e-009
    0 0 0 1.37481492567501e-009 5.6362411369211e-009 -4.46354472530844944e-009 -4.45323199408844944e-009
    0 0 0 2.7496283101822e-009 5.98687758733022e-009 -4.53024186308844944e-009 -4.51992874480844944e-009
    0 0 0 3.96482465541359e-009 4.24566520525143e-010 -4.60695213178844944e-009 -4.59663909048844944e-009
    0 0 0 5.57892045182612e-009 3.144577931317989e-010 -4.6836609790415301e-009 -4.673347848725844944e-009
    0 0 0 6.691948232880748e-009 2.308792275926998e-010 -4.750368857741868e-009 -4.73995572640844944e-009
    0 0 0 6.65919594412399e-009 1.53477234924161e-010 -4.82707673544944e-009 -4.816753604125844944e-009
    0 0 0 7.65919594412399e-009 1.53477234924161e-010 -4.89378451414944e-009 -4.88346138188844944e-009
    0 0 0 9.47920852228345e-010 5.2159381165943e-010 -4.96049229284944e-009 -4.94999655216244e-009
    0 0 0 1.37481492567501e-009 5.6362411369211e-009 -5.02720117054944e-009 -5.01688804060844944e-009
    0 0 0 2.7496283101822e-009 5.98687758733022e-009 -5.09390891824644e-009 -5.08359578740844944e-009
    0 0 0 3.96482465541359e-009 4.24566520525143e-010 -5.1610198009445367266e-009 -5.150696778521608e-009
    0 0 0 5.57892045182612e-009 3.144577931317989e-010 -5.2271376785445367266e-009 -5.21682454720844944e-009
    0 0 0 6.691948232880748e-009 2.308792275926998e-010 -5.294264447125844944e-009 -5.28395122640844944e-009
    0 0 0 6.65919594412399e-009 1.53477234924161e-010 -5.36135121590844944e-009 -5.35103809468844944e-009
    0 0 0 7.65919594412399e-009 1.53477234924161e-010 -5.42843819458844944e-009 -5.41812577336844944e-009
    0 0 0 9.47920852228345e-010 5.2159381165943e-010 -5.49553507316844944e-009 -5.48522295104844944e-009
    0 0 0 1.37481492567501e-009 5.6362411369211e-009 -5.56263185194844944e-009 -5.55231933072844944e-009
    0 0 0 2.7496283101822e-009 5.98687758733022e-009 -5.62973893072844944e-009 -5.61942675850844944e-009
    0 0 0 3.96482465541359e-009 4.24566520525143e-010 -5.69684580950844944e-009 -5.68653368728844944e-009
    0 0 0 5.57892045182612e-009 3.144577931317989e-010 -5.76395378728844944e-009 -5.75364156606844944e-009
    0 0 0 6.691948232880748e-009 2.308792275926998e-010 -5.83106266606844944e-009 -5.82075044484844944e-009
    0 0 0 6.65919594412399e-009 1.53477234924161e-010 -5.89817144384844944e-009 -5.88785822262844944e-009
    0 0 0 7.65919594412399e-009 1.53477234924161e-010 -5.96527822164844944e-009 -5.95496500042844944e-009
    0 0 0 9.47920852228345e-010 5.2159381165943e-010 -6.03237520044844944e-009 -6.02206297822844944e-009
    0 0 0 1.37481492567501e-009 5.6362411369211e-009 -6.09947217924844944e-009 -6.08915995702844944e-009
    0 0 0 2.7496283101822e-009 5.98687758733022e-009 -6.16656905804844944e-009 -6.15625683682844944e-009
    0 0 0 3.96482465541359e-009 4.24566520525143e-010 -6.23368593682844944e-009 -6
```

### 4.1.3 Working with SIMION for $V^*(R)$

Firstly, I imported the DC voltage values to the electrodes into SIMION and converted the potential values due to the electrodes in the environment into a .patxt file via SL Tools. Next, I imported the  $U_{RF_{max}}$  voltage values to the electrodes into SIMION and converted the electric field values due to the electrodes in the environment into a .patxt file in same way. The potential file contains potential and position data, as illustrated in Figure 5.

```

# ASCII text representation of a SIMION PA file.
begin_header
  model_planar
  symmetry planar
  max_voltage 100000
  nx 400
  ny 188
  nz 188
  mirror_x 0
  mirror_y 0
  mirror_z 0
  field_type electrostatic
  ng 100
  dx_m 0.1
  dy_m 0.1
  dz_m 0.1
  fast_Adjustable 0
  atoms(x,y,z) is_electrode potential
end_header
begin_points
  0 0 0 199.9999999756764
  1 0 0 199.999999975223
  2 0 0 199.999999971487
  3 0 0 199.999999970422
  4 0 0 199.999999970345
  5 0 0 199.9999999686807
  6 0 0 199.999999968525
  7 0 0 199.999999958578
  8 0 0 199.999999951615
  9 0 0 199.9999999452844
  10 0 0 199.9999999395087
  11 0 0 199.9999999310793
  12 0 0 199.9999999245116
  13 0 0 199.9999999138883
  14 0 0 199.999999807806
  15 0 0 199.99999975123
  16 0 0 199.9999998071501
  17 0 0 199.999999848565
  18 0 0 199.9999998477598
  19 0 0 199.9999998032888
  20 0 0 199.9999997757897
  21 0 0 199.999999774472
  22 0 0 199.999999788664
  23 0 0 199.999999678205
  24 0 0 199.9999996712092
  25 0 0 199.9999995679384
  26 0 0 199.9999995678653
  27 0 0 199.9999995675123
  28 0 0 199.999999518865
  29 0 0 199.9999995272636
  30 0 0 199.999999521545
  31 0 0 199.9999994848243
  32 0 0 199.9999989692315
  33 0 0 199.9999989692475
  34 0 0 199.9999985771885
  35 0 0 199.9999983748254
  36 0 0 199.9999983748259
  37 0 0 199.9999978793735
  38 0 0 199.9999975774877
  39 0 0 199.9999975752515
  40 0 0 199.999998385182
  41 0 0 199.999998383265
  42 0 0 199.999998383257
  43 0 0 199.9999952654607
  44 0 0 199.9999946152433
  45 0 0 199.9999946152436
  46 0 0 199.9999929725847
  47 0 0 199.999991971842
  48 0 0 199.9999919718423
  49 0 0 199.999995228388
  50 0 0 199.999988018074
  51 0 0 199.999988018073
  52 0 0 199.9999843799754
  53 0 0 199.99992158941
  54 0 0 199.999796159836

```

Figure 5: Position-dependent potential data

As seen in Figure 5, the first three columns show the position  $(x, y, z)$ , the 4th column is unimportant, and the 5th column corresponds to the potential in V. Details regarding scaling and SIMION's step adjustments are covered in section 4.1.2. Additionally, since the structure of the electric field .patxt file has already been provided, it is not repeated here.

## 4.2 Python

### 4.2.1 Calculation of $V(R)$

In equation (3) since I needed to use the mean of the electric field to calculate the effective potential energy  $V(R)$ , I transferred the electric field vectors that data I created for each sampling time from .patxt to Python as a matrix and summed the electric fields vectorally in Python.

$$\langle E_x \rangle = \frac{1}{N} \sum_{t=0}^N E_{x,t} \quad \langle E_y \rangle = \frac{1}{N} \sum_{t=0}^N E_{y,t} \quad \langle E_z \rangle = \frac{1}{N} \sum_{t=1}^N E_{z,t}$$

$N$  : Total number of sampling time

$\langle E_x \rangle$  : Mean of the x component of the electric field [V/mm]

$\langle E_y \rangle$  : Mean of the y component of the electric field [V/mm]

$\langle E_z \rangle$  : Mean of the z component of the electric field [V/mm]

I then calculated the magnitude of the average electric field using the following equation :

$$E_0 = \sqrt{\langle E_x \rangle^2 + \langle E_y \rangle^2 + \langle E_z \rangle^2} \quad (5)$$

After that, we determined reasonable values to the mass and charge to calculate the effective potential energy( $V(R)$ ) using equation (3). The mass we determined corresponds to the mass of a proton, and the charge corresponds to the charge of a proton.

$$m = 1.166053906892 \times 10^{-27} \text{ kg}$$

$$Q = -e = 1.602176634 \times 10^{-19} \text{ C}$$

Having calculated  $E_0$  in equation (5) and  $\Omega$  in equation (1), and determined  $m$  and  $Q$ , I computed  $V(R)$  by substituting these values into equation (3).

### 4.2.2 Calculation of $V^*(R)$

In equation (4) since I needed to use  $E_0$  and  $\Phi_s$  to calculate the effective potential energy, I transferred the electric field vector and potential value datas by from .patxt to Python as a matrix. I then calculated the magnitude of electric field by using equation (5).

Having calculated  $E_0$  in equation (5) and  $\Omega$  in equation (1), and determined  $m$  and  $Q$  in section 4.2.1, I computed  $V^*(R)$  by substituting these values into equation (4).

### 4.2.3 Plotting the graph of position and effective potential energy ( $V(R)$ )

Before plotting the graph of position and effective potential energy, I also plotted some graphs in some intermediate steps. The main reason for this was to ensure that I was on the right track by comparing them with the expected results at each intermediate step. Additionally, I avoided plotting the graphs in four dimensions ( $x, y, z$ , and effective potential energy) because it was too time-consuming and complicated to analyze. Instead, I created 3D contour graphs by keeping one of the variables (x, y, or z). When I plotted 3D contour graphs, specifically, I set one of the variables to constant value :  $x = \max(x/2)$ ,  $y = \max(y/2)$ ,  $z = \max(z/2)$ .

Firstly, I plotted graphs of position and electric field magnitude at each sampling time. In Figure 4, you can observe some graphs that I plotted for various sampling times, with  $z$  held constant at  $z = \max(z)/2$ .

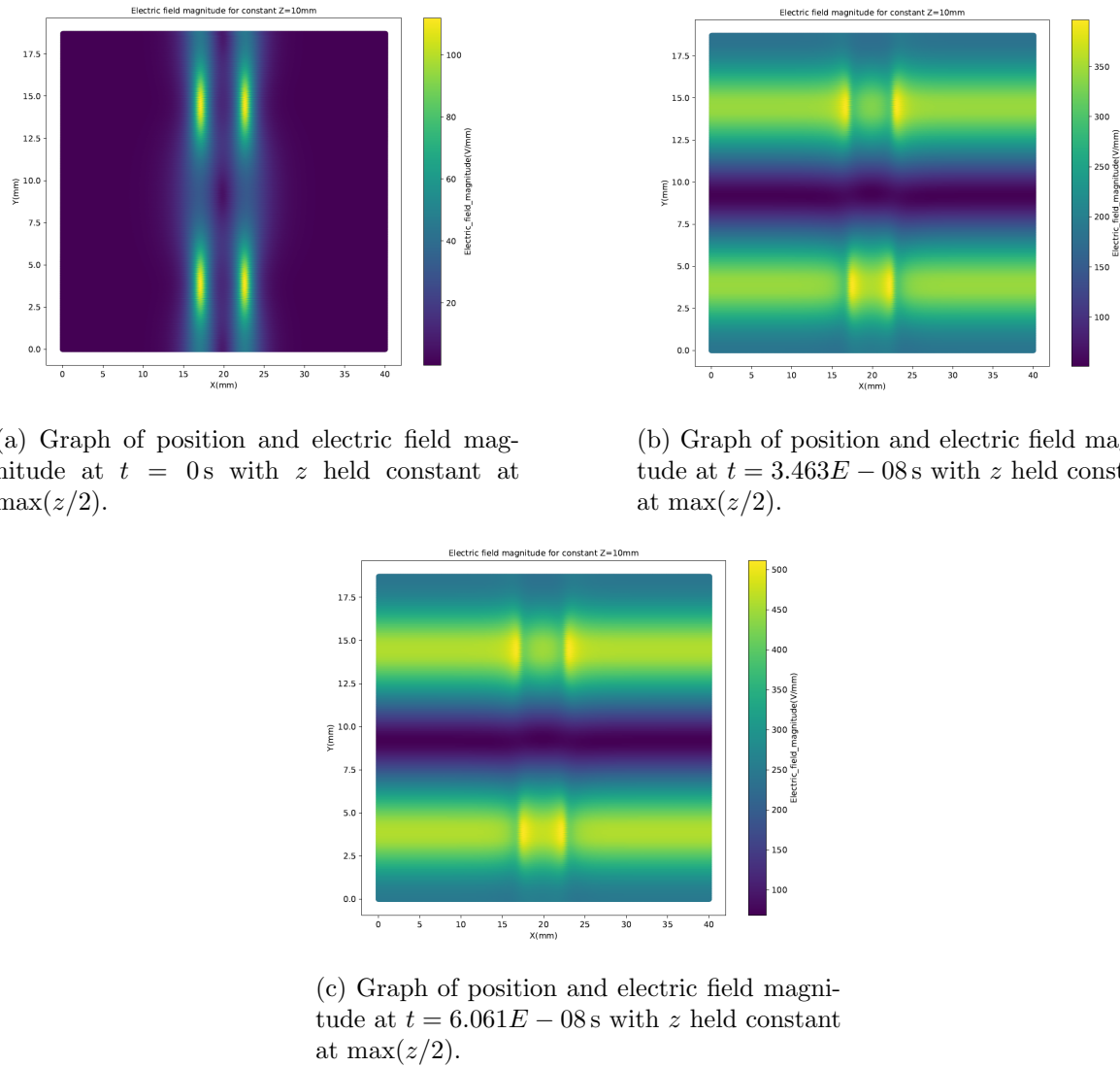


Figure 6: Graphs of position and electric field magnitude at different sampling times with  $z$  held constant at  $\max(z/2)$ .

Secondly, after calculating the magnitude of the mean electric field using equation 5, I plotted the graph of the position and magnitude of mean electric field.

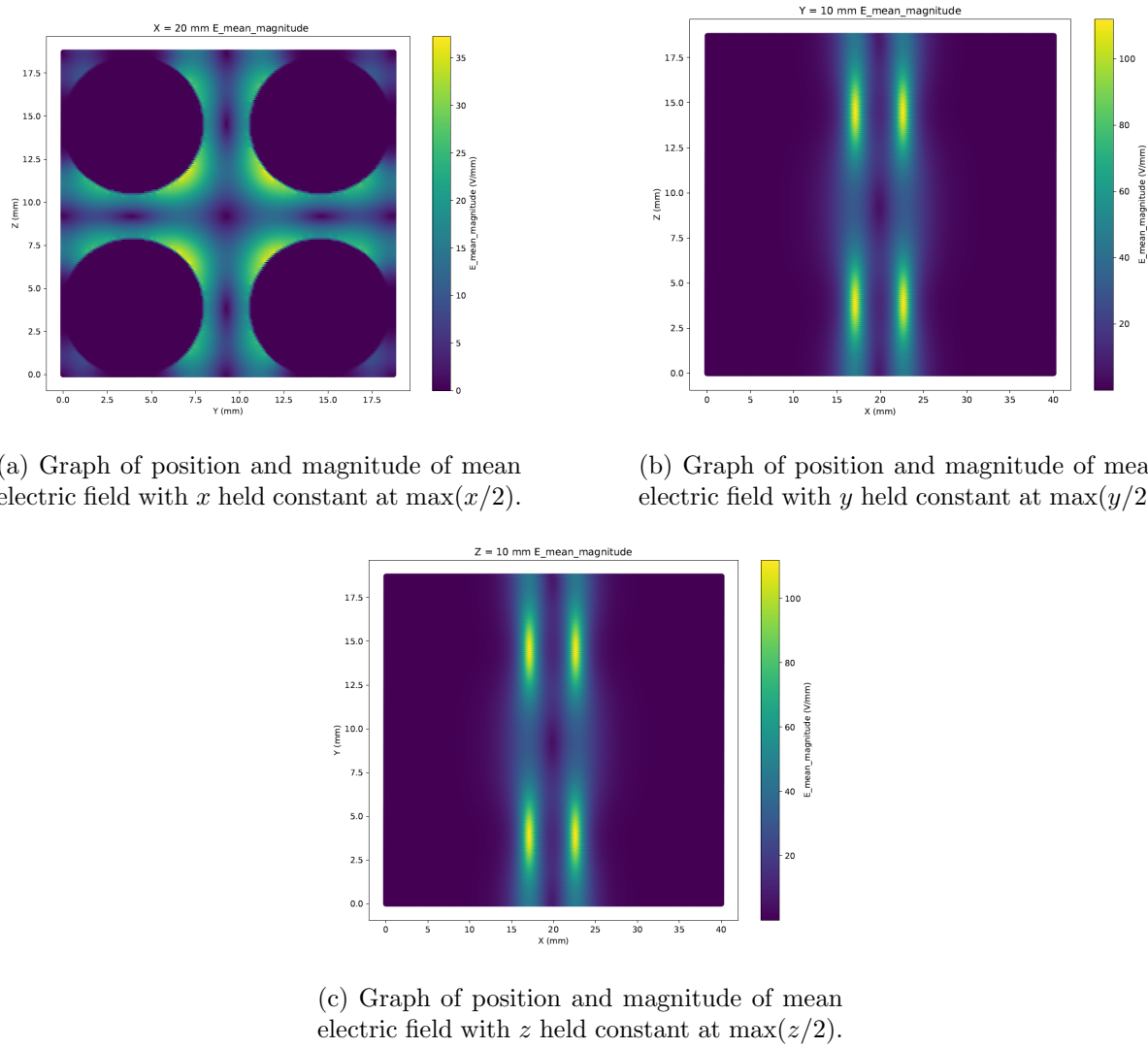
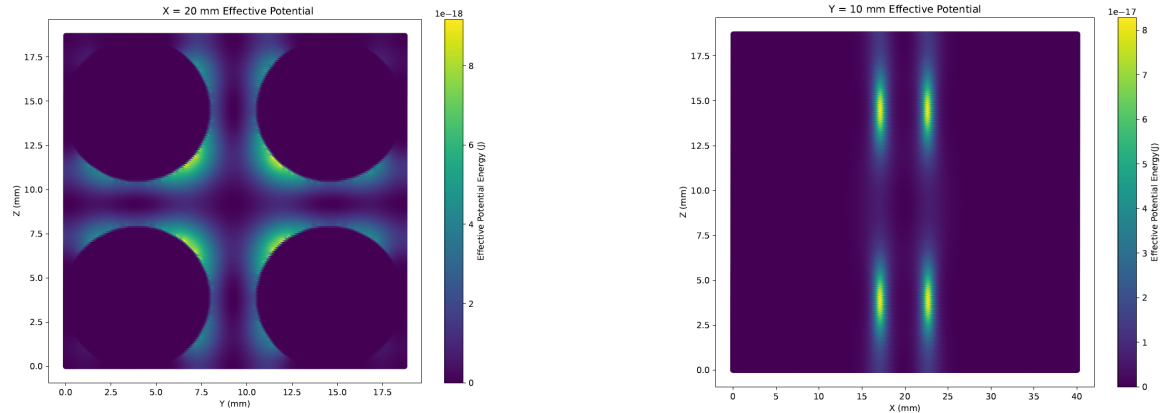


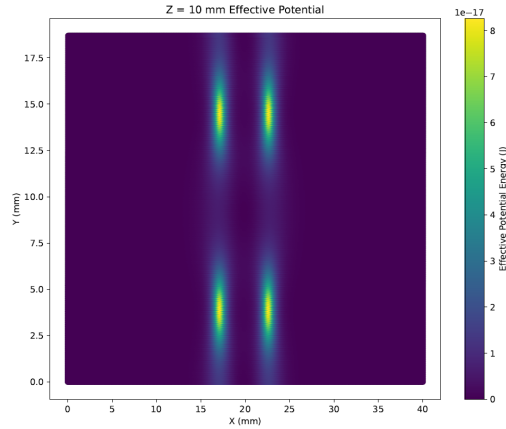
Figure 7: Graph of position and magnitude of mean electric field.

Lastly, I calculated effective potential energy by using equation (3), and plotted the graph of the position and effective potential energy ( $V(R)$ ).



(a) Graph of position and effective potential energy ( $V(R)$ ) with  $x$  held constant at  $\max(x/2)$ .

(b) Graph of position and effective potential energy ( $V(R)$ ) with  $y$  held constant at  $\max(y/2)$ .



(c) Graph of position and effective potential energy ( $V(R)$ ) with  $z$  held constant at  $\max(z/2)$ .

Figure 8: Graph of position and effective potential energy ( $V(R)$ ).

#### 4.2.4 Plotting the graph of position, DC potential and effective potential energy ( $V^*(R)$ )

In Section 4.2.2, due to the reasons discussed, I plotted graphs in some intermediate steps. Firstly, I plotted graphs of position and magnitude of electric field.

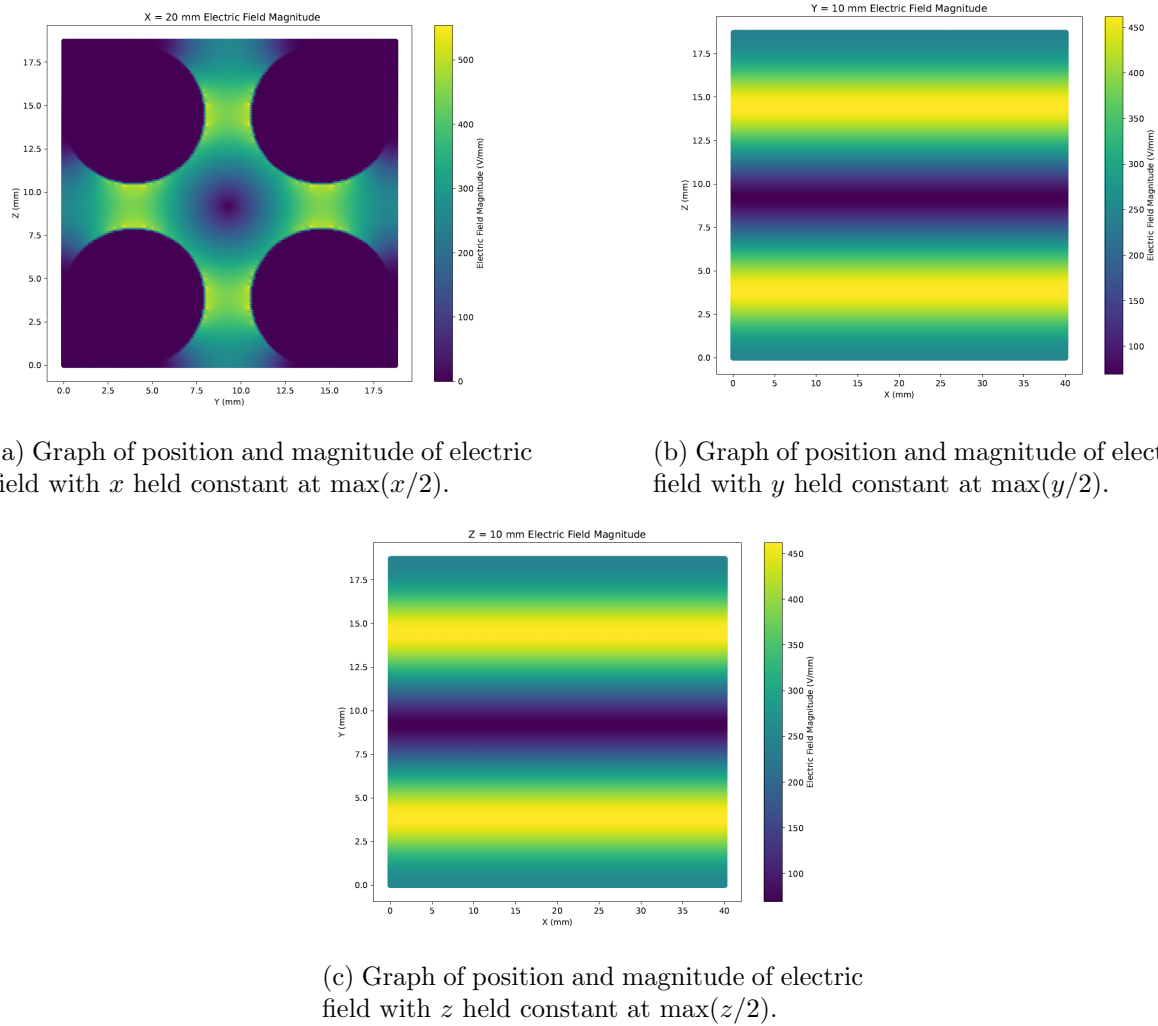


Figure 9: Graph of position and magnitude of electric field.

Secondly, I plotted graphs of position and DC potential.

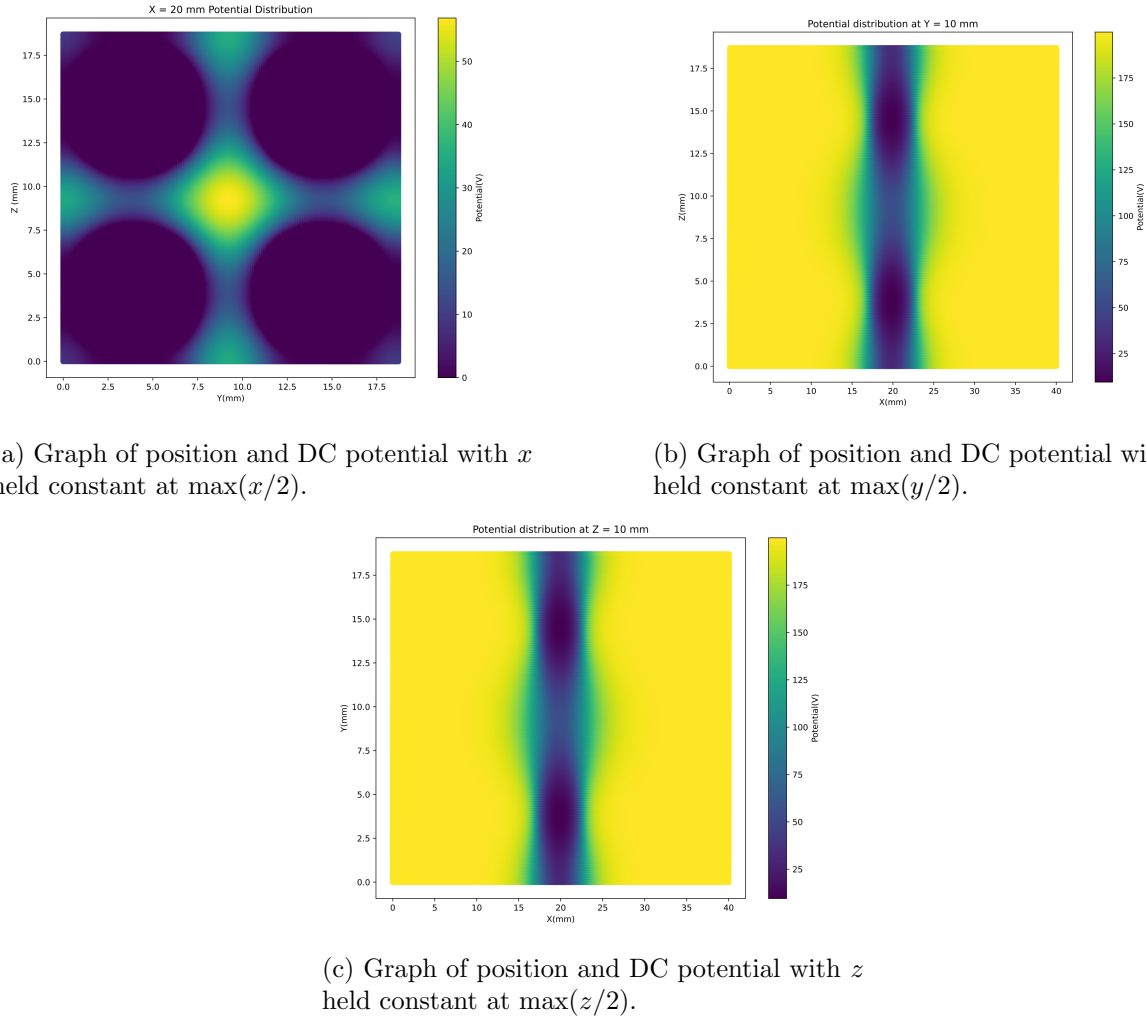


Figure 10: Graph of position and DC potential.

Lastly, I calculated the effective potential energy ( $V^*(R)$ ) by using equation (4), and plotted the graph of the position and effective potential energy ( $V^*(R)$ ).

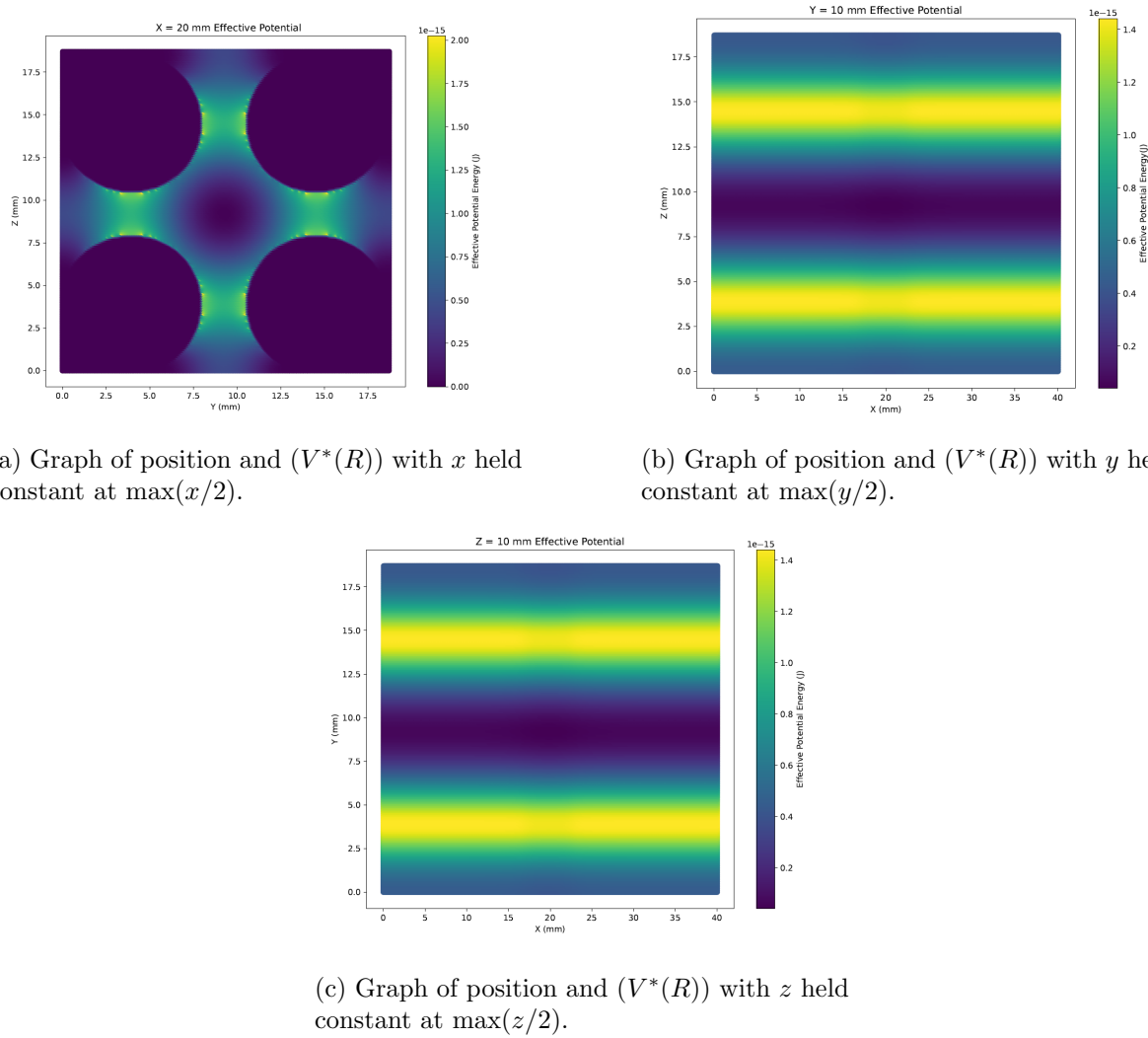
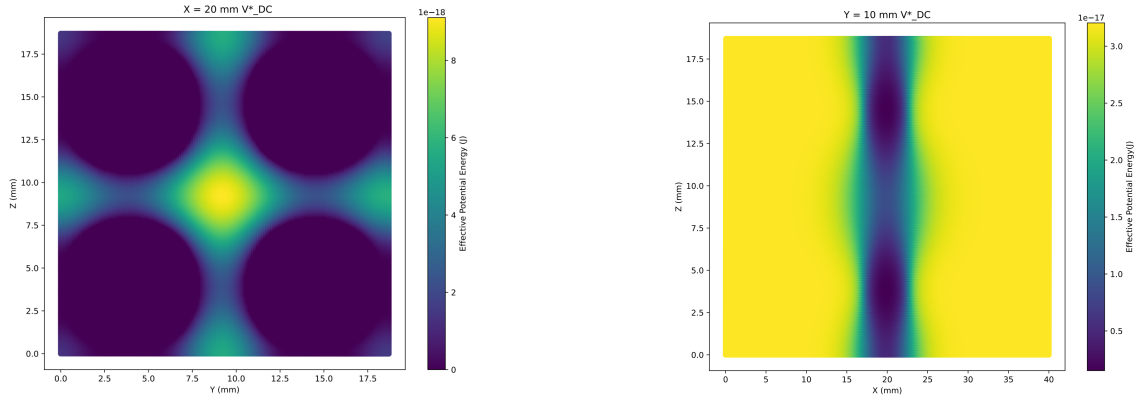


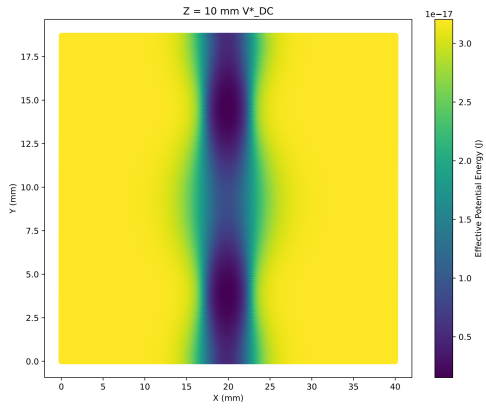
Figure 11: Graph of position and effective potential energy ( $V^*(R)$ ).

I also plotted the graphs of  $V_{\text{RF}}^*$  and  $V_{\text{DC}}^*$  in order to make a more detailed analysis of the effective potential energy.



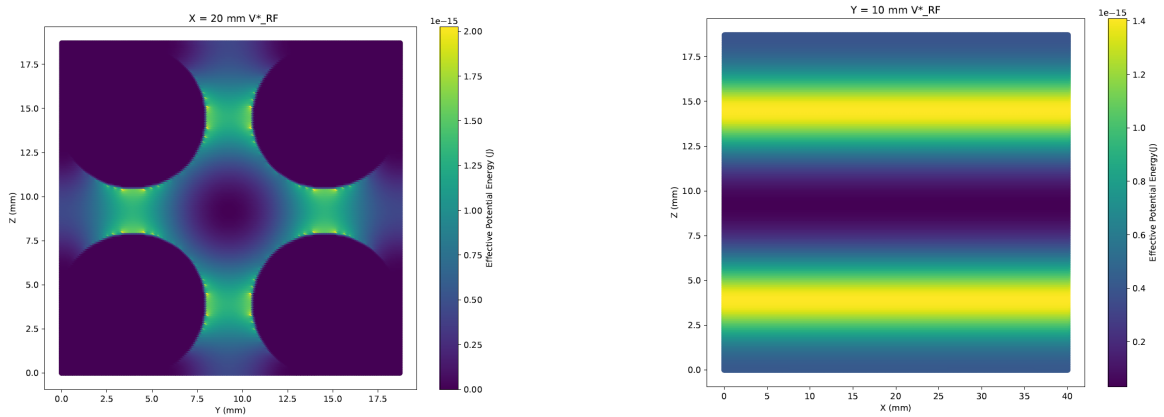
(a) Graph of position and  $V_{\text{DC}}^*$  with  $x$  held constant at  $\max(x/2)$ .

(b) Graph of position and  $V_{\text{DC}}^*$  with  $y$  held constant at  $\max(y/2)$ .



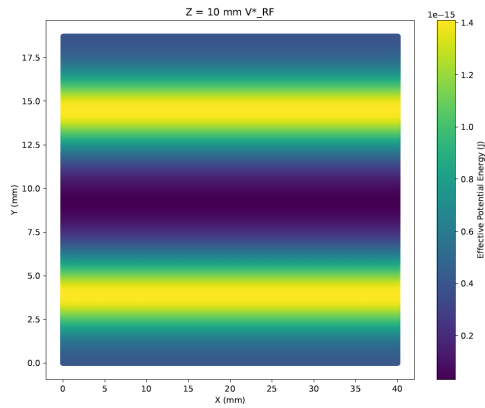
(c) Graph of position and  $V_{\text{DC}}^*$  with  $z$  held constant at  $\max(z/2)$ .

Figure 12: Graph of position and  $V_{\text{DC}}^*$ .



(a) Graph of position and  $V_{\text{RF}}^*$  with  $x$  held constant at  $\max(x/2)$ .

(b) Graph of position and  $V_{\text{RF}}^*$  with  $y$  held constant at  $\max(y/2)$ .



(c) Graph of position and  $V_{\text{RF}}^*$  with  $z$  held constant at  $\max(z/2)$ .

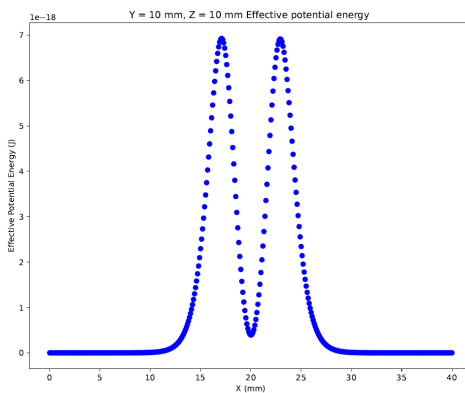
Figure 13: Graph of position and  $V_{\text{RF}}^*$ .

## 5 Results

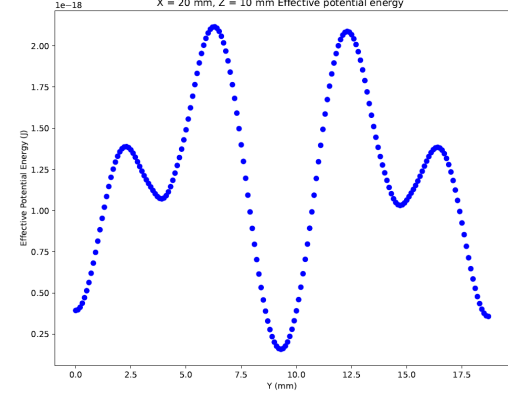
### 5.1 Results for $V(R)$

Firstly, by examining Figure 3, we anticipated the results depicted in Figure 6. As  $U_{RF\max}$  increases, we expected the magnitude of the electric field to increase in certain regions, as shown in Figure 3. Furthermore, by comparing the results in Figure 6 with the contour lines generated by the SIMION program, we confirmed the validity of our pattern.

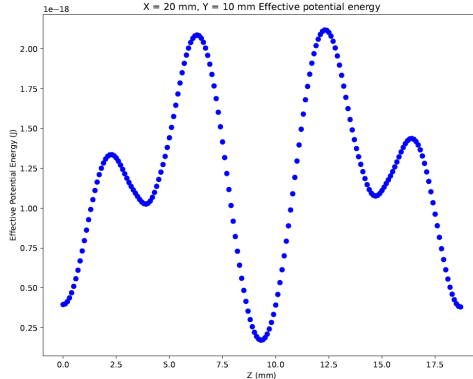
Next, to make a better inference about the graph of position and effective potential energy, I plotted 2D graphs by keeping two position variables constant.



(a) Graph of position and effective potential energy ( $V(R)$ ) with  $y$  and  $z$  held constant at  $\max(y/2)$  and  $\max(z/2)$ .



(b) Graph of position and effective potential energy ( $V(R)$ ) with  $x$  and  $z$  held constant at  $\max(x/2)$  and  $\max(z/2)$ .



(c) Graph of position and effective potential energy ( $V(R)$ ) with  $x$  and  $y$  held constant at  $\max(x/2)$  and  $\max(y/2)$ .

Figure 14: Graph of position and effective potential energy with 2 constant variables.

To obtain an approximate value for the trap depth, we used the following approximation :

$$V_{\max} \approx k_B T \quad (6)$$

$V_{\max, \text{axial}}$  : Maximum effective potential energy in the axial direction = 6.926E-20 J

$V_{\max, \text{radial}}$  : Maximum effective potential energy in the radial direction = 2.117E-20 J

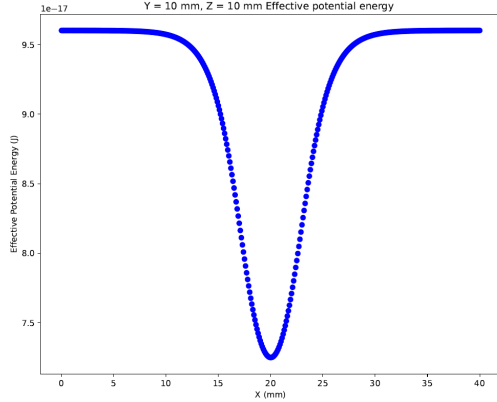
$k_B$  : Boltzmann constant = 1.380E-23 J/K

$T$  : Temperature (K)

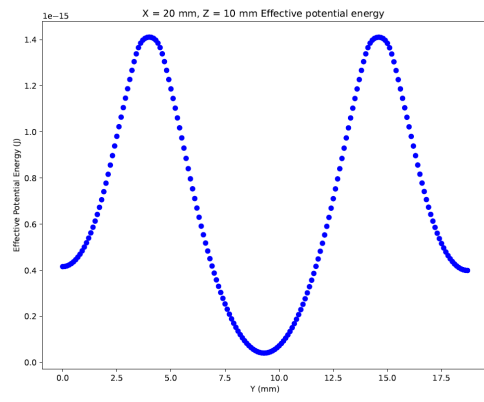
As a result, our temperature came out to be in the axial direction 5018.84 K and in the radial direction 1534.05 K. Based on the research conducted after applying this method, there are some flaws in the initial approach. Method 2, as referenced in Dehmelt 1968 [6], is the more accurate method. What we did not consider earlier was that the effective potential energy already contains the time average.

## 5.2 Results for $V^*(R)$

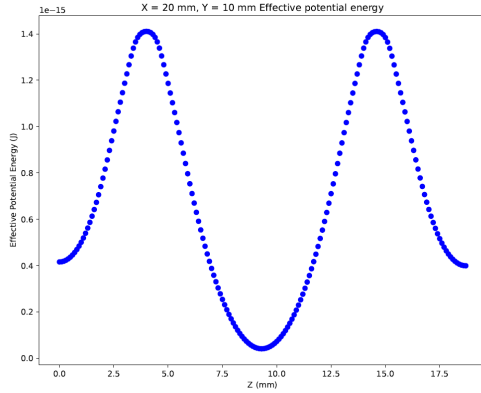
To make a better inference about the graph of position and effective potential energy, I plotted 2D graphs of  $V^*(R)$ ,  $V_{RF}^*$ , and  $V_{DC}^*$  by keeping two position variables constant.



(a) Graph of position and effective potential energy ( $V^*(R)$ ) with  $y$  and  $z$  held constant at  $\max(y/2)$  and  $\max(z/2)$ .

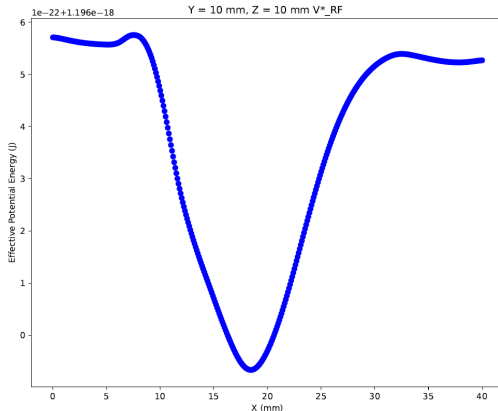


(b) Graph of position and effective potential energy ( $V^*(R)$ ) with  $x$  and  $z$  held constant at  $\max(x/2)$  and  $\max(z/2)$ .

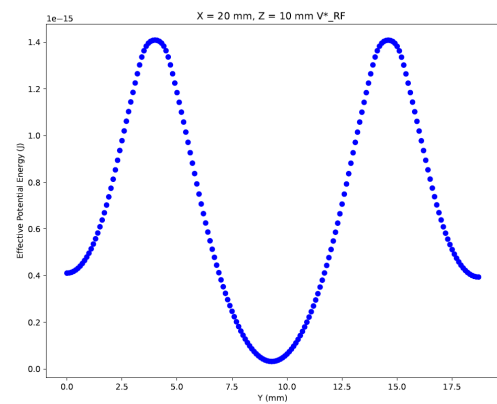


(c) Graph of position and effective potential energy ( $V^*(R)$ ) with  $x$  and  $y$  held constant at  $\max(x/2)$  and  $\max(y/2)$ .

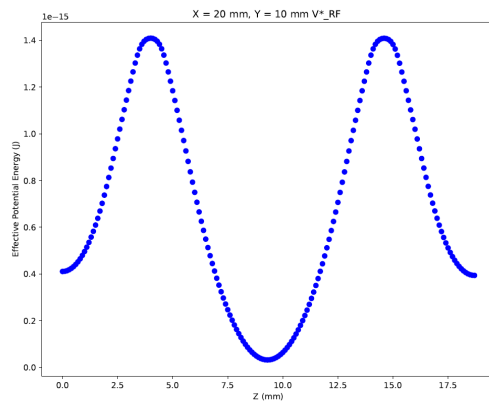
Figure 15: Graph of position and effective potential energy ( $V^*(R)$ ) with 2 constant variables.



(a) Graph of position and  $V_{\text{RF}}^*$  with  $y$  and  $z$  held constant at  $\max(y/2)$  and  $\max(z/2)$ .

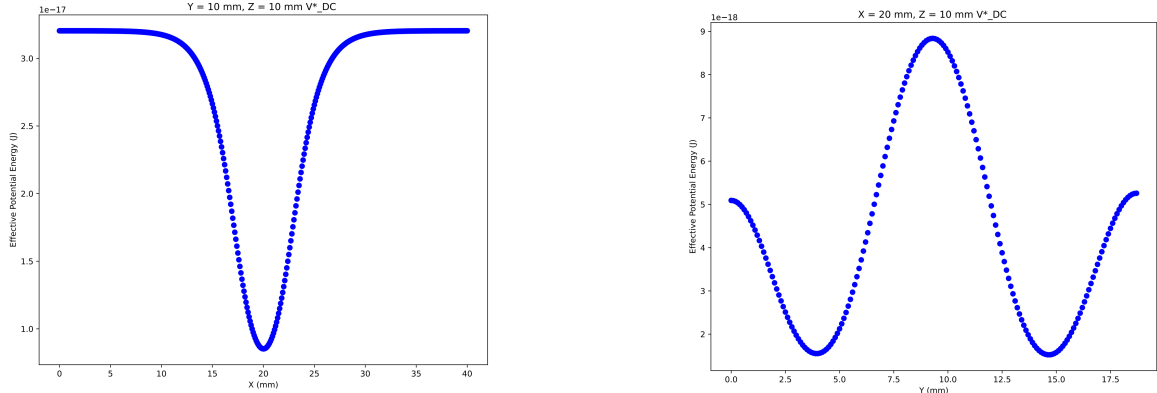


(b) Graph of position and  $V_{\text{RF}}^*$  with  $x$  and  $z$  held constant at  $\max(x/2)$  and  $\max(z/2)$ .

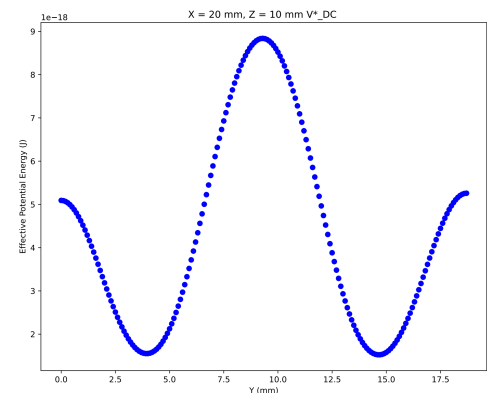


(c) Graph of position and  $V_{\text{RF}}^*$  with  $x$  and  $y$  held constant at  $\max(x/2)$  and  $\max(y/2)$ .

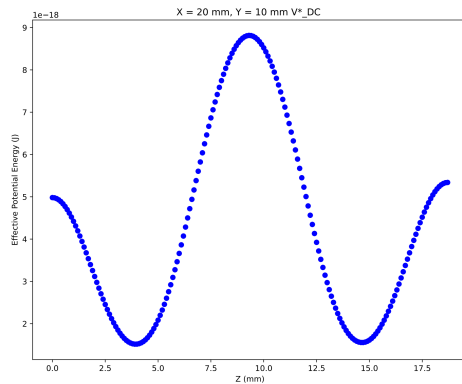
Figure 16: Graph of position and  $V_{\text{RF}}^*$  with 2 constant variables.



(a) Graph of position and  $V_{\text{DC}}^*$  with  $y$  and  $z$  held constant at  $\max(y/2)$  and  $\max(z/2)$ .



(b) Graph of position and  $V_{\text{DC}}^*$  with  $x$  and  $z$  held constant at  $\max(x/2)$  and  $\max(z/2)$ .



(c) Graph of position and  $V_{\text{DC}}^*$  with  $x$  and  $y$  held constant at  $\max(x/2)$  and  $\max(y/2)$ .

Figure 17: Graph of position and  $V_{\text{DC}}^*$  with 2 constant variables.

Then, I determined  $V_{\text{max,axial}}$  and  $V_{\text{max,radial}}$  in Python.

$$V_{\text{max,axial}} = 3.267 \times 10^{-17} \text{ J}$$

$$V_{\text{max,radial}} = 1.564 \times 10^{-17} \text{ J}$$

To obtain an approximate value for the trap depth, we used the equation (6). As a result, our temperature came out to be in the axial direction 2367391.30 K and in the radial direction 1133333.333 K. A temperature value exceeding kilokelvin was anticipated, and our result confirmed this expectation. Additionally, when examining the effective potential energy graph in Figure 15, we observe that the ions can be trapped in the region located in the middle, between the maximum and minimum points. This indicates that the method we employed is highly likely to be effective and accurate.

To better analyze the effective potential energy graph shown in Figure 15, I will plot new graphs by implementing the changes discussed in Section 7. Subsequently, I will compare these newly generated graphs with the existing ones to gain a deeper understanding of the effective potential energy.

## 6 Mathieu Equations and Stability Diagram

In this section, we will examine the theoretical background of Mathieu's equations and their connection with the stability diagram. Following this, we will compare the analytically derived Mathieu parameters and some of the corresponding results with those obtained through numerical calculations using Python. The coordinate system I use in this section is different from other sections. The derivation of Mathieu equations and numerical calculations were adjusted according to this coordinate system. Despite this change, it is important to note that the dimensions in the design of the linear Paul trap are exactly the same as the previous sections. The coordinate system used in this section is given below along with the linear Paul trap.

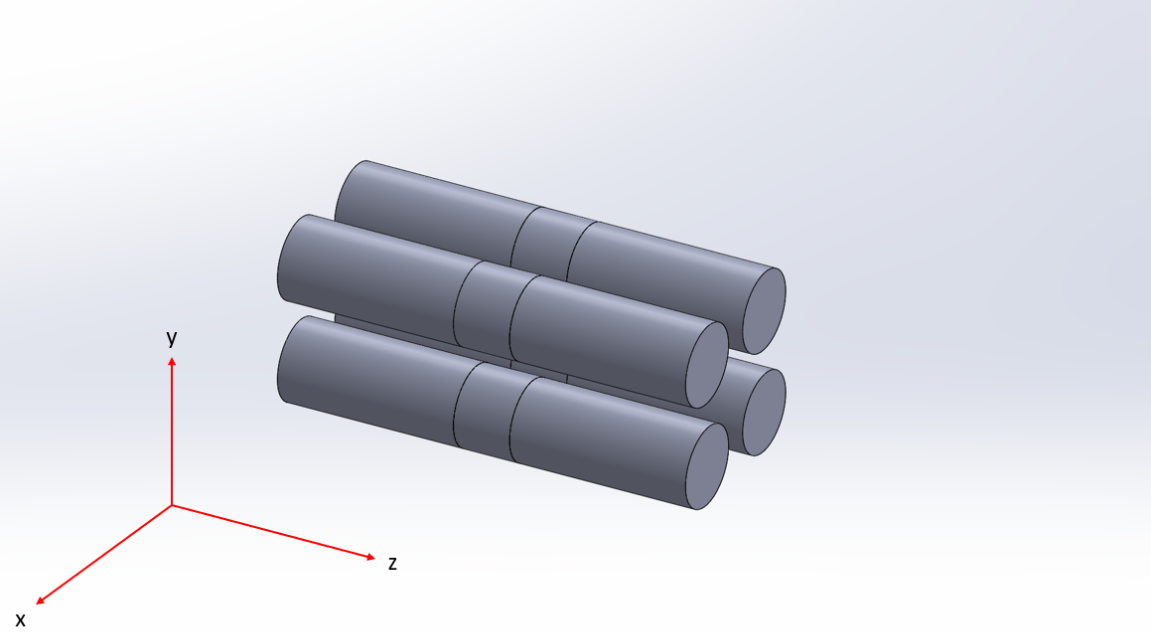


Figure 18: Coordinate system with the linear Paul trap.

### 6.1 Theoretical background of Mathieu equations

Oscillating quadrupole fields are electromagnetic fields that vary with time and have a quadrupolar spatial configuration. These fields are commonly used in devices such as ion traps (e.g., Paul traps) to confine and manipulate charged particles, such as ions. As illustrated in Section 2, we also employed oscillating quadrupole fields to trap our ions. Oscillating quadrupole fields are special for the very reason that the equations of motion can be reduced to a set of decoupled one dimensional differential equations of the Mathieu type [5]. This is advantageous because the solutions of the Mathieu equations are well understood, with the stability of a trajectory dependent on only two dimensionless parameters and not on the initial conditions of the ion [8].

To understand the connection between the equation of motion for ions and Mathieu's equations in the context of oscillating quadrupole fields, we should first express the potential contributions arising from the applied RF and DC voltages. The complete electric potential in the trap is obtained through a multipole expansion, where terms beyond quadratic order are neglected to approximate harmonic potential. This resulting harmonic potential can be expressed as follows [5]:

$$\phi_{\text{RF}}(x, y, t) = \frac{U_{\text{RF}}}{2} \left( \frac{x^2 + y^2}{r_0^2} \right) \cos(\Omega t) \quad (7)$$

$$\phi_{\text{DC}}(x, y, z) = \frac{\kappa U_{\text{DC}}}{z_0^2} \left( z^2 - \frac{x^2 + y^2}{2} \right) \quad (8)$$

$$\phi = \phi_{\text{RF}} + \phi_{\text{DC}} \quad (9)$$

The factors  $r_0$  and  $z_0$  relate to the trap geometry as indicated by Figure 1, and  $\kappa$  is also a geometric coefficient uniquely determined for a given trap design. Given the total electric potential in the form of equation 9, the Newtonian equations of motion for a particle of charge  $Q$  and mass  $m$  may be written according to  $F = ma = -QE = -Q\nabla\phi$  as [5] :

$$\ddot{x} + \left( -\frac{\kappa Q U_{\text{DC}}}{mz_0^2} + \frac{Q U_{\text{RF}}}{mr_0^2} \cos \Omega t \right) x = 0 \quad (10)$$

$$\ddot{y} + \left( -\frac{\kappa Q U_{\text{DC}}}{mz_0^2} - \frac{Q U_{\text{RF}}}{mr_0^2} \cos \Omega t \right) y = 0 \quad (11)$$

$$\ddot{z} + \left( \frac{2\kappa Q U_{\text{DC}}}{mz_0^2} \right) z = 0 \quad (12)$$

These may then be written in the form of the Mathieu equations,

$$\frac{\partial^2 u}{\partial \tau^2} + [a_u - 2q_u \cos(2\tau)] u = 0; \quad u_i \in \{x, y, z\} \quad (13)$$

by making the substitution  $\tau = \frac{\Omega t}{2}$  into equations 10, 11 and 12 [5]:

$$\frac{\partial^2 x}{\partial \tau^2} + \left( -\frac{4\kappa Q U_{\text{DC}}}{mz_0^2 \Omega^2} + \frac{4Q U_{\text{RF}}}{mr_0^2 \Omega^2} \cos 2\tau \right) x = 0 \quad (14)$$

$$\frac{\partial^2 y}{\partial \tau^2} + \left( -\frac{4\kappa Q U_{\text{DC}}}{mz_0^2 \Omega^2} - \frac{4Q U_{\text{RF}}}{mr_0^2 \Omega^2} \cos 2\tau \right) y = 0 \quad (15)$$

$$\frac{\partial^2 z}{\partial \tau^2} + \left( \frac{8\kappa Q U_{\text{DC}}}{mz_0^2 \Omega^2} \right) z = 0 \quad (16)$$

Finally, direct comparison of these equations with the form of the Mathieu equations yields the dimensionless Mathieu parameters[5]:

$$a_x = a_y = -\frac{a_z}{2} = -\frac{4\kappa Q U_{\text{DC}}}{mz_0^2 \Omega^2} \quad (17)$$

$$q_x = -q_y = \frac{2Q U_{\text{RF}}}{mr_0^2 \Omega^2}; \quad q_z = 0 \quad (18)$$

In Section 8.2, we provide a more detailed explanation of how the stability diagram is constructed using the Mathieu parameters.

## 6.2 Stability Diagram

A direct result of the decoupling of the equations of motions in the harmonic potential is that the stability of a single ion trajectory within the trap is dependent purely on the values of  $a$  and  $q$ , and not on the initial conditions. This means that a stability “map” can be generated in the  $(a, q)$  parameter space [5]. For certain values of  $a$  and  $q$ , the ion will be in a stable state, while for other values, it will not be. I used a MATLAB code from [9] that draws the stability diagram based on the  $a$  and  $q$  parameters of Mathieu’s equation. I translated this code into Python and used it to plot stability diagrams based on these parameters. You can see this graph below.

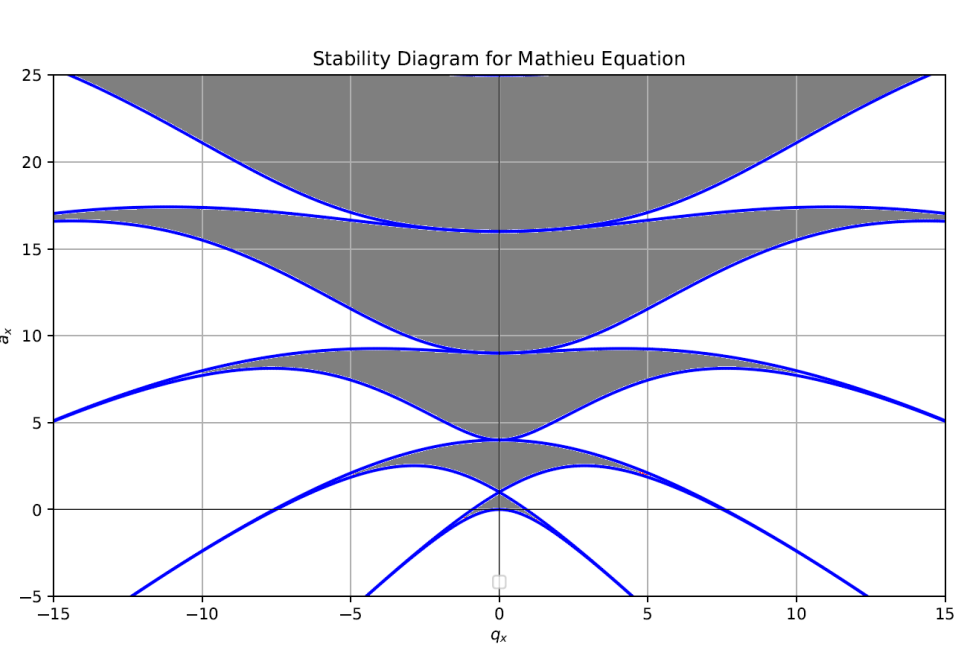


Figure 19: Stability diagram with  $a_x$  and  $q_x$ . Grey shaded areas represent regions of stable trapping.

A stability diagram can be constructed using the values of  $U_{\text{RF}}$  and  $U_{\text{DC}}$ , which allows us to identify the combinations of these voltages where ions can be effectively stabilized or trapped. By analyzing this diagram, we can determine the specific ranges or conditions under which ions remain confined, providing valuable insights into the optimal settings for ion trapping. Therefore, I formulated the values of  $U_{\text{RF}}$  and  $U_{\text{DC}}$  using Equations 17 and 18 to construct the stability diagram. It is important to note that, unlike in the previous sections where we considered a hydrogen ion, we are now focusing specifically on the calcium ion. As a result, the mass value has been adjusted to  $m = 40$  amu, while all other parameters remain unchanged.

$$U_{\text{DC}} = -\frac{a_x m z_0^2 \Omega^2}{4\kappa Q} \quad (19)$$

$$U_{\text{RF}} = \frac{q_x m r_0^2 \Omega^2}{2Q} \quad (20)$$

Then, I plotted stability diagram for  $U_{RF}$  and  $U_{DC}$ . You can see this in the graph below.

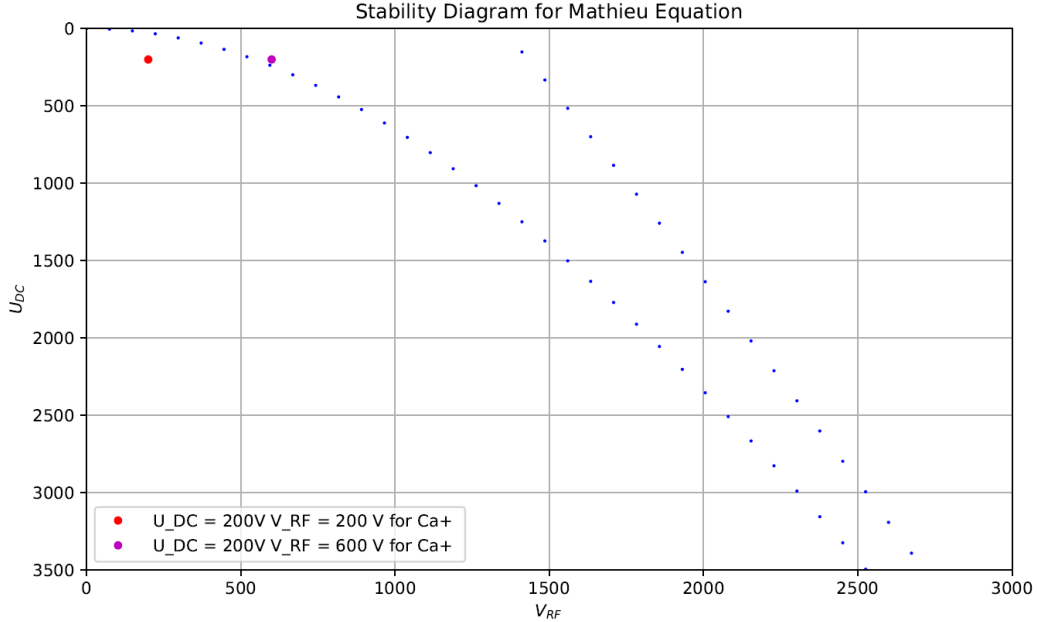


Figure 20: Stability diagram for  $U_{RF}$  and  $U_{DC}$  for  $\kappa = 0.152$ . In the area between two curves represent regions of stable trapping. Stabilized state of Ca+ ion at two different  $U_{RF}$  and  $U_{DC}$  voltage values.

Figure 20 illustrates the stability of the Ca+ ion under two different sets of  $U_{RF}$  and  $U_{DC}$  voltage values. In one configuration the ion is in a stabilized state, while in another it is not. We can interpret this by looking at the graph. However, it is important to note that this graph is based on theoretical calculations, which assume ideal conditions. In practice, the ions may not remain experimentally stabilized in all the regions where they appear stable theoretically. This discrepancy arises because these calculations assume perfect geometries, which are almost impossible achievable in real-world setups. Factors such as electrode misalignment, fabrication errors, field distortion, insulator charging, and voltage noise can lead to deviations from the theoretical predictions. As a result, while the stability regions predicted by the model provide useful guidance, they do not guarantee ion stability in actual experiments.

## 6.3 Longitudinal frequency

### 6.3.1 Calculation of longitudinal frequency analytically

We have previously formalized the time-independent effective potential energy as shown in equation 4 of Section 3.2. Note that the first term in Equation 4 is effectively a time-averaged potential resulting from the oscillating RF fields (which have amplitude  $E_0$  and angular frequency  $\Omega$ ); in the second term,  $\phi_s$  represents the potential arising from the static fields [5]. Furthermore, when trapping ions, it is important to note that the axial trapping is driven only by the DC potential, while radial trapping is driven generally by the RF potential. However, as indicated in Equation 4, there are no explicit terms for the longitudinal and radial frequencies. To address this, we represented the effective potential energy using the pseudopotential approach within the quantum harmonic oscillator framework, thereby connecting it to the effective potential energy described in Equation 4. By analogy to a quantum harmonic oscillator, the harmonic pseudopotential may also be written[5]:

$$V^*(r, z) = \frac{1}{2}m\omega_r^2 r^2 + \frac{1}{2}m\omega_z^2 z^2 \quad (21)$$

with  $r = \sqrt{x^2 + y^2}$  the radial distance from the trap axis, and  $z$  the axial distance from the trap centre (In other sections, the axial direction was taken as  $x$  axis. It is important to note that the axial direction is the  $z$  axis in this section.). The corresponding secular motional frequencies  $\omega_z$  and  $\omega_r$  are given by [5]

$$\omega_i = \sqrt{\frac{q_i^2}{2} + a_i} \frac{\Omega}{2} \quad (22)$$

Then, I determined the Mathieu parameters in the  $z$ -direction using Equations 17 and 18 for analytical calculations in the longitudinal direction. The variables used in these calculations, are presented in Table 2.

|                    |                                     |
|--------------------|-------------------------------------|
| $\kappa$           | 0.244                               |
| $Q$                | $1.602176634 \times 10^{-19}$ C     |
| $m$                | $40 \times 1.66 \times 10^{-27}$ kg |
| $\Omega$           | 24190263.43 1/s                     |
| $2r_0$             | 7 mm                                |
| $2z_0$             | 5.5 mm                              |
| $U_{DC}$           | 5 V                                 |
| $U_{RF_{max}}$     | 600 V                               |
| $a_z/U_{DC}$       | $0.0010638 \text{ V}^{-1}$          |
| $q_z/U_{RF_{max}}$ | $0 \text{ V}^{-1}$                  |

Table 2: Mathieu parameters in the  $z$ -direction and other parameters at specific  $U_{DC}$  and  $U_{RF}$  values, used for the stable trapping of Ca+ ions.

To analytically calculate the longitudinal frequency using the parameters provided in Table 2, I first calculated  $\omega_z$  by using equation 22. Then, I divided it by  $2\pi$  to find the longitudinal frequency analytically. As a result of these calculations, I found the longitudinal frequency analytically to be 140397.401 (1/s). The calculation for the longitudinal frequency ( $f_{axial}$ ) analytically is presented below equation:

$$f_{axial} = \frac{\omega_z}{2\pi} = \sqrt{\frac{8\kappa Q U_{DC}}{m z_0^2 \Omega^2}} \frac{\Omega}{4\pi} \quad (23)$$

### 6.3.2 Calculation of longitudinal frequency numerically

Since the contribution to longitudinal trapping comes from the constant DC potential, I used the second term ( $V_{DC}^*$ ) in equation 4 for the longitudinal trap frequency calculations numerically by using  $U_{DC}$  and  $Q$  parameters in table 2. I plotted the  $V_{DC}^*$  graph as a function of  $z$  using Python. To establish a relationship between the harmonic potential and the  $V_{DC}^*$  graph, I determined a coefficient  $a$  by performing a second-degree nonlinear fit on the  $V_{DC}^*$ -dependent  $z$  graph, similar to the harmonic potential. You can see the relationship between the nonlinear fit parameter and  $V_{DC}^*$  in the equations below.

$$V_{DC}^*(z) = Q\phi_s(z) \quad (24)$$

$$Q\phi_s(z) = az^2 \quad (25)$$

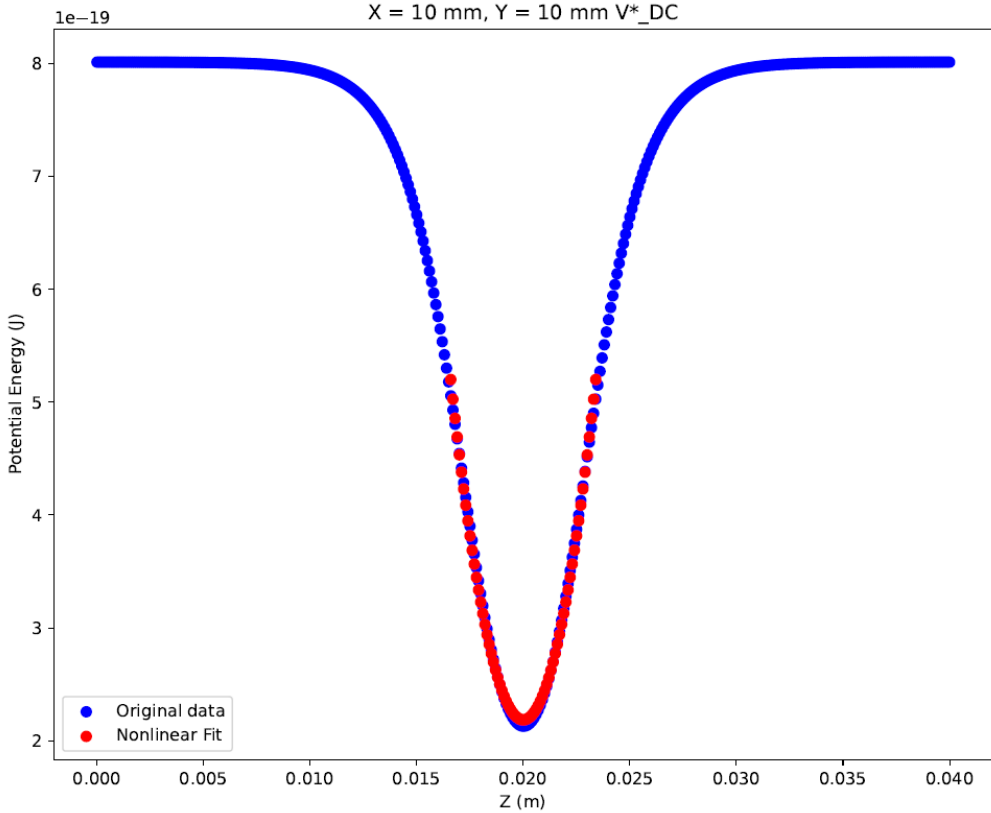


Figure 21: The  $V_{DC}^*$  versus  $z$  graph of the original data alongside the second-degree nonlinear fit applied to the  $V_{DC}^*$ -dependent  $z$  graph. The nonlinear fit was performed over an  $z$ -range of 0.0165 to 0.0235 m.

The relationship between second terms of the equations 4 and 21 is shown in below equation.

$$\frac{1}{2}m\omega_z^2z^2 = V_{DC}^*(z) = az^2 \quad (26)$$

The  $\omega_z$  can be formulated numerically as follows using equation 26.

$$\omega_z = \sqrt{\frac{2a}{m}} \quad (27)$$

In summary, I determined the  $a$  coefficient from the  $V_{DC}^*$  graph by doing nonlinear fit and subsequently calculated the  $\omega_z$  using Equation 27. Then, I calculated the longitudinal frequency( $\omega_z/2\pi$ ) and found it to be 140996.33 (1/s). The calculation for the longitudinal frequency ( $f_{\text{axial}}$ ) numerically is presented below equation:

$$f_{\text{axial}} = \frac{\omega_z}{2\pi} = \sqrt{\frac{2a}{m}} \frac{1}{2\pi} \quad (28)$$

Finally, I used Equation 29 to compare my numerical and analytical results, finding a percent error of 0.42. As a result, the analytical and numerical results I obtained were in close agreement, which confirms the accuracy of my  $V_{DC}^*$  position graphs.

$$\text{Percentage Error} = \left| \frac{\text{Theoretical Value} - \text{Experimental Value}}{\text{Theoretical Value}} \right| \times 100 \quad (29)$$

### 6.3.3 Calculation of $\kappa$ with numerical methods

To calculate  $\kappa$  numerically, I performed a linear fit using  $U_{DC}$  as the independent variable and the coefficient  $a$  obtained from the  $V_{DC}^*$  graph as the dependent variable. The value of  $\kappa$  was numerically determined using the constant  $C$  derived from this linear fit. The relationship between  $a$  and  $U_{DC}$  was established based on Equations 21 and 27.

$$\frac{\sqrt{\frac{2a}{m}}}{2\pi} = \sqrt{\frac{8\kappa Q U_{DC}}{m z_0^2 \Omega^2}} \frac{\Omega}{4\pi} \quad (30a)$$

Equation (30a) was squared on both sides:

$$\frac{2a}{4m\pi^2} = \frac{8\kappa Q U_{DC}}{m z_0^2 \Omega^2} \frac{\Omega^2}{16\pi^2} \quad (30b)$$

Following this, Equation (30b) was simplified, isolating the variable  $a$ :

$$a = \frac{\kappa Q U_{DC}}{z_0^2} \quad (30c)$$

The relationship between coefficient  $C$  and linear fit is shown below.

$$\frac{a}{U_{DC}} = \frac{\kappa Q}{z_0^2} = C \quad (31)$$

Then, I determined the coefficient  $a$  values numerically for various  $U_{DC}$  values and subsequently calculated the coefficient  $C$  by performing a linear fit using these  $a$  values. The  $U_{DC}$  values and their corresponding  $a$  values are presented in Table 3.

|                 |                   |
|-----------------|-------------------|
| $U_{DC} = 1V$   | $a = 5.162E - 15$ |
| $U_{DC} = 5V$   | $a = 2.580E - 14$ |
| $U_{DC} = 20V$  | $a = 1.032E - 13$ |
| $U_{DC} = 50V$  | $a = 2.580E - 13$ |
| $U_{DC} = 200V$ | $a = 1.028E - 12$ |

Table 3: Various  $U_{DC}$  values and corresponding  $a$  coefficient values to make a linear fit.

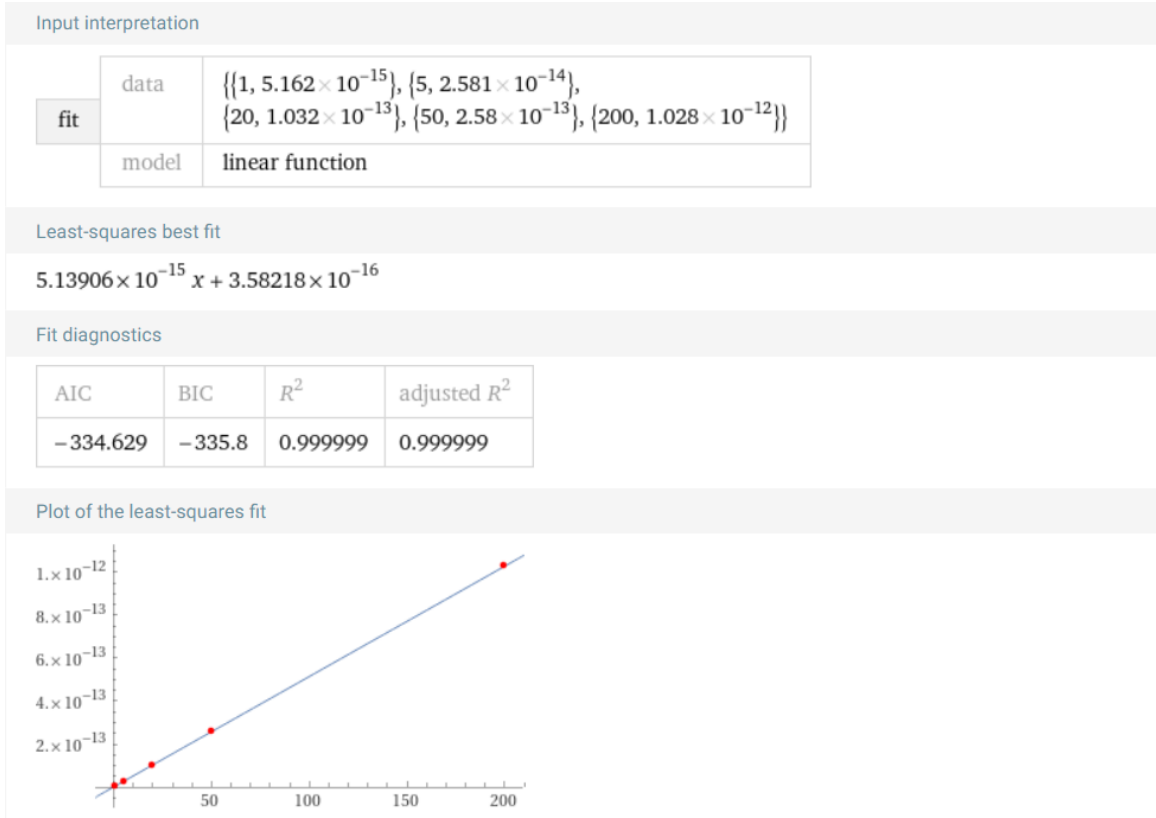


Figure 22: Linear fit using  $U_{DC}$  (x-axis) and  $a$  coefficient (y-axis) values (graph plotted with WolframAlpha).

The  $C$  coefficient was found to be  $5.13906E - 15$  as a result of the above linear fit process. I found the  $\kappa$  by substituting this  $C$  coefficient into the equation below.

$$\kappa = \frac{Cz_0^2}{Q} \quad (32)$$

It was calculated as  $\kappa = 0.242$ . Then, using Equation 29, the percent error was calculated as 0.52 by substituting the numerical  $\kappa$  results and the  $\kappa$  value provided in Alex Gingell's thesis[5].

## 6.4 Radial frequency

Trapping in the radial direction arises from the combined effects of both the constant  $U_{DC}$  voltage and the time-dependent  $U_{RF}(t)$ . However, in our pseudopotential approach, the contribution to radial trapping comes only from the first term ( $V_{RF}^*$ ) of Equation 4. In other words, in our approach, only the contribution from  $U_{RF,max}$  is taken into account, ignoring the contribution of  $U_{DC}$  for radial trapping. Therefore, only the  $U_{RF,max}$  value will be used in our radial frequency calculations numerically. However,  $U_{DC}$  also plays a crucial role in calculating the radial frequency analytically, as will be addressed in Section 6.4.1 and shown in Equation 35. Therefore, we will primarily focus on radial frequency calculations where  $U_{DC}$  is near zero.

Although the pseudopotential approach is not valid for large  $U_{DC}$  values, this approach is quite practical and useful in predicting real-life experimental results, because  $U_{DC}$  voltage values do not need to be large for longitudinal trapping and there may be deviations in radial frequency for large  $U_{DC}$  values, the  $U_{DC}$  value is usually chosen below 20 volts in real-life experiments. This voltage selection complies with our  $U_{DC}$  near-zero limit and allows us to make reasonable predictions about the experimental results.

### 6.4.1 Calculation of radial frequency analytically

Since the radial direction is actually equivalent to the x and y direction, I can write the following equation.

$$\omega_r = \omega_x = \omega_y \quad (33)$$

$$\omega_r = \omega_y = \sqrt{\frac{q_y^2}{2} + a_y \frac{\Omega}{2}} \quad (34)$$

In order to calculate  $\omega_r$  in Equation 34, I substituted the parameters  $a_y$  and  $q_y$  from Equations 17 and 18 and obtained the following equation:

$$\omega_r = \sqrt{\frac{2Q^2 U_{RF}^2}{m^2 r_0^4 \Omega^4} - \frac{4\kappa_z Q U_{DC}}{m z_0^2 \Omega^2} \frac{\Omega}{2}} \quad (35)$$

If  $|a_y| \ll q_y^2 \ll 1$ , which corresponds to small values of  $U_{DC}$ , equation 35 can be approximated as follows:

$$\omega_r = \sqrt{\frac{2Q^2 U_{RF}^2}{m^2 r_0^4 \Omega^4} \frac{\Omega}{2}} \quad (36)$$

$$f_{rad} = \frac{\omega_r}{2\pi} = \sqrt{\frac{2Q^2 U_{RF}^2}{m^2 r_0^4 \Omega^4} \frac{\Omega}{4\pi}} \quad (37)$$

When calculating  $\omega_r$  analytically,  $U_{RF}$  is considered as peak-to-peak, so it is represented as  $U_{RF} = 2 \times U_{RF,max}$  in the equations. Additionally,  $U_{DC}$  is not taken as the value given in Table 2 but rather as a very small value close to 0. In fact, you can assume that  $U_{DC}$  is taken as 0 in the calculations, leading to the derivation of equation 36. In the light of this information, I calculated radial frequency ( $f_{rad}$ ) by using equation 37. As a result of this calculation, I found the radial frequency analytically to be 1099165.614 (1/s).

#### 6.4.2 Calculation of radial frequency numerically

Since the contribution to radial trapping comes from the  $U_{\text{RF}}(t)$  in our approach, I used the first term ( $V_{\text{RF}}^*$ ) in equation 4 for the radial trap frequency calculations numerically by using  $U_{\text{RF}_{\max}}$ ,  $\Omega$ ,  $m$  and  $Q$  parameters in table 2. I plotted the  $V_{\text{RF}}^*$  graph as a function of  $y$  using Python. To establish a relationship between the harmonic potential and the  $V_{\text{RF}}^*$  graph, I determined  $b$  coefficient by performing a second-degree nonlinear fit on the  $V_{\text{RF}}^*$ -dependent  $y$  graph, similar to the harmonic potential. You can see the relationship between the nonlinear fit parameter and  $V_{\text{RF}}^*$  in the equations below.

$$V_{\text{RF}}^*(y) = \frac{Q^2 E_0^2}{4m\Omega^2} = by^2 \quad (38)$$

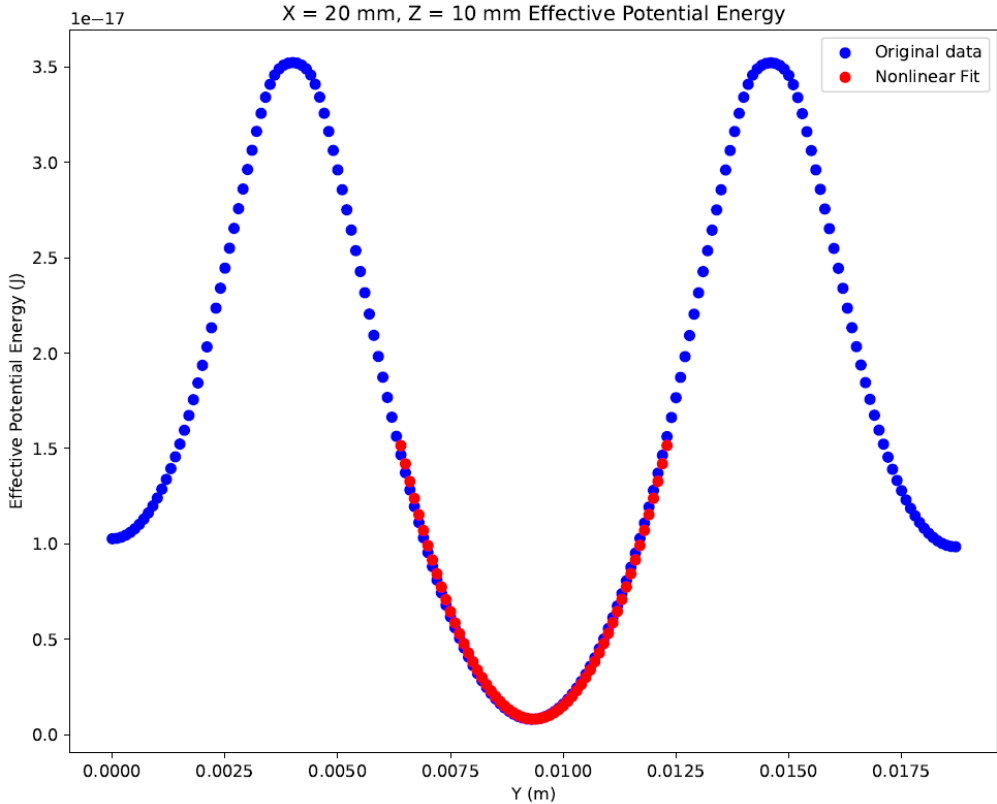


Figure 23: The  $V_{\text{RF}}^*$  versus  $y$  graph of the original data alongside the second-degree nonlinear fit applied to the  $V_{\text{RF}}^*$ -dependent  $y$  graph. The nonlinear fit was performed over an  $y$ -range of 0.00635 to 0.01235 m.

The relationship between second terms of the equations 4 and 21 is shown in below equation.

$$\frac{1}{2}m\omega_r^2y^2 = V_{\text{RF}}^*(y) = by^2 \quad (39)$$

The  $\omega_r$  can be formulated numerically as follows using equation 39.

$$\omega_r = \sqrt{\frac{2b}{m}} \quad (40)$$

In summary, I determined the  $b$  coefficient from the  $V_{\text{RF}}^*$  graph by doing nonlinear fit and subsequently calculated the  $\omega_r$  using Equation 40. Then, I calculated the frequency( $f_{\text{rad}}$ ) numerically and found it to be 1125223.886 (1/s). The calculation for the radial frequency numerically is presented below equation:

$$f_{\text{rad}} = \frac{\omega_r}{2\pi} = \sqrt{\frac{2b}{m}} \frac{1}{2\pi} \quad (41)$$

Finally, I used Equation 29 to compare my numerical and analytical results, finding a percent error of 2.370. As a result, the analytical and numerical results I obtained were in close agreement.

### 6.4.3 A novel approach to analytical calculation of radial frequency

H. X. Li et al. point out in their article that the equation 35 I used for the radial frequency, is not entirely accurate. They indicate that just as there is a  $\kappa$  factor in front of  $U_{DC}$ , there should also be a  $\kappa_r$  factor in front of  $U_{RF}$ . The geometric parameter in the radial direction  $\kappa_r$  shows the effect of the non-ideal hyperboloid shaped electrodes used in the linear Paul trap[10]. In my SIMION simulations, factors such as resolution, electrode size, and grid size affect the ideality of the electrode shapes. Because of this reason,  $\kappa_r$  will not be calculated numerically. However, due to the significance of this aspect for experimental studies, it is included in this internship report.

An alternative version of Equation 35, which includes this correction, is presented below[10].

$$\omega_r = \sqrt{\frac{2\kappa_r^2 Q^2 U_{RF}^2}{m^2 r_0^4 \Omega^4} - \frac{4\kappa Q U_{DC}}{m z_0^2 \Omega^2} \frac{\Omega}{2}} \quad (42)$$

In his thesis, Alex Gingell essentially assumes that the  $\kappa_r$  factor is equal to 1. However, while  $\kappa_r$  is indeed close to 1, it is not exactly equal to 1 .If  $|a_y| \ll q_y^2 \ll 1$ , which corresponds to small values of  $U_{DC}$ , equation 42 can be approximated as follows:

$$\omega_r = \sqrt{\frac{2\kappa_r^2 Q^2 U_{RF}^2}{m^2 r_0^4 \Omega^4} \frac{\Omega}{2}} \quad (43)$$

$$f_{rad} = \frac{\omega_r}{2\pi} = \sqrt{\frac{2\kappa_r^2 Q^2 U_{RF}^2}{m^2 r_0^4 \Omega^4} \frac{\Omega}{4\pi}} \quad (44)$$

I would also like to highlight that, upon examining the error calculations for longitudinal frequency in section 6.3.2 and radial frequency in section 6.4.2, the percentage error in the radial direction is larger. This discrepancy in the margin of error may be attributed to the difference in  $\kappa_r$  values, with Alex Gingell using  $\kappa_r = 1$  while my  $\kappa_r$  value differs.

## 7 An alternative design for linear Paul trap

To trap Ca<sup>+</sup> ions, I used an alternative design to the three-section linear Paul trap shown in Figure 1. In this design, I demonstrated that Ca<sup>+</sup> ions can be trapped for some specific  $U_{DC}$  and  $U_{RF}$  voltage values by plotting position-dependent effective potential graphs. I also calculated the longitudinal frequency, radial frequency and  $\kappa$ . The main purpose of this trap is to use it as a starting point for a new trap that will ensure that both positive and negative ions are captured in separate potential wells.

### 7.1 Designing the ion trap model in SolidWorks

This design comprises four cylindrical rods arranged in a parallel configuration forming a rectangular shape. By applying time-dependent  $U_{RF}(t)$  voltage to the rods, ions are trapped in the radial direction. In the middle of these cylindrical rods, there are opposite two hollow cylinder. The function of these cylinders is to ensure the trapping of the ion in the axial direction by applying constant  $U_{DC}$  voltage.

The specific components can be found in appendix A.1. Figure 24 shows a sketch of the trap and Figure 25 shows the SolidWorks model. Additionally, the construction of each component followed the dimensional specifications outlined in table 4.

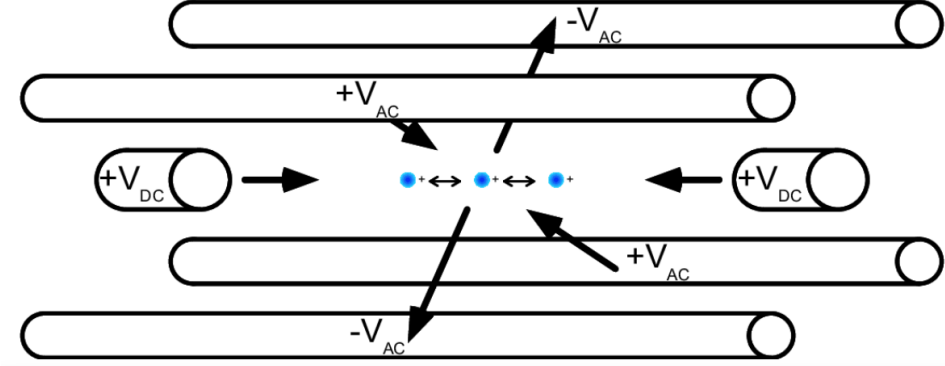


Figure 24: Linear Paul trap design. The figure also presents the voltage configuration required for ion trapping. This figure is taken from Ref. [7]

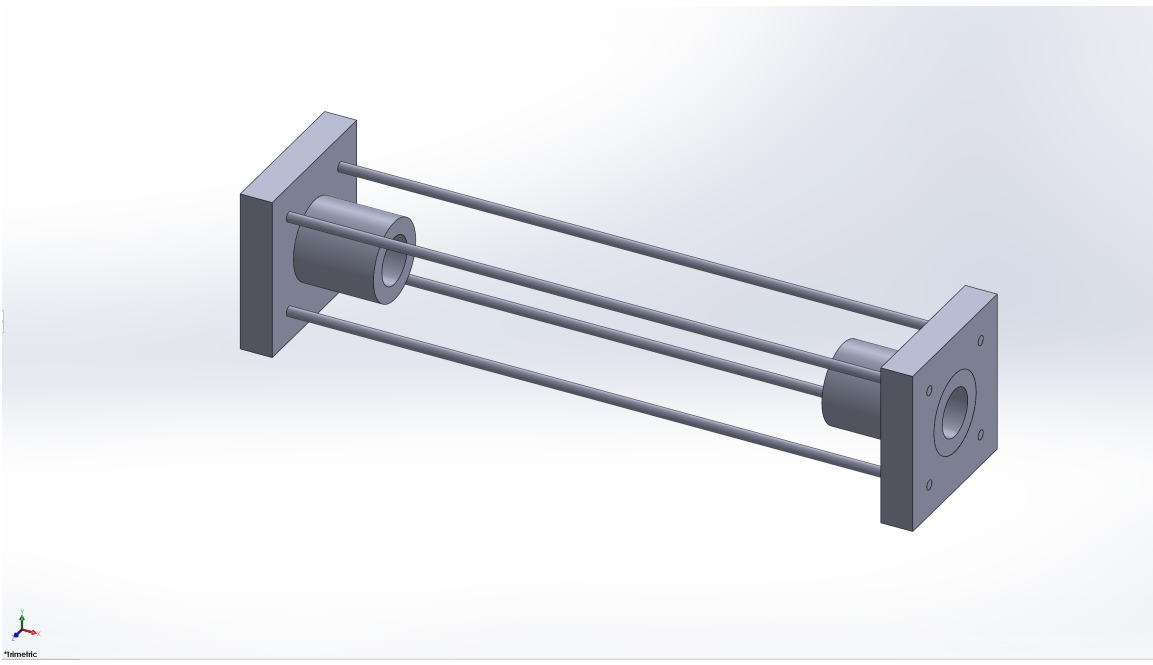


Figure 25: The linear Paul trap, which was constructed using SolidWorks. (This design was inspired by the linear paul trap design of Sam White, a doctoral student at the University of Innsbruck). The design parameters and dimensions for this replica are specified in table 4.

|                                       |                        |          |
|---------------------------------------|------------------------|----------|
| RF electrode length                   | $L_{RF}$               | 21.00 mm |
| DC electrode length                   | $L_{DC}$               | 3.50 mm  |
| RF Electrode radius                   | $r_{RF}$               | 0.15 mm  |
| DC Electrode inner radius             | $r_{DC, \text{inner}}$ | 0.75 mm  |
| DC Electrode outer radius             | $r_{DC, \text{outer}}$ | 1.25 mm  |
| Diagonal electrode surface separation | $2r_0$                 | 4.00 mm  |
| End-cap separation                    | $2z_0$                 | 14.00 mm |

Table 4: Necessary parameters for constructing the linear Paul trap.

## 7.2 Difficulties

### 7.2.1 Grid cell size

One of the critical factors impacting the accuracy of potential and electric field values is the grid cell size, or grid unit size, in the potential array. This parameter defines the dimensions of the elements that constitute the electrode surfaces and is typically set to a default value of 1 mm per grid unit. Essentially, it can be seen as the number of "grid points" that compose the electrodes. A higher number of grid points results in smoother representations of curved surfaces, while a lower grid size corresponds to a higher resolution of the electrodes and a more refined depiction of the resulting fields. The smaller the size of the electrodes imported into SIMION, the lower the resolution of the electrodes in SIMION. Therefore, since I chose the radius of the RF electrodes to be a small size of 0.15 mm, I chose the grid cell size 0.05 for higher resolution results.

### 7.2.2 Importing Solidworks design into SIMION

To import a SolidWorks design into SIMION, it is necessary to first convert the SolidWorks parts into STL files. For detailed guidance on this process, you can refer to Beke's thesis[2]. The main point I want to emphasize is a potential issue you may encounter during the STL conversion. If two parts of your design intersect in a specific area, the STL file may not accurately represent the intersection, causing parts of your design to lose detail or resolution in that region. This issue is particularly problematic in designs where electrodes intersect with holders. I used the following way to solve this problem. After completing my design, I deleted the holders from my design and converted only the electrodes into STL files. However, if you prefer not to delete the holders, you can use the location dimension feature on your holders to resolve this issue.

In SolidWorks, the Location Dimension tool is crucial for defining the precise location of sketch elements relative to reference points or other geometry. A key aspect of this tool is its ability to incorporate tolerance settings, which allow for slight variations in manufacturing while ensuring that parts align and function correctly. By applying tolerance to your holder, you significantly improve the overall reliability and quality of the assembly. The figure below illustrates the Location Dimension feature applied to the holder used in the linear Paul trap design.

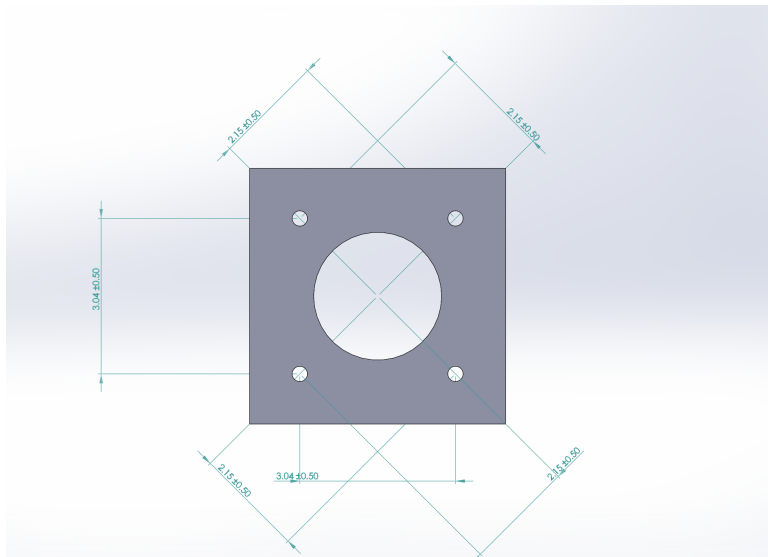


Figure 26: The Location Dimension feature applied to the holder used in the linear Paul trap design.

### 7.3 Calculation of $V^*(R)$

To calculate  $V^*(R)$  I used the method in the Section 3.2. Initially, I applied only the constant DC voltage to some of the electrodes for the potential data. The specific voltages applied to the electrodes are detailed below:

- Electrode01:  $U_{DC}$
- Electrode02:  $U_{DC}$
- Electrode03: 0
- Electrode04: 0
- Electrode05: 0
- Electrode06: 0

Secondly, I applied  $U_{RF_{max}}$  to the electrodes for the electric field data. The specific voltages applied to the electrodes are detailed below:

- Electrode01: 0
- Electrode02: 0
- Electrode03:  $U_{RF_{max}}$
- Electrode04:  $U_{RF_{max}}$
- Electrode05:  $-U_{RF_{max}}$
- Electrode06:  $-U_{RF_{max}}$

In Figure 27, you can also see the more detailed numbering of the electrodes.

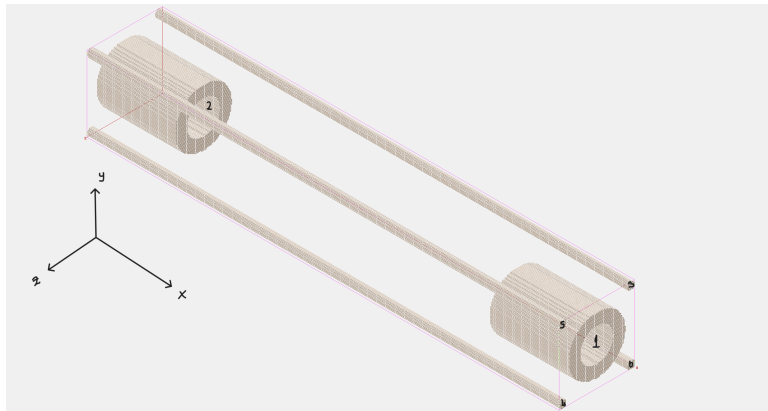


Figure 27: Detailed numbering of the electrodes in the linear Paul trap design.

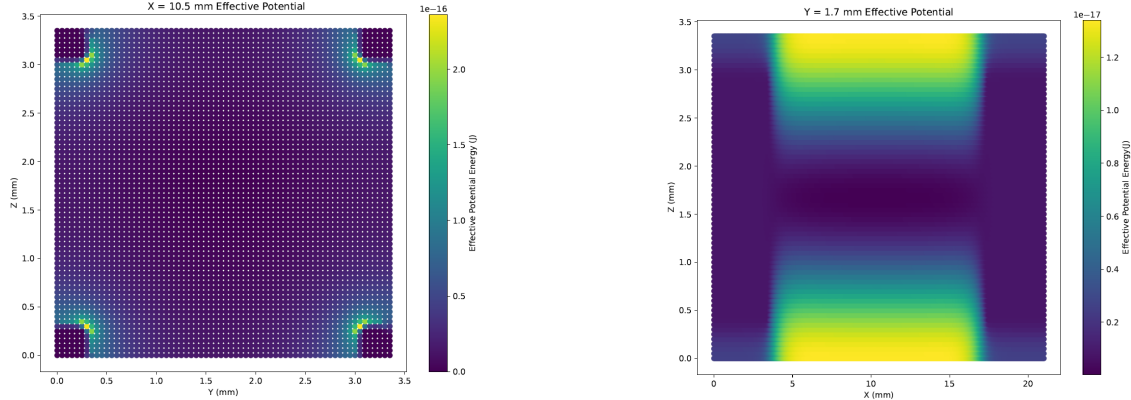
Then, I calculated the effective potential energy  $V^*(R)$  by using Equation (4), and you can find the values of the parameters I used in Equation (4) in the table below.

|                        |                                      |
|------------------------|--------------------------------------|
| $U_{\text{DC}}$        | 5.00 V                               |
| $U_{\text{RF}_{\max}}$ | 600.00 V                             |
| $\Omega$               | 24190263.43 1/s                      |
| $m$                    | $40 \times 1.66 \times 10^{-27}$ kg  |
| $q$                    | $-e = 1.602176634 \times 10^{-19}$ C |

Table 5: Values of the parameters used in Equation (4).

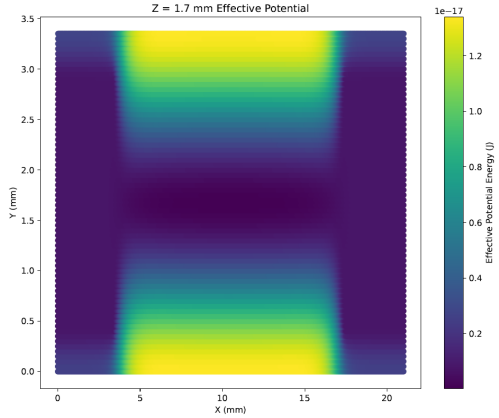
## 7.4 Result graphs

Firstly, I plotted the graph of the position and effective potential energy ( $V^*(R)$ ).



(a) Graph of position and  $(V^*(R))$  with  $x$  held constant at  $\max(x/2)$ .

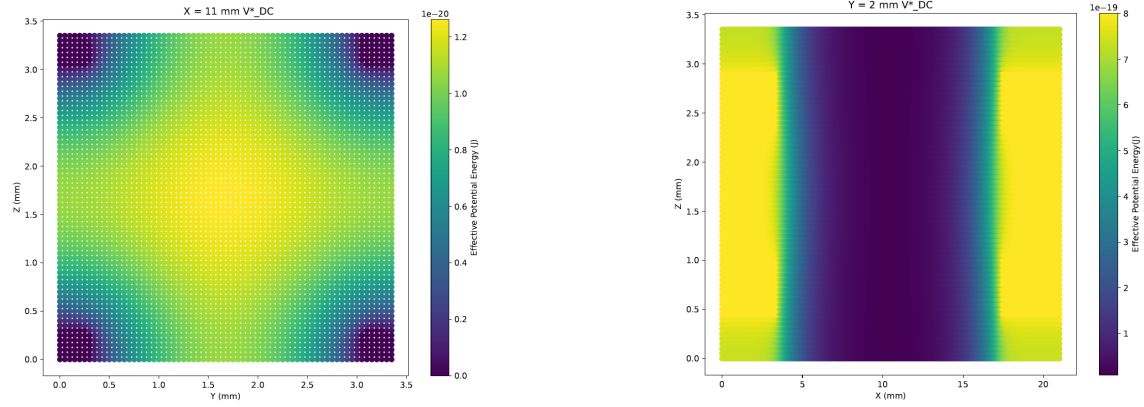
(b) Graph of position and  $(V^*(R))$  with  $y$  held constant at  $\max(y/2)$ .



(c) Graph of position and  $(V^*(R))$  with  $z$  held constant at  $\max(z/2)$ .

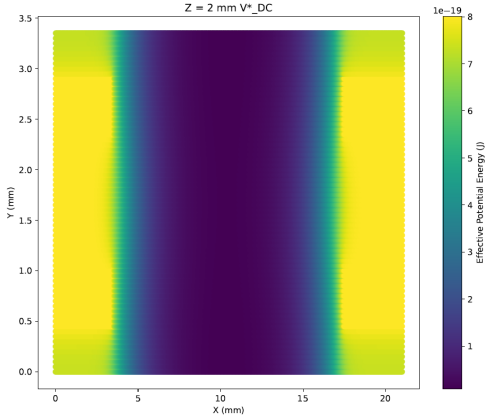
Figure 28: Graph of position and effective potential energy ( $V^*(R)$ ).

I also plotted the graphs of  $V_{\text{RF}}^*$  and  $V_{\text{DC}}^*$  in order to make a more detailed analysis of the effective potential energy.



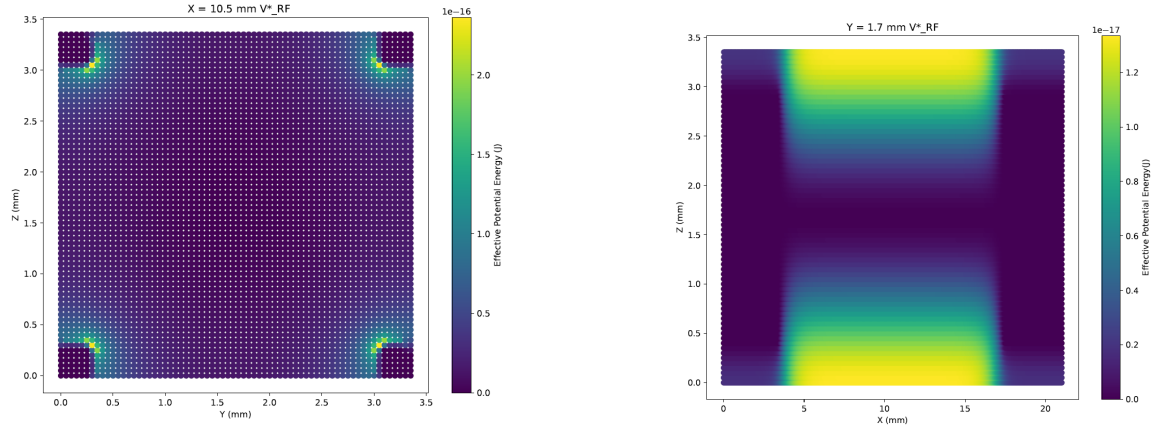
(a) Graph of position and  $V_{\text{DC}}^*$  with  $x$  held constant at  $\max(x/2)$ .

(b) Graph of position and  $V_{\text{DC}}^*$  with  $y$  held constant at  $\max(y/2)$ .



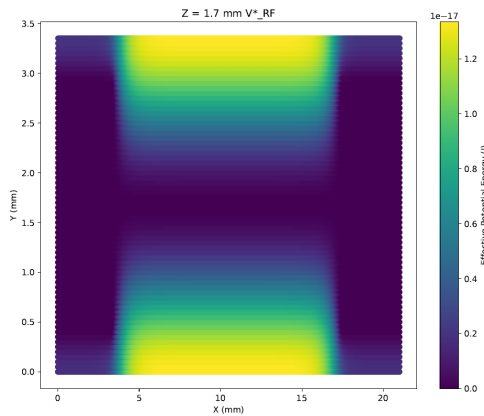
(c) Graph of position and  $V_{\text{DC}}^*$  with  $z$  held constant at  $\max(z/2)$ .

Figure 29: Graph of position and  $V_{\text{DC}}^*$ .



(a) Graph of position and  $V_{\text{RF}}^*$  with  $x$  held constant at  $\max(x/2)$ .

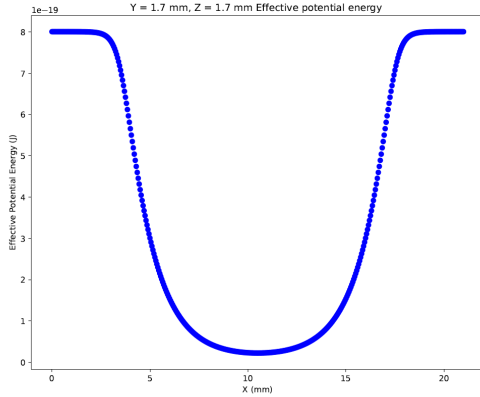
(b) Graph of position and  $V_{\text{RF}}^*$  with  $y$  held constant at  $\max(y/2)$ .



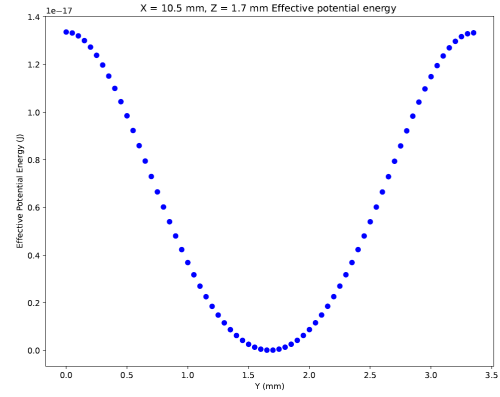
(c) Graph of position and  $V_{\text{RF}}^*$  with  $z$  held constant at  $\max(z/2)$ .

Figure 30: Graph of position and  $V_{\text{RF}}^*$ .

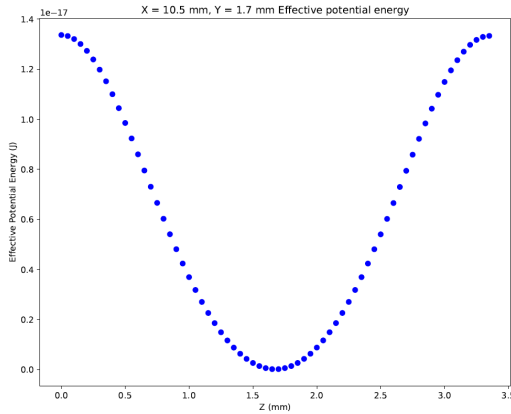
To make a better inference about the graph of position and effective potential energy, I plotted 2D graphs of  $V^*(R)$ ,  $V_{RF}^*$ , and  $V_{DC}^*$  by keeping two position variables constant.



(a) Graph of position and effective potential energy ( $V^*(R)$ ) with  $y$  and  $z$  held constant at  $\max(y/2)$  and  $\max(z/2)$ .



(b) Graph of position and effective potential energy ( $V^*(R)$ ) with  $x$  and  $z$  held constant at  $\max(x/2)$  and  $\max(z/2)$ .



(c) Graph of position and effective potential energy ( $V^*(R)$ ) with  $x$  and  $y$  held constant at  $\max(x/2)$  and  $\max(y/2)$ .

Figure 31: Graph of position and effective potential energy ( $V^*(R)$ ) with 2 constant variables.

As shown in Figures 31 (a), (b), and (c), our ions can be effectively trapped at the midpoints where the potential energy reaches its minimum. This outcome was anticipated, and the graphs align well with our expectations.

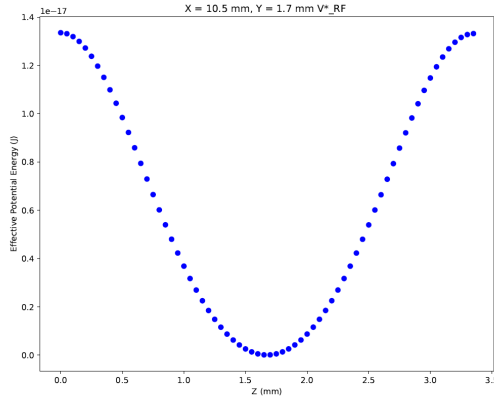
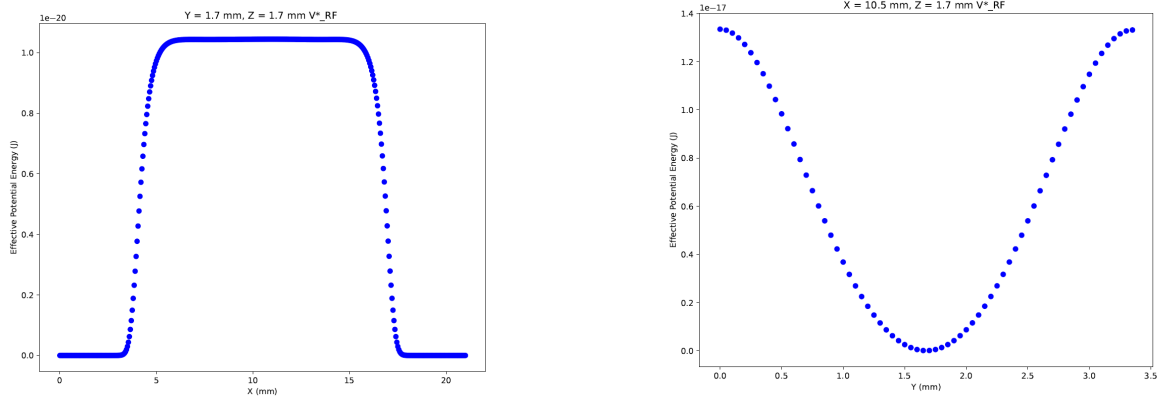
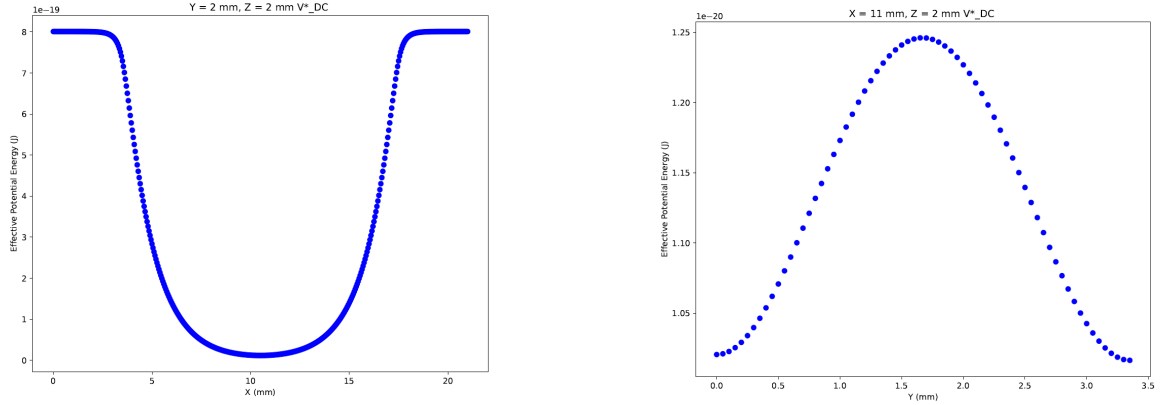
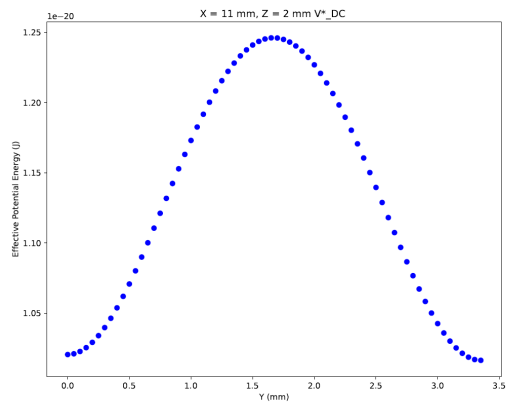


Figure 32: Graph of position and  $V_{\text{RF}}^*$  with 2 constant variables.

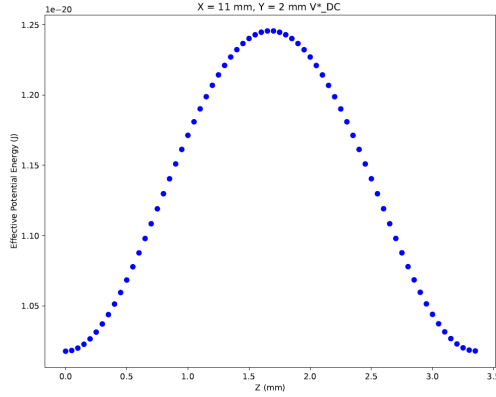
Figures 32(b) and 32(c) demonstrate that the restriction in the radial direction ( $y$  and  $z$  axes) originates from the  $V_{\text{RF}}^*$  component. This outcome was anticipated, and the graphs correspond well with the predicted results.



(a) Graph of position and  $V_{\text{DC}}^*$  with  $y$  and  $z$  held constant at  $\max(y/2)$  and  $\max(z/2)$ .



(b) Graph of position and  $V_{\text{DC}}^*$  with  $x$  and  $z$  held constant at  $\max(x/2)$  and  $\max(z/2)$ .



(c) Graph of position and  $V_{\text{DC}}^*$  with  $x$  and  $y$  held constant at  $\max(x/2)$  and  $\max(y/2)$ .

Figure 33: Graph of position and  $V_{\text{DC}}^*$  with 2 constant variables.

In Figure 33(a), it is evident that the axial direction ( $x$ ) is constrained by the  $V_{\text{DC}}^*$  component, a result that aligns with our expectations and is clearly illustrated in the chart.

Then, I calculated trap depths by using Python.

$$V_{\text{max,axial}} - V_{\text{min,axial}} = 8.01 \text{E-19 J}$$

$$V_{\text{max,radial}} - V_{\text{min,radial}} = 1.38 \text{E-17 J}$$

$$V_{\max} - V_{\min} \approx k_B T \quad (45)$$

To obtain an approximate value for temperature, we used the equation (45). As a result, our temperature came out to be in the axial direction 58043.47 K and in the radial direction 999500.249 K. A temperature value exceeding kilokelvin was anticipated, and our result confirmed this expectation. Additionally, when examining the effective potential energy graphs in Figure 33, we observe that the ions can be trapped in the region located in the middle, between the maximum and minimum points. This indicates that the results are highly likely to be accurate.

## 7.5 Calculation of longitudinal and radial frequency

For this design, the information and equations given in Section 8 will be used to calculate longitudinal and radial frequencies. However, when using the equations, it should never be forgotten that the axial direction in our design is  $x$  and the radial directions are  $y$  and  $z$ . (In Section 8, the axial direction is  $z$  and the radial directions are  $x$  and  $y$ .) Additionally, the values used in calculating the frequencies are given in the table below.

|                |                                     |
|----------------|-------------------------------------|
| $Q$            | $1.602176634 \times 10^{-19}$ C     |
| $m$            | $40 \times 1.66 \times 10^{-27}$ kg |
| $\Omega$       | $24190263.43$ 1/s                   |
| $2r_0$         | 4.0 mm                              |
| $2z_0$         | 14.0 mm                             |
| $U_{DC}$       | 5 V                                 |
| $U_{RF_{max}}$ | 600 V                               |

Table 6: Parameters for calculation frequencies.

As can be seen, there is no  $\kappa$  value in table 6. Therefore, I could not calculate the longitudinal frequency analytically, but I calculated it numerically. I also tried to find an approximate value for  $\kappa$  from our numerical calculations.

### 7.5.1 Calculation of longitudinal frequency numerically

While determining the longitudinal and radial frequencies in Sections 6.3.2 and 6.4.2, I selected a nonlinear fit range and performed my numerical calculations within that range. Since changing the range had minimal impact on the results, I chose an average range centered around the middle point for my calculations. However, as shown in Figure 35, for this linear Paul trap design, the second-order derivative of my effective potential energy graph in the axial direction varies significantly depending on the range selected around the minimum. For this reason, before choosing my nonlinear fit range, I plotted a graph showing the quality of the fit ( $R^2$ ) according to the nonlinear fit range I would choose. The quality of fit describes how well the model's predictions match the observed data, often evaluated by metric as  $R^2$ .

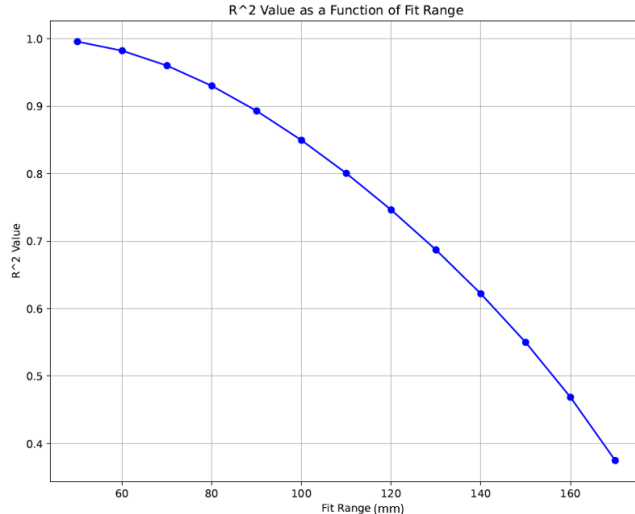


Figure 34:  $R^2$  value as a function of fit range.

The coefficient of determination,  $R^2$ , ranges from 0 to 1, with a value of 1 indicating a perfect fit. However, to ensure that the fit range is not too narrow while maintaining  $R^2$  close to 1, I selected a nonlinear fit range between  $x = 0.007$  and  $x = 0.014$  m. This choice balances achieving a high  $R^2$  value with ensuring the fit range is sufficiently broad.

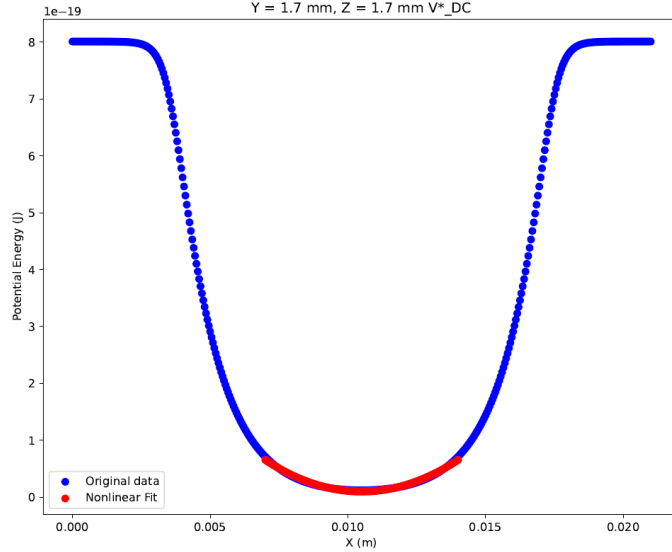


Figure 35: The  $V_{\text{DC}}^*$  versus  $x$  graph of the original data alongside the second-degree nonlinear fit applied to the  $x$ -dependent  $V_{\text{DC}}^*$  graph. The nonlinear fit was performed over an  $x$ -range of 0.007 to 0.014 m. ( $R^2 = 0.9870$ )

Then I calculated the axial frequency ( $f_{\text{axial}}$ ) numerically using equation 28. As a result of this calculation, I found the axial frequency to be 58817.720 (1/s).

### 7.5.2 Calculation of $\kappa$ with numerical methods

To calculate  $\kappa$ , I performed the linear fit using the coefficient  $a$  obtained from the nonlinear fit and the variable  $U_{DC}$ , following the same method described in Section 6.3.3. Additionally, for the reasons outlined in Section 7.5.1, I chose the nonlinear fit range as  $x = 0.007$  m to  $x = 0.014$  m for the calculation of  $\kappa$ .

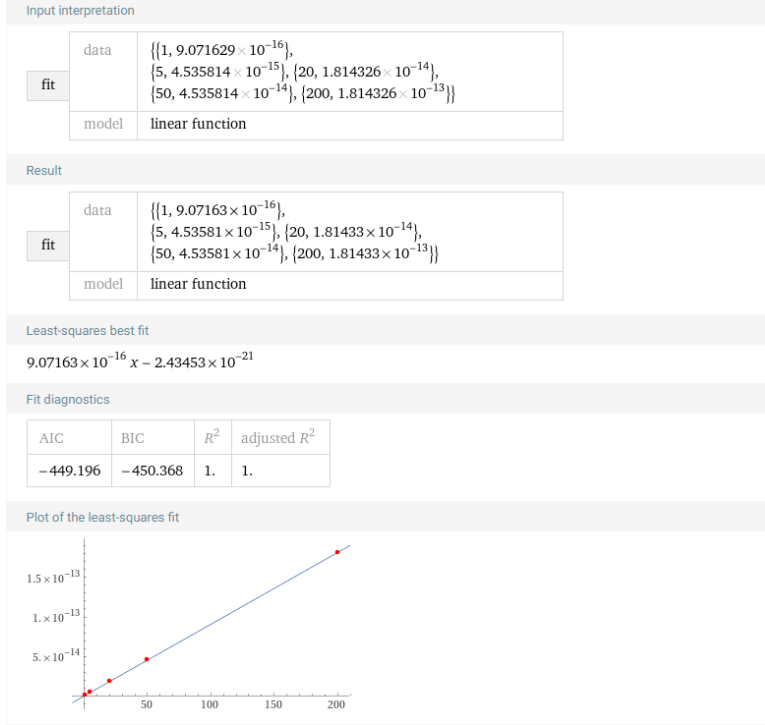


Figure 36: Linear fit using  $U_{DC}$  ( $x$ -axis) and  $a$  coefficient ( $y$ -axis) values (graph plotted with WolframAlpha).

The slope coefficient in the linear fit was calculated by Wolfram Alpha as  $9.07163 \times 10^{-16}$ . (This coefficient is the coefficient of the  $x$  term shown in the Least-Squares Best Fit section of Figure 36.) It was named  $C$  as in Section 6.3.3, and  $\kappa$  was calculated as 0.277 using Equation 32.

## 7.6 Calculation of radial frequency

### 7.6.1 Calculation of radial frequency analytically

As mentioned in Section 6.4, we chose  $U_{DC}$  at the limit of 0 to ensure that the radial frequency calculated numerically using the pseudopotential approach matches the radial frequency calculated analytically. For the analytical calculation of the radial frequency ( $f_{rad}$ ), I used Equation 37 and the values from Table 6. As a result of this calculation, I found the radial frequency to be 3366194.69 (1/s) .

### 7.6.2 Calculation of radial frequency numerically

I plotted the  $y$ -dependent graph of  $V_{RF}^*$  for table 5 values and found the coefficient b by doing a nonlinear fit on this graph. (Details on this are in section 6.4.2.) Then I calculated the radial frequency ( $f_{rad}$ ) numerically using equation 41. As a result of this calculation, I found the radial frequency to be 2478852.528 (1/s).

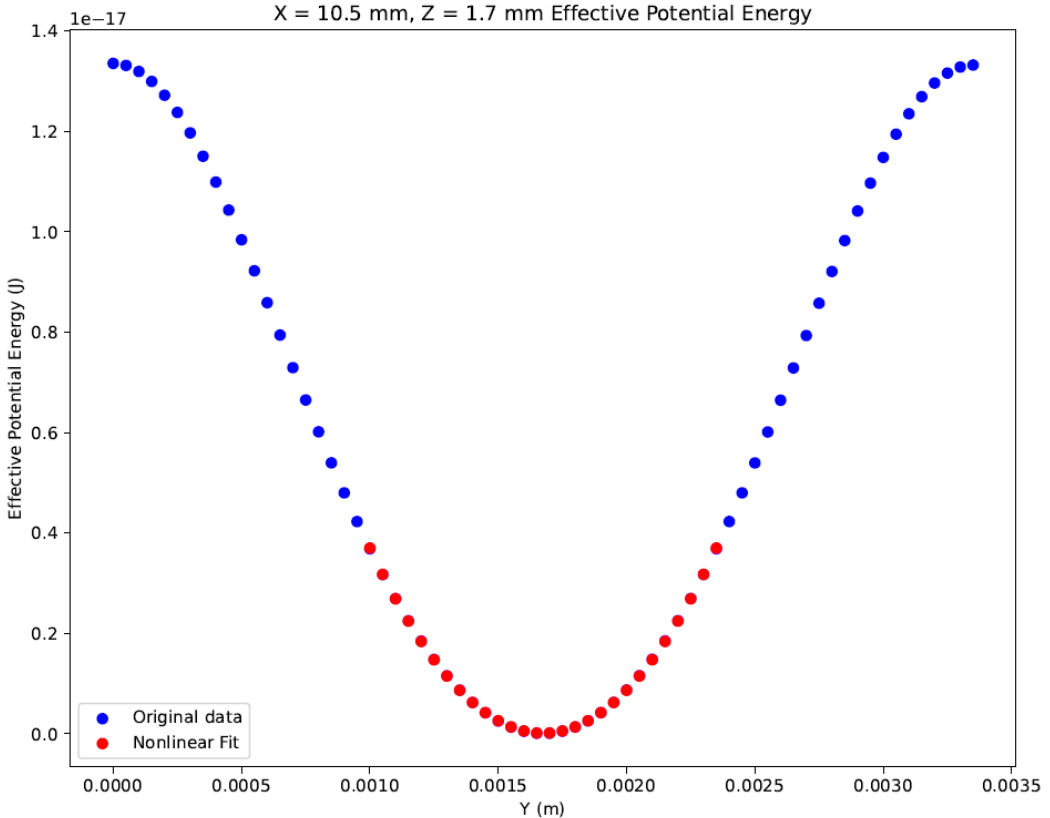


Figure 37: The  $V_{RF}^*$  versus  $y$  graph of the original data alongside the second-degree nonlinear fit applied to the  $V_{RF}^*$ -dependent  $y$  graph. The nonlinear fit was performed over an  $y$ -range of 0.00100 to 0.00235 m.

Finally, I used Equation 29 to compare my numerical and analytical results, finding a percent error of 26.36. As a result, my analytical and numerical values are not very close to each other. The reason for this deviation may be the  $\kappa_r$  I mentioned in Section 6.4.3, or it may indicate the need for different analytical calculations for this design.

## 8 A trap design for trapping both positive and negative ions simultaneously

In her thesis[2], Beke demonstrated that both positive and negative ions could be trapped simultaneously using a three-segmented linear Paul trap by employing a non-standard voltage configuration. However, in the three segmented linear Paul trap, the positive and negative ions were confined to the same region within the trap. The goal of the trap design described in this section is to improve upon this by trapping positive and negative ions in distinct, separate regions. Figure 38 illustrates the ion trapping of positive and negative ions using a three-segmented linear Paul trap, while Figure 39 shows the trapping of positive and negative ions using the trap design presented in this section. These figures are schematic presentations with no numeric data.

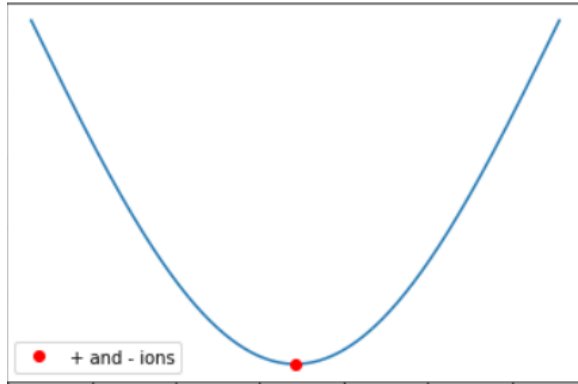


Figure 38: Ion trapping of positive and negative ions using the three segmented linear Paul trap.

**x-axis : Position in axial direction**  
**y-axis : Effective Potential Energy**

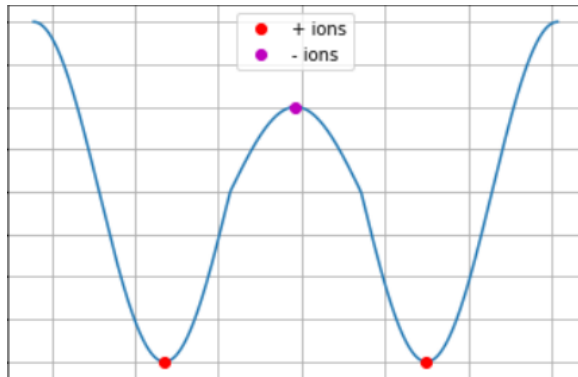


Figure 39: Ion trapping of positive and negative ions using the design presented in this section.

**x-axis : Position in axial direction**  
**y-axis : Effective Potential Energy**

To trap both positive and negative ions simultaneously, I designed a trap in SolidWorks, aiming to confine them in separate but closely located regions. The reason for trapping ions in this way is to examine the behavior of positive ions and negative ions in separate regions using the sympathetic cooling method. Sympathetic cooling is a method where one species of ions is directly cooled (e.g., using lasers), and through their interactions, they indirectly cool another species of ions that cannot be directly cooled. This process works by coupling the external degrees of freedom of both positive and negative ions through the Coulomb forces they exert on

each other, thus allowing them to exchange energy[11]. In other words, since couloumb forces are effective in the sympathetic cooling method, the distance between the ions should not be large and this design was designed according to this requirement.

I demonstrated that both positive and negative ions can be trapped for some specific  $U_{DC}$  and  $U_{RF}$  voltage values by plotting position-dependent effective potential energy graphs, showing that these ions are trapped in separate but closely located regions.

## 8.1 Designing the ion trap model in Solidworks

This design was created by making some modifications to the linear Paul trap shown in section 7.1. In the design, four cylindrical rods are used to apply the RF voltage for radial trapping, similar to the design described in Section 7.1. However, unlike the linear Paul trap design, five washers are used instead of two opposing hollow cylinders to apply DC voltage for axial trapping. In this design, one washer is placed at the center of the trap ( $x = 5.0\text{mm}$ ) along the x-axis, while the other four washers are symmetrically positioned around it along the x-axis, with two on each side, spaced at equal intervals from the center washer. Refer to Figure 41 for a more detailed illustration of the washer placement. The reason why DC electrodes (washers) are preferred in this way is to trap both positive and negative ions in the axial direction at the midpoint and points close to the midpoint. The overall design concept was proposed by my supervisor, Professor Dulitz, and I subsequently determined several parameters independently, as detailed in Section 10.2.

The specific components are detailed in Appendix A.2. Figure 40 shows the SolidWorks model of the ion trap, while Figures 41 and 42 display the sketches in the XY and ZY planes, respectively. Each component was constructed according to the dimensional specifications provided in Table 7.

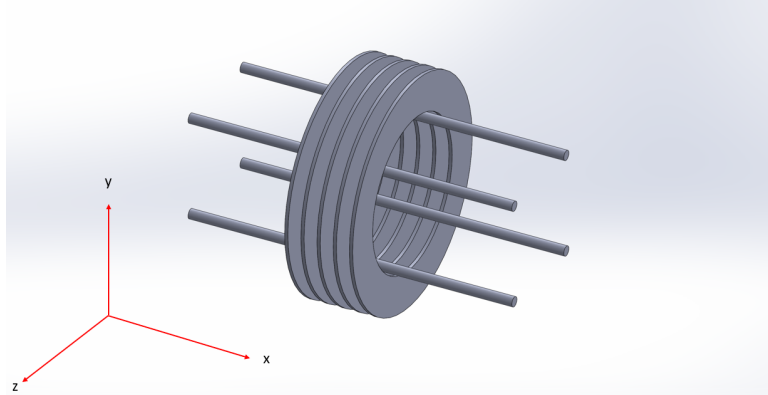


Figure 40: The linear Paul trap, which was constructed using SolidWorks. The design parameters are specified in table 7.

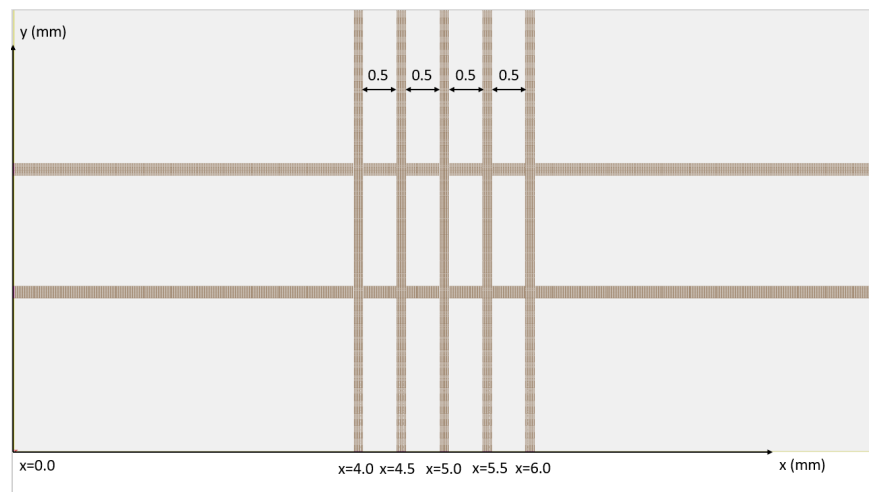


Figure 41: XY-Axis Sketch of the Ion Trap

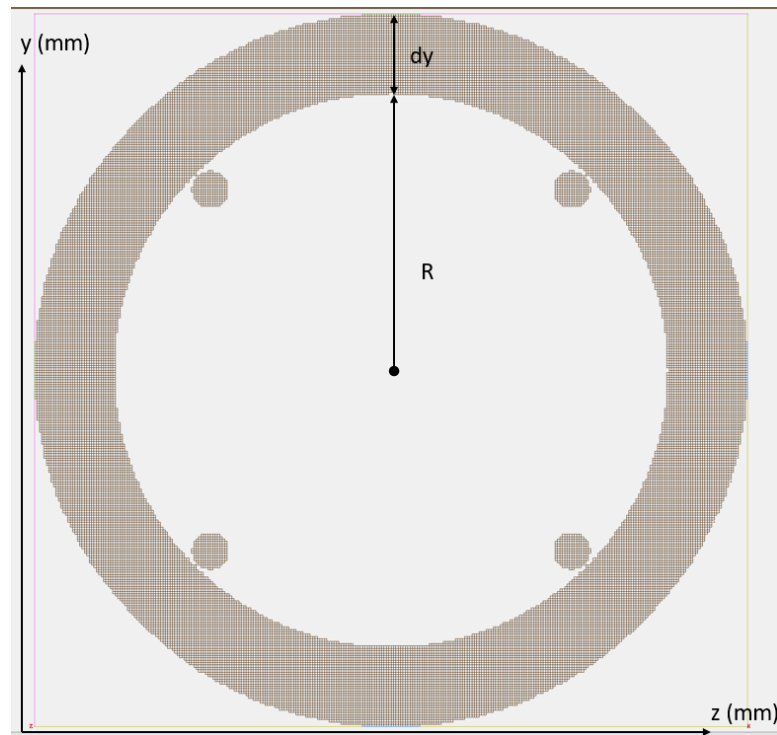


Figure 42: ZY-Axis Sketch of the Ion Trap

|   |                        |          |
|---|------------------------|----------|
| RF electrode length   | $L_{RF}$               | 10.00 mm |
| DC electrode (washer) length  | $L_{DC}$               | 0.10 mm  |
| RF Electrode radius   | $r_{RF}$               | 0.15 mm  |
| DC Electrode (washer) inner radius  | $r_{DC, \text{inner}}$ | 2.33 mm  |
| DC Electrode (washer) outer radius  | $r_{DC, \text{outer}}$ | 3.00 mm  |
| Diagonal electrode surface separation                                     | $2r_0$                 | 4.00 mm  |
| Distance between two washers  | $dx$                   | 0.50 mm  |
| Distance between inner radius and outer radius of washer                  | $dy$                   | 0.67 mm  |
| Distance from the center to the inner radius of the washer on the ZY axis | $R$                    | 2.33 mm  |

Table 7: Necessary parameters for constructing the ion trap.

## 8.2 Determination of parameters used in the design of the ion trap

While determining the parameters in the design of the ion trap, position-dependent effective potential energy graphs were used. When determining the design parameters, the voltage configurations applied to the electrodes in SIMION for calculating effective potential energy and generating corresponding graphs are as follows:

Initially, I applied only a constant DC voltage to DC electrodes (washers) for potential datas. The specific voltages applied to the electrodes are detailed below:

- Electrode01: 0
- Electrode02: 0
- Electrode03: 0
- Electrode04: 0
- Electrode05:  $U_{DC}$
- Electrode06:  $-U_{DC}$
- Electrode07:  $U_{DC}$
- Electrode08:  $-U_{DC}$
- Electrode09:  $U_{DC}$

The DC voltage configuration applied to the washers shown above made it possible to trap both positive and negative ions in the axial direction at different points.

Secondly, I applied  $U_{RF_{max}}$  to the RF electrodes for electric field datas. The specific voltages applied to the electrodes are detailed below :

- Electrode01:  $-U_{RF_{max}}$
- Electrode02:  $U_{RF_{max}}$
- Electrode03:  $U_{RF_{max}}$
- Electrode04:  $-U_{RF_{max}}$
- Electrode05: 0
- Electrode06: 0
- Electrode07: 0
- Electrode08: 0
- Electrode09: 0

In Figure 67, you can also see the more detailed numbering of the electrodes. For a clearer explanation of why separate voltages are applied for DC voltage and  $U_{RF_{max}}$  voltage, as well as for the  $V^*(R)$  calculations, refer to Section 3.2.

While changing various parameters in the design, the changes in the  $x$ -dependent  $V_{DC}^*$  graph for axial trapping were interpreted, and the changes in the  $y$ -dependent  $V_{RF}^*$  graph for radial trapping were interpreted. In the  $x$ -dependent graph of  $V_{DC}^*$ , the minimum is targeted at the center of the trap's  $x$ -axis, while the maximum is aimed at points near this central position for trapping both positive and negative ions. Additionally, in order to trap in both axial and radial directions, the parameters were determined so that the trap depth was large at the midpoint of both graphs.

### 8.2.1 RF electrode length ( $L_{RF}$ )

Modifying the RF electrode length parameter does not result in any noticeable changes in the effective potential energy graphs. However, to allow for the selection of a finer grid size, the RF electrode length was deliberately kept short, specifically set to 10 mm.

### 8.2.2 Distance between two washers ( $dx$ )

The distance between the two washers was intentionally selected to be small to allow for a strong Coulomb interaction in between the positive and negative ions. However, when the distance was reduced too much, distortions appeared in the  $V_{DC}^*$  graph, preventing both positive and negative ions from being axial trapped effectively. This problem is shown in Figure 4. Therefore the distance between the washers was chosen as 0.50 mm in order to both apply the sympathetic cooling method and maintain the trap depth in the axial direction.

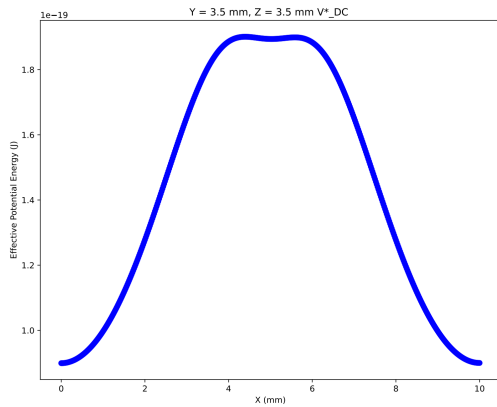


Figure 43:  $V_{DC}^*$  graph along the  $x$ -axis for  $R = 2.33$  mm,  $dy = 1.17$  mm,  $dx = 0.25$  mm.

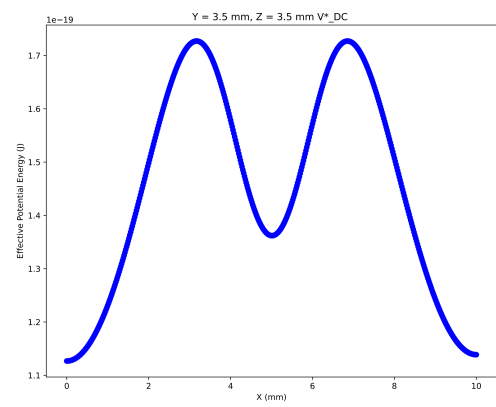


Figure 44:  $V_{DC}^*$  graph along the  $x$ -axis for  $R = 2.33$  mm,  $dy = 1.17$  mm,  $dx = 0.50$  mm.

### 8.2.3 Distance between inner radius and outer radius of washer ( $dy$ )

This parameter can be observed in Figure 3. All parameters except  $dy$  were kept constant and the effect on the effective potential energy graphs was examined by changing the  $dy$  parameter. The graphs below show the effect of changing the  $dy$  parameter on the  $V_{DC}^*$  and  $V_{RF}^*$  graphs.

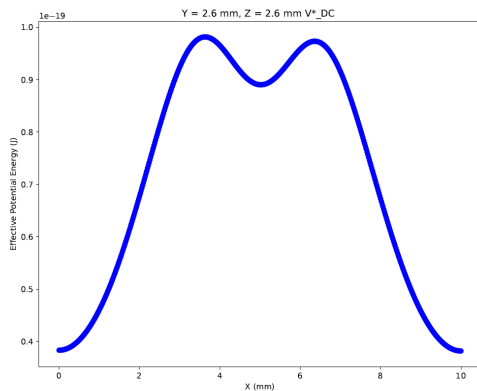


Figure 45:  $V_{DC}^*$  graph along the  $x$ -axis for  $R = 2.5$  mm,  $dy = 0.1$  mm,  $dx = 0.5$  mm.

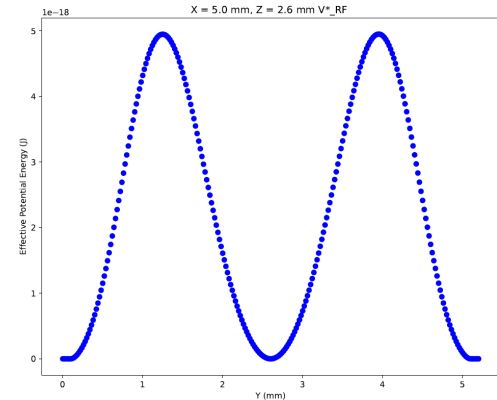


Figure 48:  $V_{RF}^*$  graph along the  $y$ -axis for  $R = 2.5$  mm,  $dy = 0.1$  mm,  $dx = 0.5$  mm.

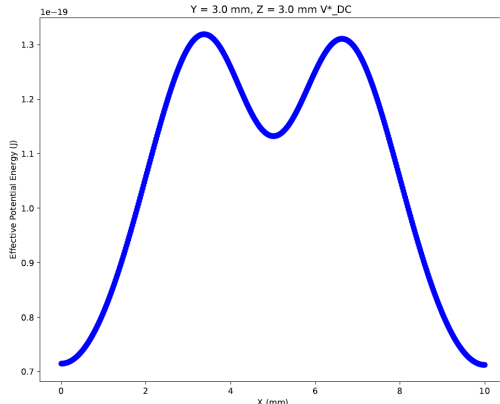


Figure 46:  $V_{DC}^*$  graph along the  $x$ -axis for  $R = 2.5$  mm,  $dy = 0.5$  mm,  $dx = 0.5$  mm.

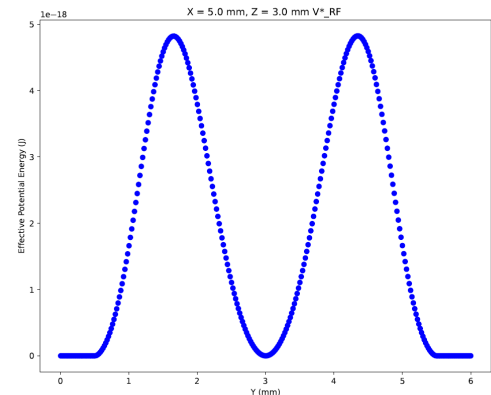


Figure 49:  $V_{RF}^*$  graph along the  $y$ -axis for  $R = 2.5$  mm,  $dy = 0.5$  mm,  $dx = 0.5$  mm.

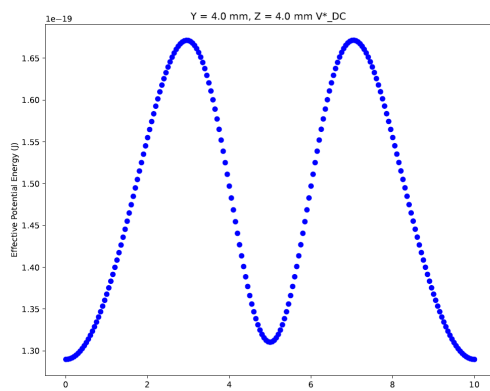


Figure 47:  $V_{DC}^*$  graph along the  $x$ -axis for  $R = 2.5$  mm,  $dy = 1.5$  mm,  $dx = 0.5$  mm.

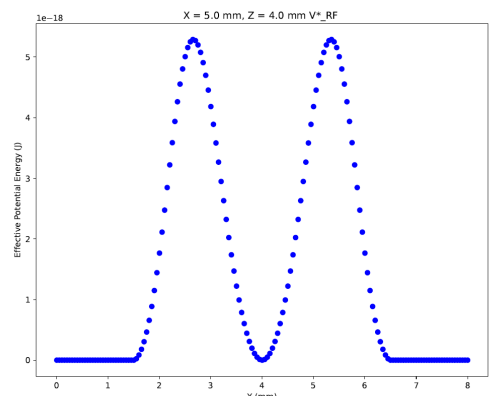


Figure 50:  $V_{RF}^*$  graph along the  $y$ -axis for  $R = 2.5$  mm,  $dy = 1.5$  mm,  $dx = 0.5$  mm.

As a result of the above graphs, it can be seen that as the  $dy$  value increases, both the trapping depth in the axial direction and the trapping depth in the radial direction increase.

#### 8.2.4 Distance from the center of the trap to the inner radius of the washer on the ZY axis ( $R$ )

This parameter can be observed in Figure 3. It also corresponds to the inner radius of the washer. The reason why this parameter affects the effective potential energy is the relationship between the washer and RF electrodes. When the washer and electrodes are further away from each other, their effects on each other decrease. All parameters except  $R$  were kept constant and the effect on the effective potential energy graphs was examined by changing the  $R$  parameter. The graphs below show the effect of changing the  $R$  parameter on the  $V_{DC}^*$  and  $V_{RF}^*$  graphs.

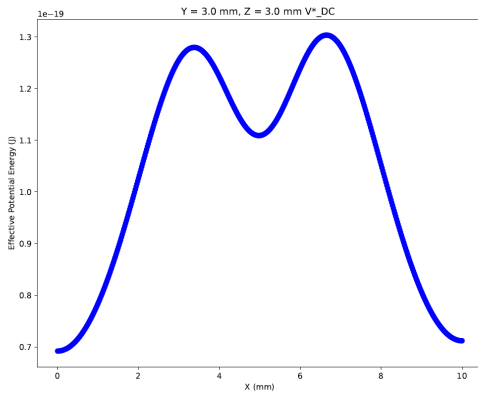


Figure 51:  $V_{DC}^*$  graph along the  $x$ -axis for  $R = 2.5$  mm,  $dy = 0.5$  mm,  $dx = 0.5$  mm.

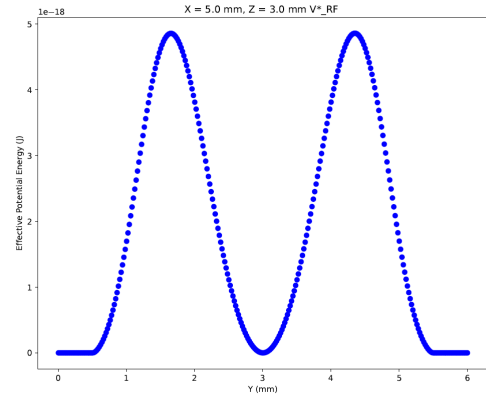


Figure 53:  $V_{RF}^*$  graph along the  $y$ -axis for  $R = 2.5$  mm,  $dy = 0.5$  mm,  $dx = 0.5$  mm.

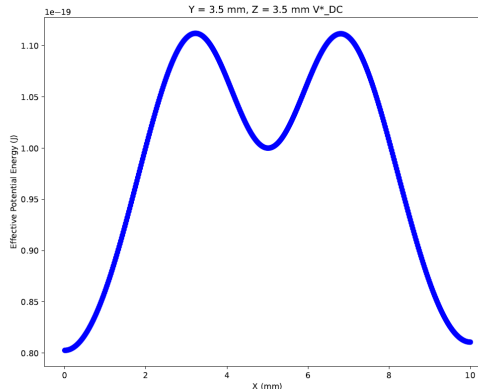


Figure 52:  $V_{DC}^*$  graph along the  $x$ -axis for  $R = 3.0$  mm,  $dy = 0.5$  mm,  $dx = 0.5$  mm.

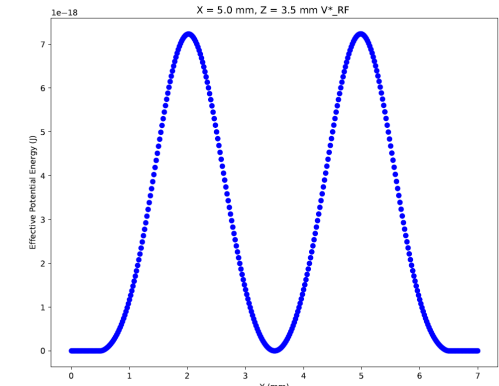


Figure 54:  $V_{RF}^*$  graph along the  $y$ -axis for  $R = 3.0$  mm,  $dy = 0.5$  mm,  $dx = 0.5$  mm.

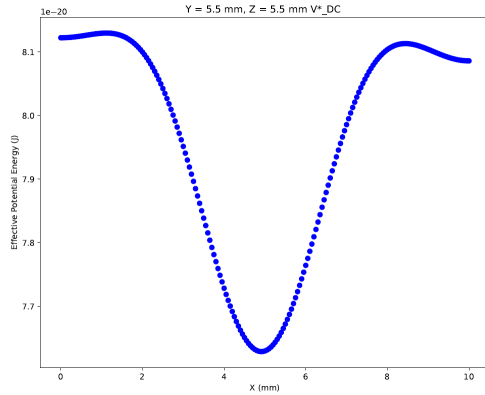


Figure 55:  $V^*_{\text{DC}}$  graph along the  $x$ -axis for  $R = 5.0$  mm,  $dy = 0.5$  mm,  $dx = 0.5$  mm.

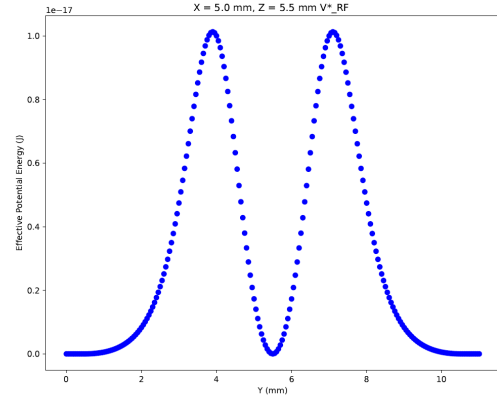


Figure 56:  $V^*_{\text{RF}}$  graph along the  $y$ -axis for  $R = 5.0$  mm,  $dy = 0.5$  mm,  $dx = 0.5$  mm.

As a result of the above graphs, it can be seen that as the  $R$  value increases, while the trapping depth in the axial direction decreases, the trapping depth in the radial direction increases.

### 8.2.5 Conclusion

Various configurations were tested by adjusting different parameters to achieve the optimal design for both axial and radial trap depths. As a result of these tests, the trap was optimized and designed to achieve large radial and axial trap depths in both the  $V_{RF}^*$  and  $V_{DC}^*$  graphs. The finalized parameters for the most suitable design are provided in Table 7. However, even with the most suitable trap design, several problems persisted: the positions where positive and negative ions were trapped were significantly distant from each other, and the axial trap depth in the  $V_{DC}^*$  graph for positive ions was not sufficiently large. To address these issues, the DC voltage configuration applied to the DC electrodes was adjusted.

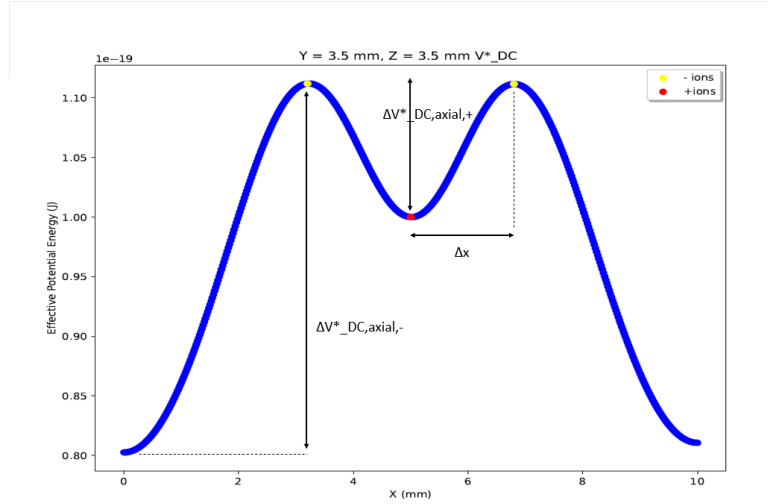


Figure 57:  $V_{DC}^*$  graph in the axial direction. The distance between the trap minima for positive and negative ions is shown as  $\Delta x$ . Additionally, for positive ions, the trap depth ( $\Delta V_{DC,axial,+}^*$ ) corresponds to the difference between two local maxima and the central local minimum, as shown in the graph. Similarly, for negative ions, the trap depth ( $\Delta V_{DC,axial,-}^*$ ) is defined as the difference between the local maxima near the center and the absolute minimum, which is also depicted in the graph.

The trap depth parameters for  $V_{DC}^*$  defined above are also defined in the other effective potential energy graphs below.

- $\Delta V_{DC,axial,+}^*$  : The axial trap depth in the  $V_{DC}^*$  graph for positive ions [J]
- $\Delta V_{RF,radial,+}^*$  : The radial trap depth in the  $V_{RF}^*$  graph for positive ions [J]
- $\Delta E_{axial,+}$  : The axial trap depth in the  $V^*(R)$  graph for positive ions [J]
- $\Delta E_{radial,+}$  : The radial trap depth in the  $V^*(R)$  graph for positive ions [J]
- $\Delta V_{DC,axial,-}^*$  : The axial trap depth in the  $V_{DC}^*$  graph for negative ions [J]
- $\Delta V_{RF,radial,-}^*$  : The radial trap depth in the  $V_{RF}^*$  graph for negative ions [J]
- $\Delta E_{axial,-}$  : The axial trap depth in the  $V^*(R)$  graph for negative ions [J]
- $\Delta E_{radial,-}$  : The radial trap depth in the  $V^*(R)$  graph for negative ions [J]
- $\Delta x$  : Distance in between trap wells [mm]

### 8.3 Determination of the configuration of the DC voltage applied to the DC electrodes (washers)

As mentioned in Section 8.2.5, since our main problem is related to the  $V_{DC}^*$  graphs, the  $V_{DC}^*$  graphs were interpreted by changing the DC voltage configurations applied to the electrodes, and an effort was made to find the most appropriate DC voltage configuration. During this process, the ion trap designed according to the parameters listed in Table 7 and the  $U_{DC}$  voltage value in Table 5 were used.

#### 8.3.1 DC voltage applied to the central washer (Electrode07)

The figures below illustrate how the  $V_{DC}^*$  graph and various parameters change in response to the DC voltage applied to the center washer, while keeping the DC voltage on all other washers constant.

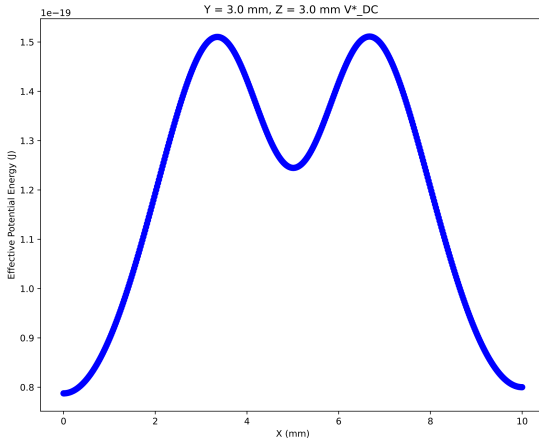


Figure 58: DC voltage values applied to washers: Electrode05:  $U_{DC}$ , Electrode06:  $-U_{DC}$ , Electrode07:  $U_{DC}$ , Electrode08:  $-U_{DC}$ , Electrode09:  $U_{DC}$ .  $\Delta V_{DC,\text{axial},+}^* = 0.311 \times 10^{-19} \text{ J}$ ,  $\Delta x = 1.68 \text{ mm}$ .

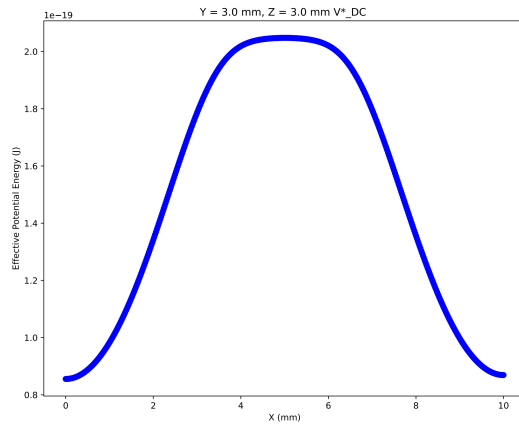


Figure 59: DC voltage values applied to washers: Electrode05:  $U_{DC}$ , Electrode06:  $-U_{DC}$ , Electrode07:  $2 \times U_{DC}$ , Electrode08:  $-U_{DC}$ , Electrode09:  $U_{DC}$ .

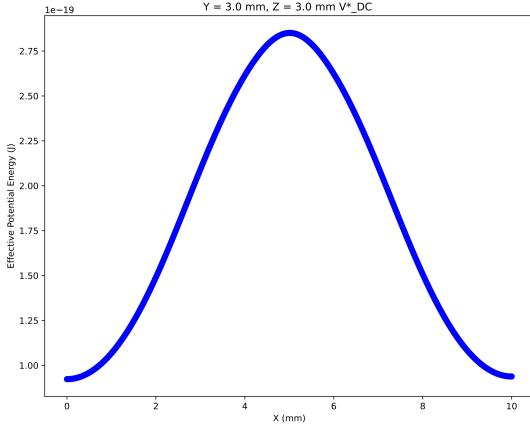


Figure 60: DC voltage values applied to washers: Electrode05:  $U_{DC}$ , Electrode06:  $-U_{DC}$ , Electrode07:  $3 \times U_{DC}$ , Electrode08:  $-U_{DC}$ , Electrode09:  $U_{DC}$ .

As observed from the figures above, as the DC voltage supplied to the central washer increases, the trap depth in the axial direction disappears and it is not possible to trap both positive and negative ions. For this reason, the central washer should be kept lower than other washers.

### 8.3.2 DC voltage applied to the washers between the end and central washers (Electrode06 and Electrode08)

The figures below illustrate how the  $V_{DC}^*$  graph and various parameters change in response to the DC voltage applied to the washers between the end and central washers, while keeping the DC voltage on all other washers constant.

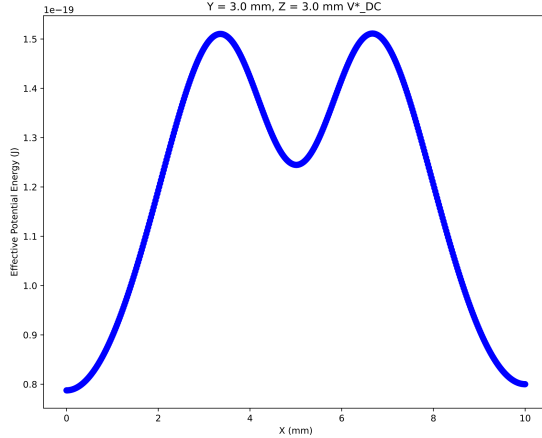


Figure 61: DC voltage values applied to washers: Electrode05:  $U_{DC}$ , Electrode06:  $-U_{DC}$ , Electrode07:  $U_{DC}$ , Electrode08:  $-U_{DC}$ , Electrode09:  $U_{DC}$ .  $\Delta V_{DC,\text{axial},+}^* = 0.311 \times 10^{-19} \text{ J}$ ,  $\Delta x = 1.68 \text{ mm}$ .

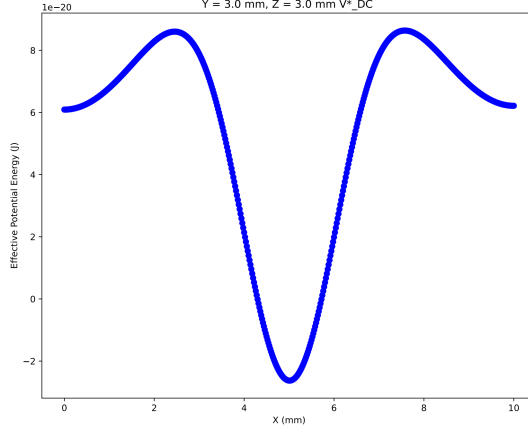


Figure 62: DC voltage values applied to washers: Electrode05:  $U_{DC}$ , Electrode06:  $-2 \times U_{DC}$ , Electrode07:  $U_{DC}$ , Electrode08:  $-2 \times U_{DC}$ , Electrode09:  $U_{DC}$ .  $\Delta V_{DC,\text{axial},+}^* = 1.125 \times 10^{-19} \text{ J}$ ,  $\Delta x = 2.58 \text{ mm}$ .

As observed from the figures above, when the DC voltage applied to the washers between the end and center washers is set to  $-2 \times U_{DC}$ , the axial trap depth increases. However, this also causes the points where positive and negative ions are trapped to move further apart.

### 8.3.3 DC voltage applied to the end washers (Electrode05 and Electrode09)

The figures below illustrate how the  $V_{DC}^*$  graph and various parameters change in response to the DC voltage applied to the end washers, while keeping the DC voltage on all other washers constant.

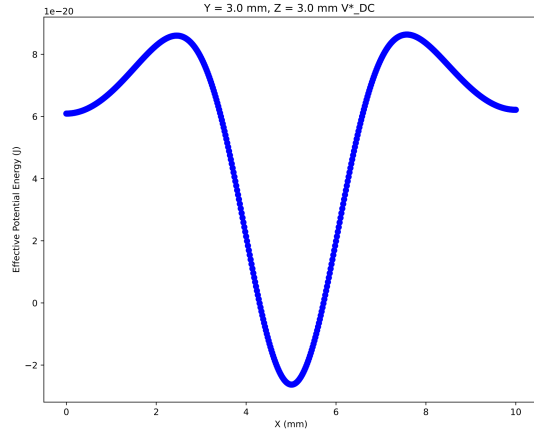


Figure 63: DC voltage values applied to washers: Electrode05:  $U_{DC}$ , Electrode06:  $-2 \times U_{DC}$ , Electrode07:  $U_{DC}$ , Electrode08:  $-2 \times U_{DC}$ , Electrode09:  $U_{DC}$ .  $\Delta V_{DC,axial,+}^* = 1.125 \times 10^{-19} \text{ J}$ ,  $\Delta x = 2.58 \text{ mm}$ .

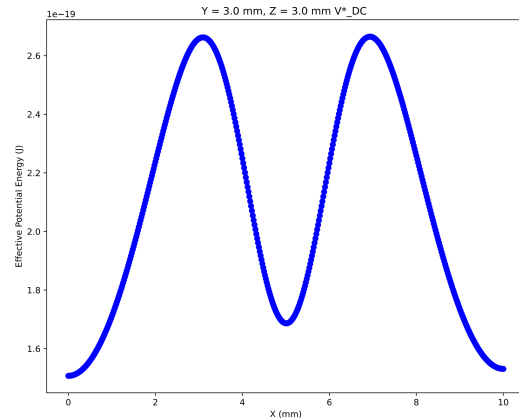


Figure 64: DC voltage values applied to washers: Electrode05:  $2 \times U_{DC}$ , Electrode06:  $-2 \times U_{DC}$ , Electrode07:  $U_{DC}$ , Electrode08:  $-2 \times U_{DC}$ , Electrode09:  $2 \times U_{DC}$ .  $\Delta V_{DC,axial,+}^* = 0.98 \times 10^{-19} \text{ J}$ ,  $\Delta x = 1.94 \text{ mm}$ .

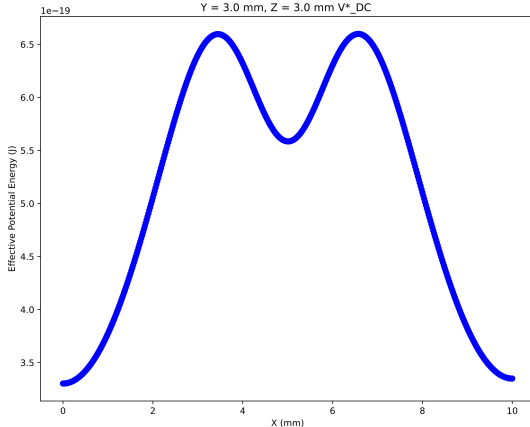


Figure 65: DC voltage values applied to washers: Electrode05:  $4 \times U_{DC}$ , Electrode06:  $-2 \times U_{DC}$ , Electrode07:  $U_{DC}$ , Electrode08:  $-2 \times U_{DC}$ , Electrode09:  $4 \times U_{DC}$ .  $\Delta V_{DC,axial,+}^* = 1.01 \times 10^{-19} \text{ J}$ ,  $\Delta x = 1.56 \text{ mm}$ .

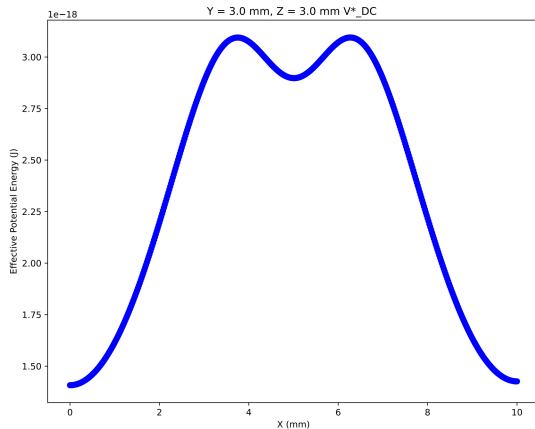


Figure 66: DC voltage values applied to washers: Electrode05:  $16 \times U_{DC}$ , Electrode06:  $-2 \times U_{DC}$ , Electrode07:  $U_{DC}$ , Electrode08:  $-2 \times U_{DC}$ , Electrode09:  $16 \times U_{DC}$ .  $\Delta V_{DC,axial,+}^* = 1.97 \times 10^{-19} \text{ J}$ ,  $\Delta x = 1.28 \text{ mm}$ .

As observed from the figures above, as the DC voltage applied to the end washers increases, the axial trap depth initially decreases, then increases, and eventually stabilizes at a nearly constant value. Similarly, the distance between the regions where positive and negative ions are trapped decreases initially but also becomes constant after a certain point, similar to the behavior of the trap depth.

#### 8.3.4 Conclusion

Various configurations were tested by adjusting different parameters to achieve the optimal configuration of the DC voltage applied to the DC electrodes (washers). As a result of various configuration tests, I tried to find the most suitable configuration. I showed the configuration that I thought was the most suitable in Section 8.5, and I plotted the effective potential energy graphs in Section 8.6, using the data I obtained as a result of this configuration in  $V^*(R)$  calculations.

## 8.4 Difficulties

### 8.4.1 Slow reading of data depending on grid cell size

I mentioned the importance of grid cell size for high-resolution data and graphics in Section 7.2.1. However, when the grid cell size was kept small, reading the electric field and potential data from SIMION and drawing the effective potential energy graphs in Python took a long time. To address this, I researched optimization techniques and found that using the `low_memory=False` setting in the Pandas library significantly accelerated the data reading and graph drawing processes by approximately 50 times. The `low_memory=False` setting allows the program to use more memory, enhancing performance and speeding up processing, especially when working with large datasets or complex operations. After updating my Python code with this feature, I could plot all my graphs at high resolution with a grid size of 0.02 quickly.

## 8.5 Calculation of $V^*(R)$

To calculate  $V^*(R)$  I used the method in section 3.2. Initially, I applied only a constant DC voltage to DC electrodes (washers) for potential data. The specific voltages applied to the electrodes are detailed below:

- Electrode01: 0
- Electrode02: 0
- Electrode03: 0
- Electrode04: 0
- Electrode05:  $16 \times U_{DC}$
- Electrode06:  $-2 \times U_{DC}$
- Electrode07:  $U_{DC}$
- Electrode08:  $-2 \times U_{DC}$
- Electrode09:  $16 \times U_{DC}$

The DC voltage configuration applied to the washers shown above made it possible to trap both positive and negative ions in the axial direction at different points.

Secondly, I applied  $U_{RF_{max}}$  to the RF electrodes for electric field data. The specific voltages applied to the electrodes are detailed below :

- Electrode01:  $-U_{RF_{max}}$
- Electrode02:  $U_{RF_{max}}$
- Electrode03:  $-U_{RF_{max}}$
- Electrode04:  $U_{RF_{max}}$
- Electrode05: 0
- Electrode06: 0
- Electrode07: 0
- Electrode08: 0
- Electrode09: 0

In Figure 67, you can also see the more detailed numbering of the electrodes.

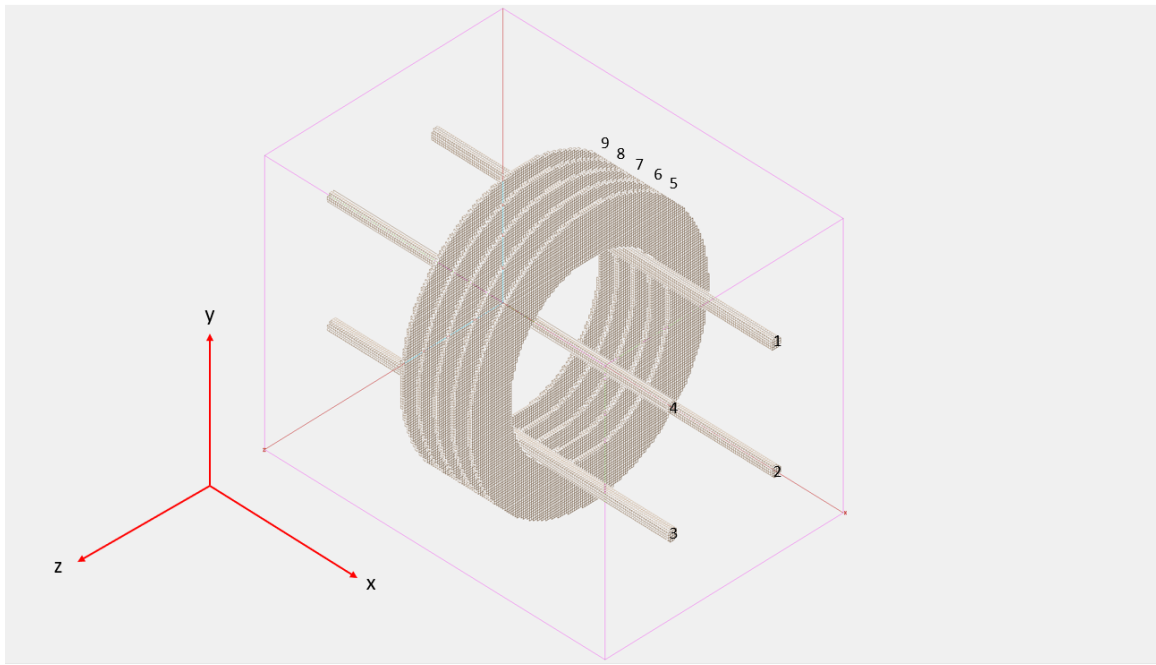


Figure 67: Detailed numbering of the electrodes in the ion trap design.

After obtaining the necessary data and performing the required some transformations (I mentioned it in Section 3.2), I calculated the effective potential energy  $V^*(R)$  using Equation (4). The parameter values utilized in this equation can be found in Table 5 of Section 7.3.

## 8.6 Result graphs

In contrast to the previous sections, where result graphs were plotted at a constant value of  $x = \max(x)/2$  in the radial direction, in this section, I extended the analysis by plotting the graphs at additional constant values:  $x = \max(x)/2 + \Delta x/2$  and  $x = \max(x)/2 + \Delta x$  for 2D representations. Due to the symmetry of the washers in our design, the graphs drawn at  $x = \max(x)/2 + \Delta x/2$  are also applicable for  $x = \max(x)/2 - \Delta x/2$ , and similarly, the graphs at  $x = \max(x)/2 + \Delta x$  are valid for  $x = \max(x)/2 - \Delta x$ . For the DC voltage configuration I used in Section 10.5 and the trap designed for the parameters given in Table 7,  $\max(x/2)$  was equal to 0.5 mm and the  $\Delta x$  value was found to be 1.28 mm.

The graphs were plotted differently from the usual approach for the following reason: Previously, only positive ions were trapped near the midpoint in the axial direction, making it sufficient to control trapping in the radial direction at that position. However, with both positive and negative ions now being trapped at different positions along the axial direction, it is necessary to verify that trapping occurs in the radial direction at those positions as well.

### 8.6.1 $x = \max(x/2)$

Firstly, I plotted the graph of the position and effective potential energy ( $V^*(R)$ ).

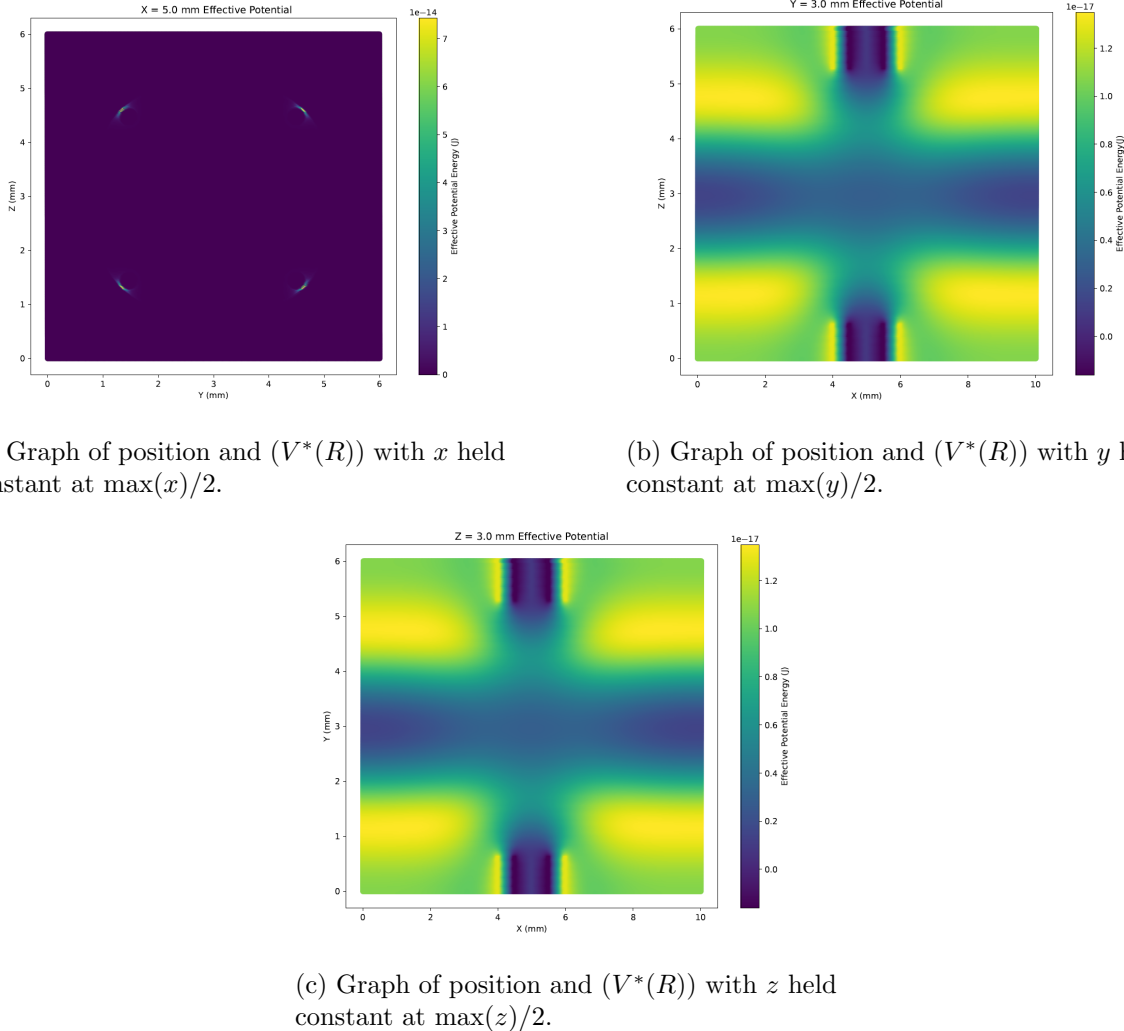
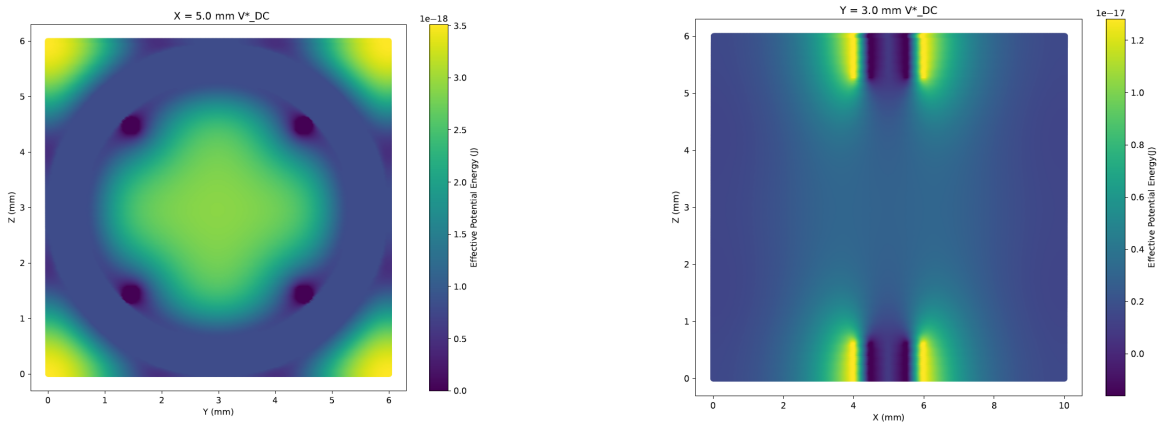
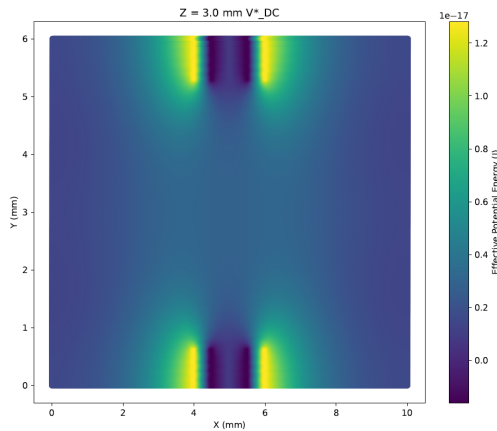


Figure 68: Graph of position and effective potential energy ( $V^*(R)$ ).



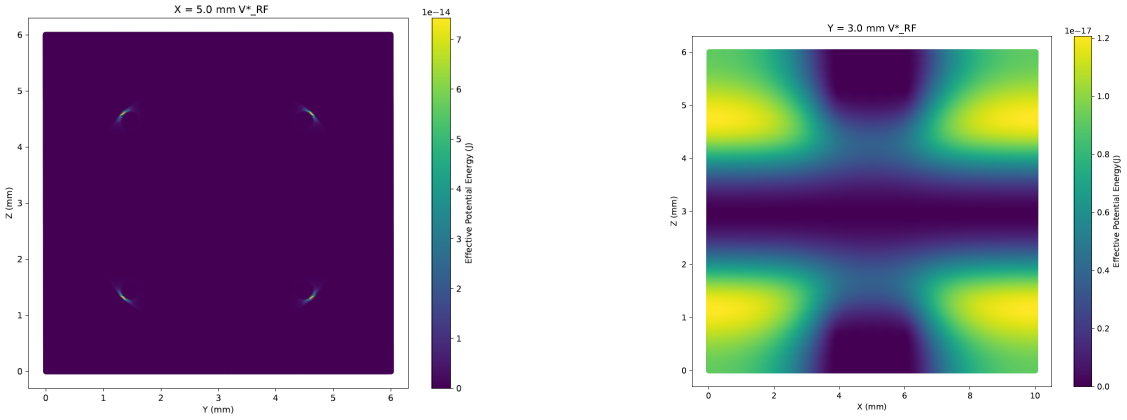
(a) Graph of position and  $V_{DC}^*$  with  $x$  held constant at  $\max(x)/2$ .

(b) Graph of position and  $V_{DC}^*$  with  $y$  held constant at  $\max(y)/2$ .



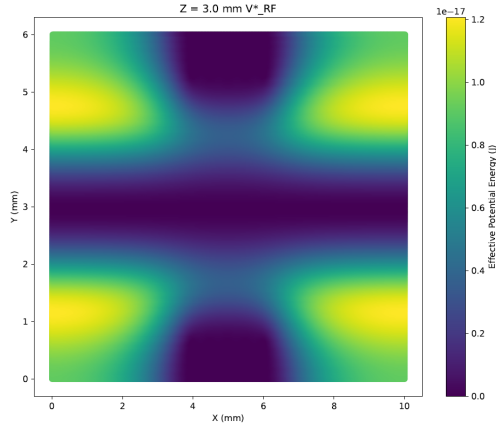
(c) Graph of position and  $V_{DC}^*$  with  $z$  held constant at  $\max(z)/2$ .

Figure 69: Graph of position and  $V_{DC}^*$ .



(a) Graph of position and  $V_{\text{RF}}^*$  with  $x$  held constant at  $\max(x)/2$ .

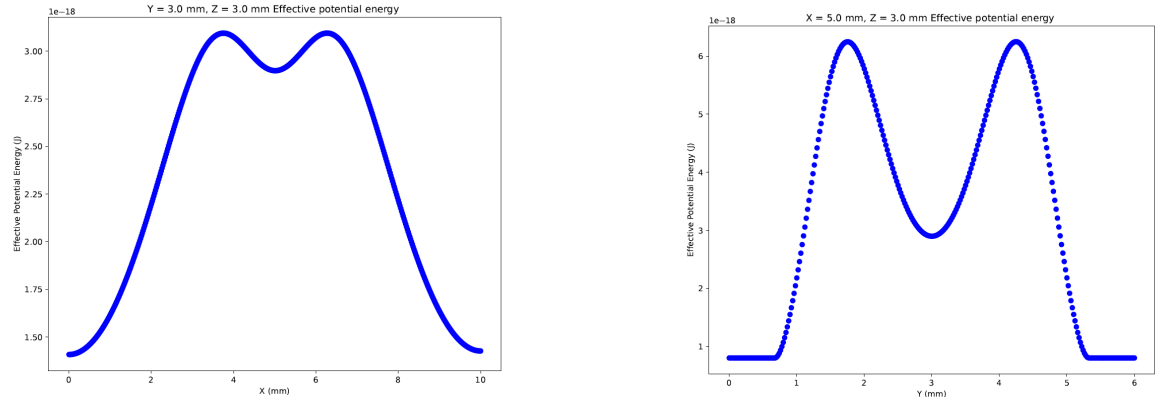
(b) Graph of position and  $V_{\text{RF}}^*$  with  $y$  held constant at  $\max(y)/2$ .



(c) Graph of position and  $V_{\text{RF}}^*$  with  $z$  held constant at  $\max(z)/2$ .

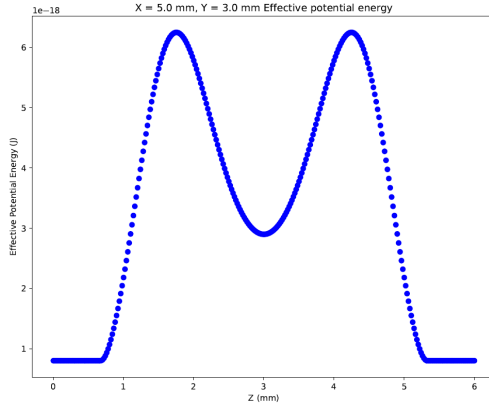
Figure 70: Graph of position and  $V_{\text{RF}}^*$ .

To make a better inference about the graph of position and effective potential energy, I plotted 2D graphs of  $V^*(R)$ ,  $V_{\text{RF}}^*$ , and  $V_{\text{DC}}^*$  by keeping two position variables constant.



(a) Graph of position and effective potential energy ( $V^*(R)$ ) with  $y$  and  $z$  held constant at  $\max(y)/2$  and  $\max(z)/2$ .

(b) Graph of position and effective potential energy ( $V^*(R)$ ) with  $x$  and  $z$  held constant at  $\max(x)/2$  and  $\max(z)/2$ .



(c) Graph of position and effective potential energy ( $V^*(R)$ ) with  $x$  and  $y$  held constant at  $\max(x)/2$  and  $\max(y)/2$ .

Figure 71: Graph of position and effective potential energy ( $V^*(R)$ ) with 2 constant variables.

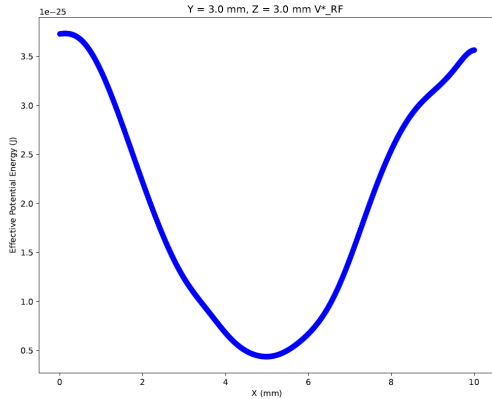
I calculated trap depths by using Python.

$$\begin{cases} \Delta E_{\text{axial},+} = 1.97 \times 10^{-19} \text{ J} \\ \Delta E_{\text{radial},+} = 3.35 \times 10^{-18} \text{ J} \end{cases}$$

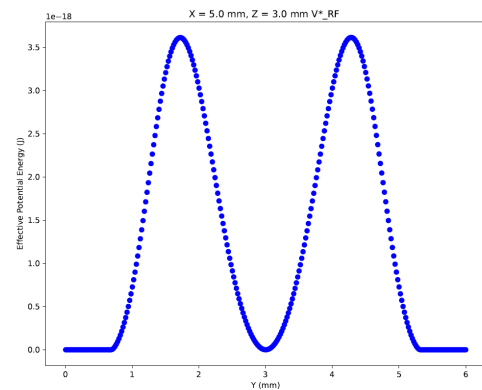
I found the trap depth in the axial direction to be  $1.97 \times 10^{-19} \text{ J}$  and the trap depth in the radial direction to be  $3.35 \times 10^{-18} \text{ J}$  for positive ions.

$$\Delta E_{\text{axial},-} = 1.68 \times 10^{-18} \text{ J}$$

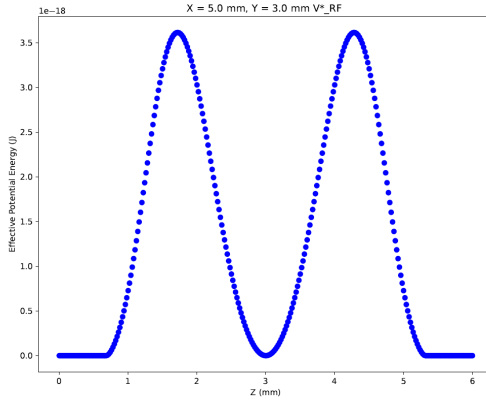
I found the the trap depth in the axial direction to be  $1.68 \times 10^{-18} \text{ J}$  for negative ions.



(a) Graph of position and  $V_{\text{RF}}^*$  with  $y$  and  $z$  held constant at  $\max(y)/2$  and  $\max(z)/2$ .



(b) Graph of position and  $V_{\text{RF}}^*$  with  $x$  and  $z$  held constant at  $\max(x)/2$  and  $\max(z)/2$ .



(c) Graph of position and  $V_{\text{RF}}^*$  with  $x$  and  $y$  held constant at  $\max(x)/2$  and  $\max(y)/2$ .

Figure 72: Graph of position and  $V_{\text{RF}}^*$  with 2 constant variables.

$$\Delta V_{\text{RF}, \text{radial}, +}^* = 3.61 \times 10^{-18} \text{ J}$$

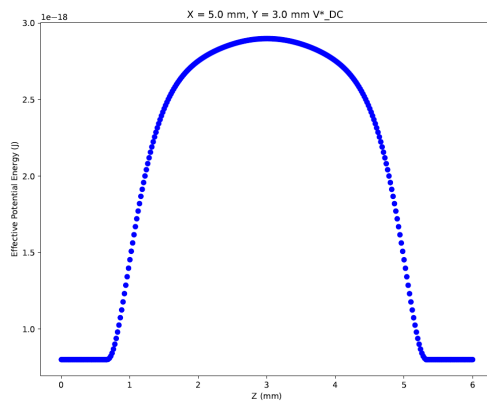
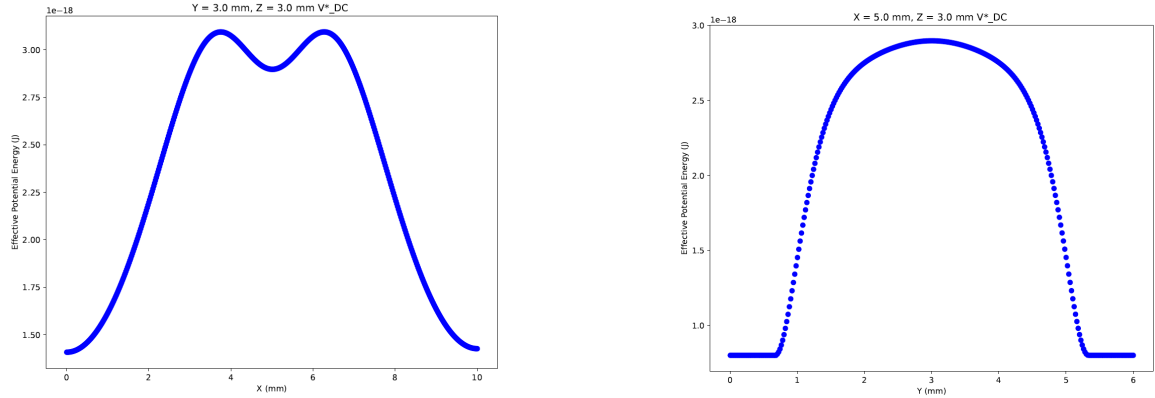
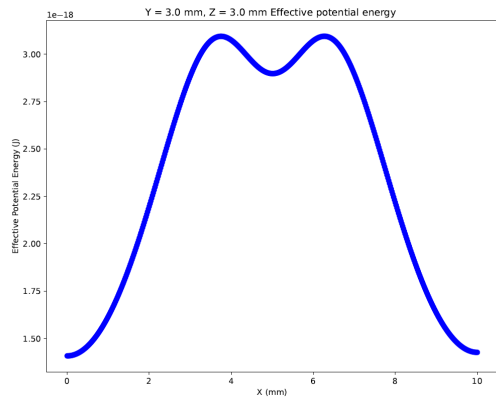


Figure 73: Graph of position and  $V_{DC}^*$  with 2 constant variables.

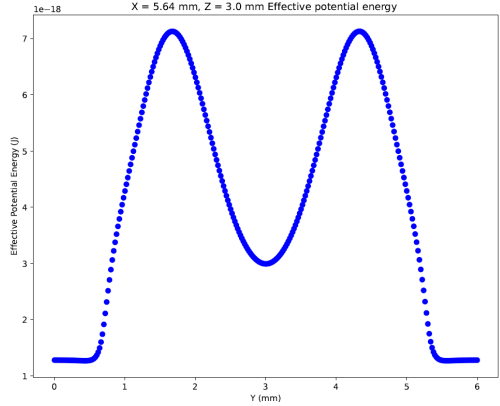
$$\Delta V_{DC, \text{axial},+}^* = 1.97 \times 10^{-19} \text{ J}$$

$$\Delta V_{DC, \text{axial},-}^* = 1.68 \times 10^{-18} \text{ J}$$

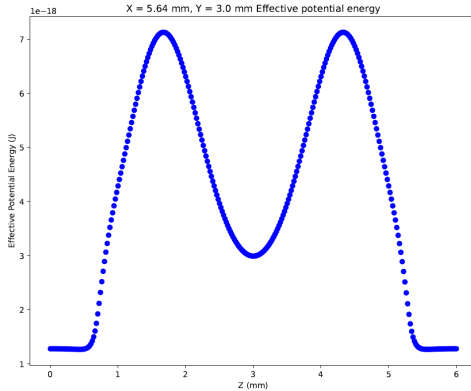
### 8.6.2 $x = \max(x/2) \pm \Delta x/2$



(a) Graph of position and effective potential energy ( $V^*(R)$ ) with  $y$  and  $z$  held constant at  $\max(y)/2$  and  $\max(z)/2$ .



(b) Graph of position and effective potential energy ( $V^*(R)$ ) with  $x$  and  $z$  held constant at  $\max(x)/2 + \Delta x/2$  and  $\max(z)/2$ .

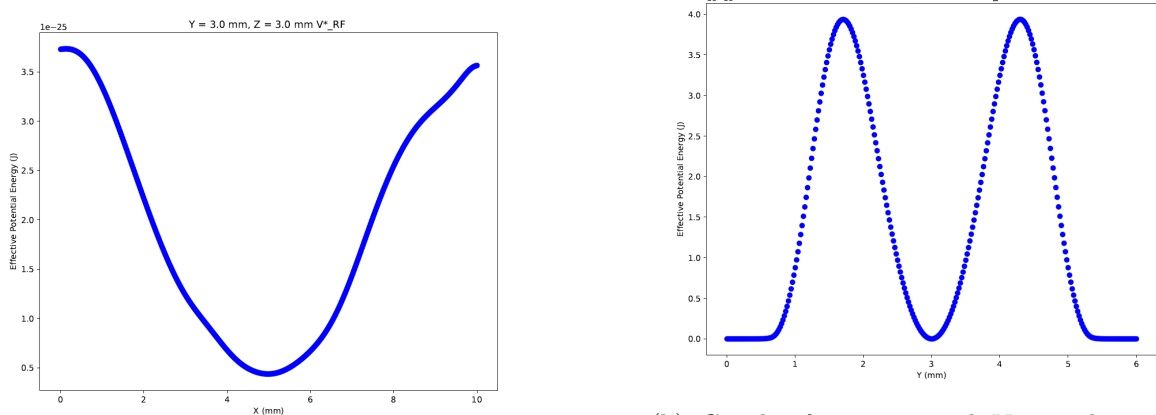


(c) Graph of position and effective potential energy ( $V^*(R)$ ) with  $x$  and  $y$  held constant at  $\max(x)/2 + \Delta x/2$  and  $\max(y)/2$ .

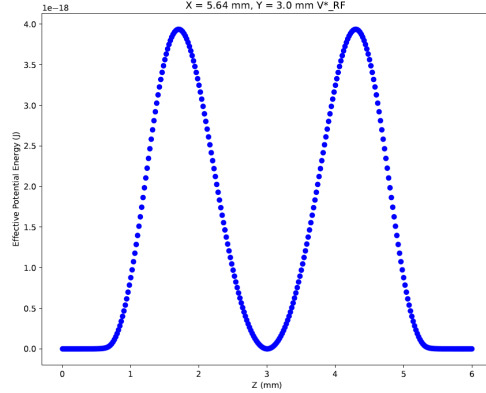
Figure 74: Graph of position and effective potential energy ( $V^*(R)$ ) with 2 constant variables.

$$\Delta E_{\text{radial},+} = 4.14 \times 10^{-18} \text{ J}$$

$$\Delta E_{\text{radial},-} = 4.14 \times 10^{-18} \text{ J}$$



(b) Graph of position and  $V_{\text{RF}}^*$  with  $x$  and  $z$  held constant at  $\max(x)/2 + \Delta x/2$  and  $\max(z)/2$ .

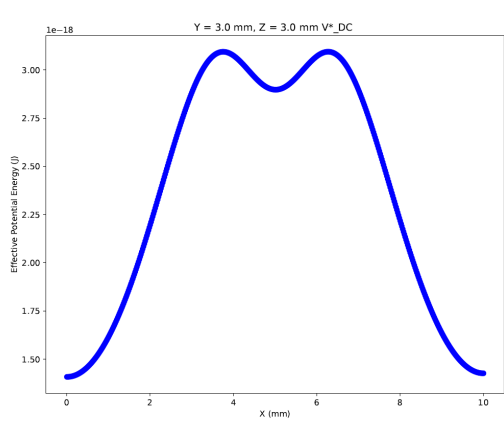


(c) Graph of position and  $V_{\text{RF}}^*$  with  $x$  and  $y$  held constant at  $\max(x)/2 + \Delta x/2$  and  $\max(y)/2$ .

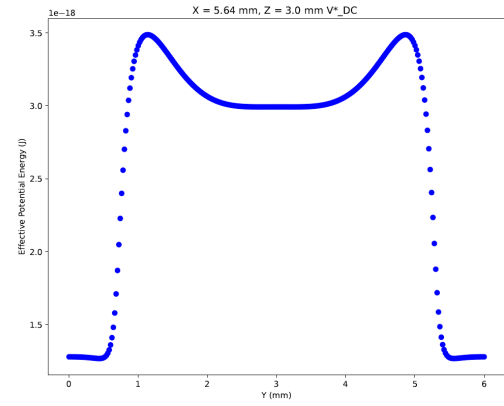
Figure 75: Graph of position and  $V_{\text{RF}}^*$  with 2 constant variables.

$$\Delta V_{\text{RF},\text{radial},+}^* = 3.93 \times 10^{-18} \text{ J}$$

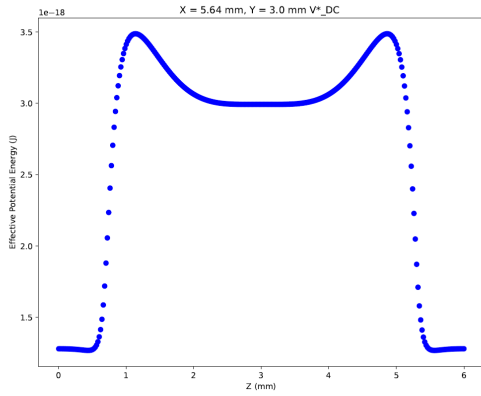
$$\Delta V_{\text{RF},\text{radial},-}^* = 3.93 \times 10^{-18} \text{ J}$$



(a) Graph of position and  $V^*_{DC}$  with  $y$  and  $z$  held constant at  $\max(y)/2$  and  $\max(z)/2$ .



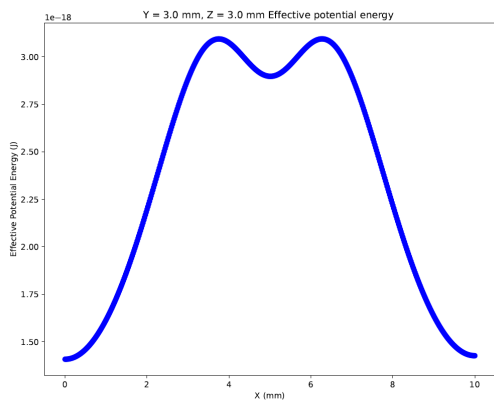
(b) Graph of position and  $V^*_{DC}$  with  $x$  and  $z$  held constant at  $\max(x)/2 + \Delta x/2$  and  $\max(z)/2$ .



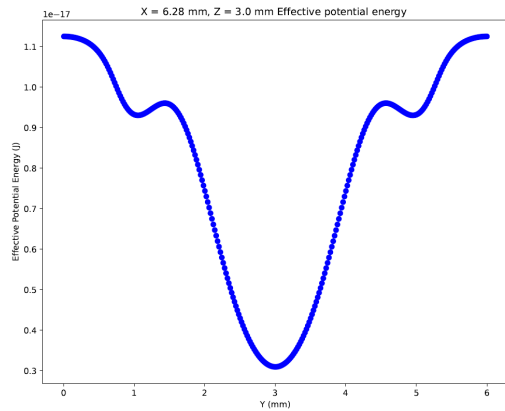
(c) Graph of position and  $V^*_{DC}$  with  $x$  and  $y$  held constant at  $\max(x)/2 + \Delta x/2$  and  $\max(y)/2$ .

Figure 76: Graph of position and  $V^*_{DC}$  with 2 constant variables.

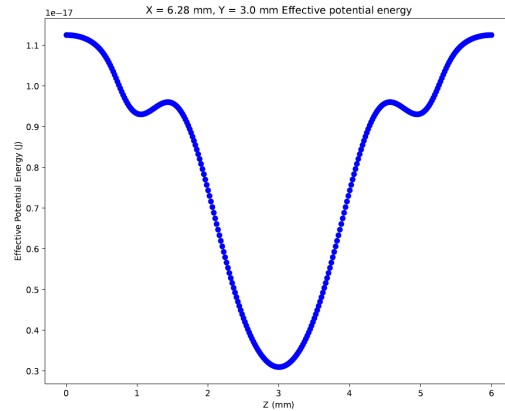
### 8.6.3 $x = \max(x/2) \pm \Delta x$



(a) Graph of position and effective potential energy ( $V^*(R)$ ) with  $y$  and  $z$  held constant at  $\max(y)/2$  and  $\max(z)/2$ .



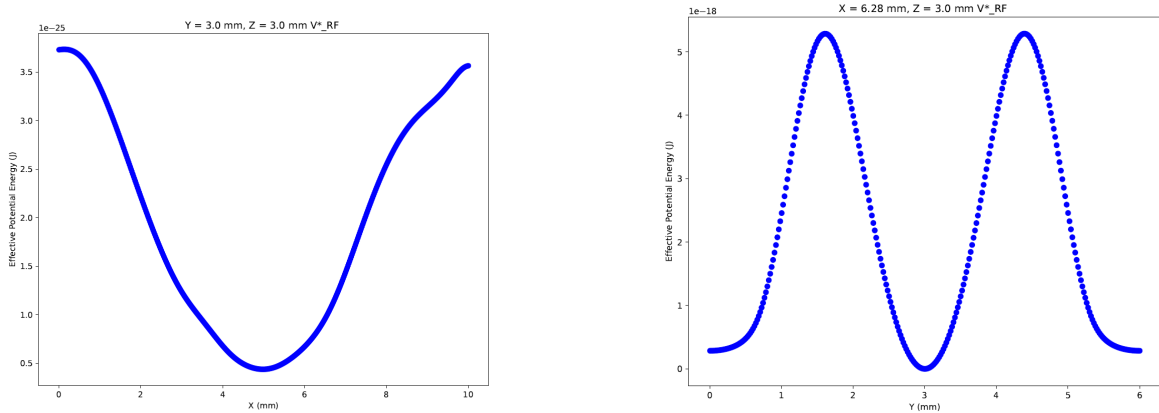
(b) Graph of position and effective potential energy ( $V^*(R)$ ) with  $x$  and  $z$  held constant at  $\max(x)/2 + \Delta x$  and  $\max(z)/2$ .



(c) Graph of position and effective potential energy ( $V^*(R)$ ) with  $x$  and  $y$  held constant at  $\max(x)/2 + \Delta x$  and  $\max(y)/2$ .

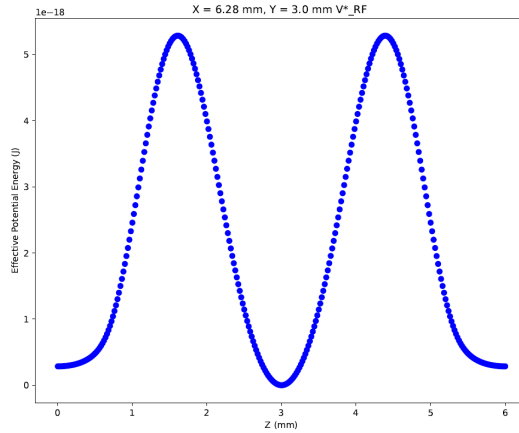
Figure 77: Graph of position and effective potential energy ( $V^*(R)$ ) with 2 constant variables.

$$\Delta E_{\text{radial},-} = 6.50 \times 10^{-18} \text{ J}$$



(a) Graph of position and  $V_{\text{RF}}^*$  with  $y$  and  $z$  held constant at  $\max(y)/2$  and  $\max(z)/2$ .

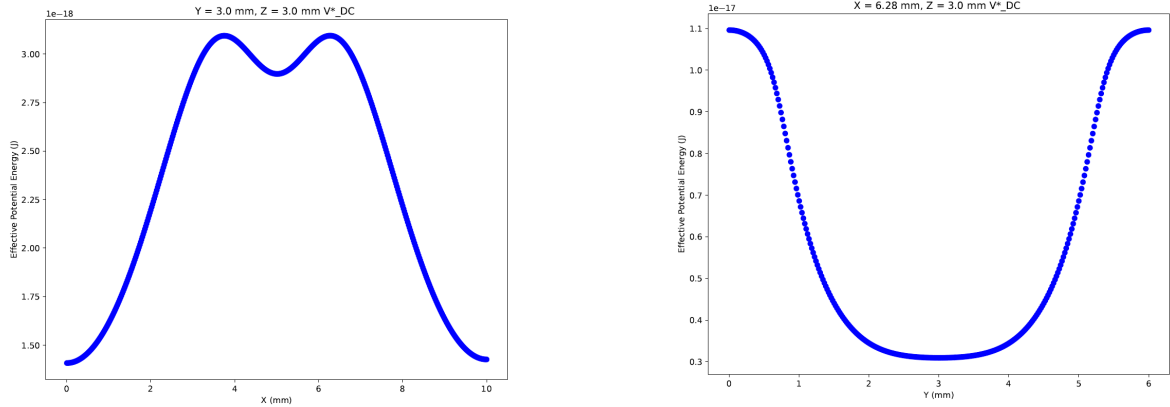
(b) Graph of position and  $V_{\text{RF}}^*$  with  $x$  and  $z$  held constant at  $\max(x)/2 + \Delta x$  and  $\max(z)/2$ .



(c) Graph of position and  $V_{\text{RF}}^*$  with  $x$  and  $y$  held constant at  $\max(x)/2 + \Delta x$  and  $\max(y)/2$ .

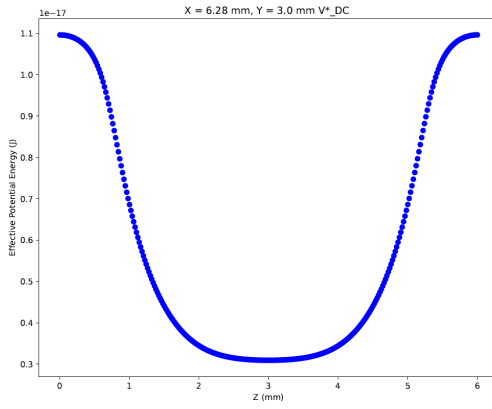
Figure 78: Graph of position and  $V_{\text{RF}}^*$  with 2 constant variables.

$$\Delta V_{\text{RF},\text{radial},-}^* = 5.28 \times 10^{-18} \text{ J}$$



(a) Graph of position and  $V^*_{DC}$  with  $y$  and  $z$  held constant at  $\max(y)/2$  and  $\max(z)/2$ .

(b) Graph of position and  $V^*_{DC}$  with  $x$  and  $z$  held constant at  $\max(x)/2 + \Delta x$  and  $\max(z)/2$ .



(c) Graph of position and  $V^*_{DC}$  with  $x$  and  $y$  held constant at  $\max(x)/2 + \Delta x$  and  $\max(y)/2$ .

Figure 79: Graph of position and  $V^*_{DC}$  with 2 constant variables.

Finally, I plotted graphs showing the trap depths of positive and negative ions in the radial direction.

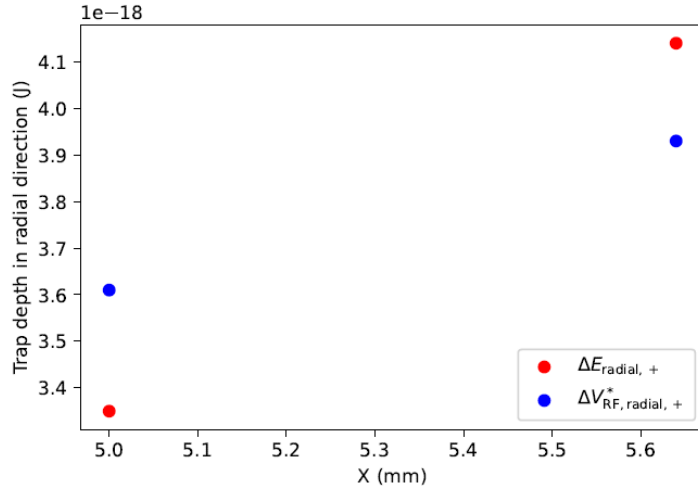


Figure 80: Graphs showing the trap depth in the radial direction for positive ions.  $\Delta E_{\text{radial},+}$  : The radial trap depth in the  $V^*(R)$  graph for positive ions [J] ,  $\Delta V_{\text{RF, radial},+}^*$  : The radial trap depth in the  $V_{\text{RF}}^*$  graph for positive ions [J] .

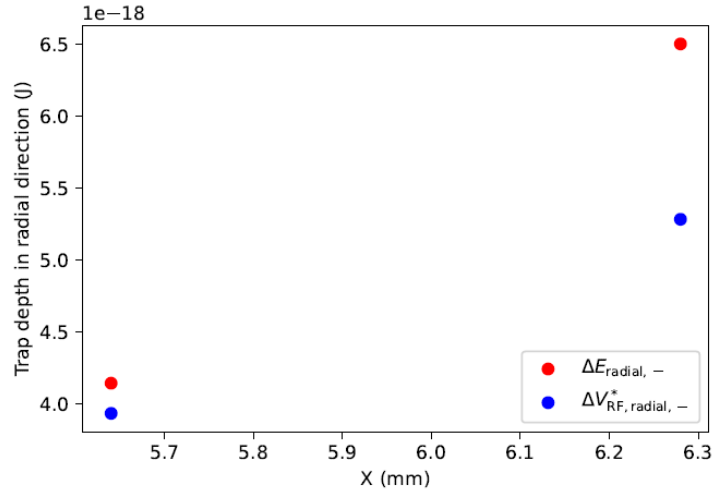


Figure 81: Graphs showing the trap depth in the radial direction for negative ions.  $\Delta E_{\text{radial},-}$  : The radial trap depth in the  $V^*(R)$  graph for negative ions [J] ,  $\Delta V_{\text{RF, radial},-}^*$  : The radial trap depth in the  $V_{\text{RF}}^*$  graph for negative ions [J] .

## 9 Using SIMION for ion trajectory simulations

### 9.1 General overview

SIMION is a powerful and widely-used software tool for modeling and simulating ion traps and charged particle trajectories. It provides a platform to calculate electrostatic and magnetic fields and then uses these fields to simulate the motion of ions within complex geometries. In this way, before assembling the actual ion trap experiment, the ion trap design can first be imported into the SIMION software for testing. This allows potential issues in the setup to be identified and corrected, enabling optimizations to be made before the physical implementation.

To run ion trajectory simulations in SIMION, the ion trap first needs to be designed using software like CAD or SolidWorks. Afterward, the design can be imported into SIMION for testing. (Detailed steps are available in the SIMION documentation.)

The User Program feature enables users to run their own scripts through an embedded scripting language like Lua. With these custom scripts, users can adjust simulation parameters, manage particle trajectories, conduct advanced data analysis, and incorporate external data sources, providing greater flexibility and control over simulations. As part of this internship, the user code was mainly utilized to simulate time-dependent potentials applied to the RF electrodes and to model the behavior of positive and negative ions within the ion trap, as shown in Figure 40. A more detailed examination of the Lua code for this simulation is provided in Section 9.2.

Finally, simulations can be performed by determining the parameters of the simulation and the properties of the ions such as speed, position, mass and distribution.

In the simulation, ion trapping is considered successful when the ions remain confined within the trap and do not collide with any electrodes or escape the trapping region. If 'Flying particles' is still displayed in the yellow box at the bottom left of the SIMION program some time after the simulation has started, it indicates that the simulation has been successful and ions has been trapped successfully. However, after the SIMION simulation runs for a while, if the green box in the lower left corner displays a message like "Fly completed. 20 splats," it indicates that the ion was not successfully trapped and either collided with a surface or escaped the trap. The number of splats represents how many ions failed to remain trapped during the simulation.

## 9.2 Lua code for ion trajectory simulation

The main structure of the Lua code, originally developed by Beke Breitmeier [2] for the three-segmented linear Paul trap, was modified with minor adjustments to fit my own design and voltage configuration. Therefore, this section focuses solely on the changes made to the code, without detailing its overall construction. For a comprehensive understanding of the general structure of the Lua code, please refer to Section 4 of Beke's thesis. You can also find the entire code I used for my simulations in Appendix B.1.

In the Lua code, instructions were implemented to vary the RF voltage applied to the RF electrodes over time, while keeping the DC voltage applied to the washers constant. The code section related to setting the voltage configuration can be found between lines 44 and 55 of the Lua code in Appendix B.1. Here, `tempvolts` corresponds to the RF voltage,  $U_{RF}(t)$ , and `_dc` corresponds to the DC voltage,  $U_{DC}$ .

- Electrode01:  $-U_{RF}(t)$
- Electrode02:  $U_{RF}(t)$
- Electrode03:  $-U_{RF}(t)$
- Electrode04:  $U_{RF}(t)$
- Electrode05:  $16 \times U_{DC}$
- Electrode06:  $-2 \times U_{DC}$
- Electrode07:  $U_{DC}$
- Electrode08:  $-2 \times U_{DC}$
- Electrode09:  $16 \times U_{DC}$

In Figure 67, you can also see the more detailed numbering of the electrodes.

## 9.3 Simulation parameters

As simulation parameters in SIMION, a trajectory quality of 3 was selected, which offers a balanced compromise between computational speed and accuracy by controlling the number of time steps for path calculations. The charge repulsion was modeled using Coulomb repulsion, accurately representing the electrostatic interactions between charged particles. Additionally, the parameters used in the simulations of ions are given in table 8.

| Name            | Type                    | Value   | Unit     |
|-----------------|-------------------------|---|----------|
| Num particles   |                         | 10  |          |
| Mass            | single value            | 40  | u        |
| Charge          | single value            | 1 or -1   | e        |
| Source position | gaussian3d distribution | Mean{x: 5.0, y: 3.0, z: 3.0}, Stdev{x: 0.1, y: 0.1, z: 0.1} | mm or gu |
| Velocity format | direction + speed       |   |          |
| Direction       | single vector           | {x: 0, y: 0, z: 0}  | unitless |
| Speed           | single value            | 0.1   | mm/usec  |
| TOB             | single value            | 0   | usec     |
| CWF             | single value            | 1   | unitless |
| Color           | single value            | 0 (for positive ions) or 1 (for negative ions)              | index    |

Table 8: Particle parameters used for simulating  $^{40}\text{Ca}^+$  and  $^{40}\text{Ca}^-$  ions in SIMION. Each row represents a distinct configuration option, encompassing the parameter name, type, value, and corresponding unit.

#### 9.4 Comparison between effective potential energy graphs and SIMION simulation results

In Section 9.1, I discussed that the primary use of the SIMION program is to test ion trap designs within a virtual environment before physical implementation. However, in this project, SIMION simulations served an additional purpose: validating the accuracy of effective potential energy graphs developed as an alternative to direct SIMION simulations.

To achieve this, various voltage configurations were applied to the electrodes, and the resulting effective potential energy graphs were compared with those obtained from SIMION simulations. Effective potential energy was calculated using parameters detailed in Table 7 of Section 8, employing the method described in Section 8.5. SIMION simulations were conducted using the code provided in Appendix B.1, with modifications only to the `_dc` and `rfvolts` for different voltage configurations. The parameters specified in Section 9.3 were consistently applied during these SIMION simulations.

### 9.4.1 $U_{RF,max} = 300V$ and $U_{DC} = 5V$

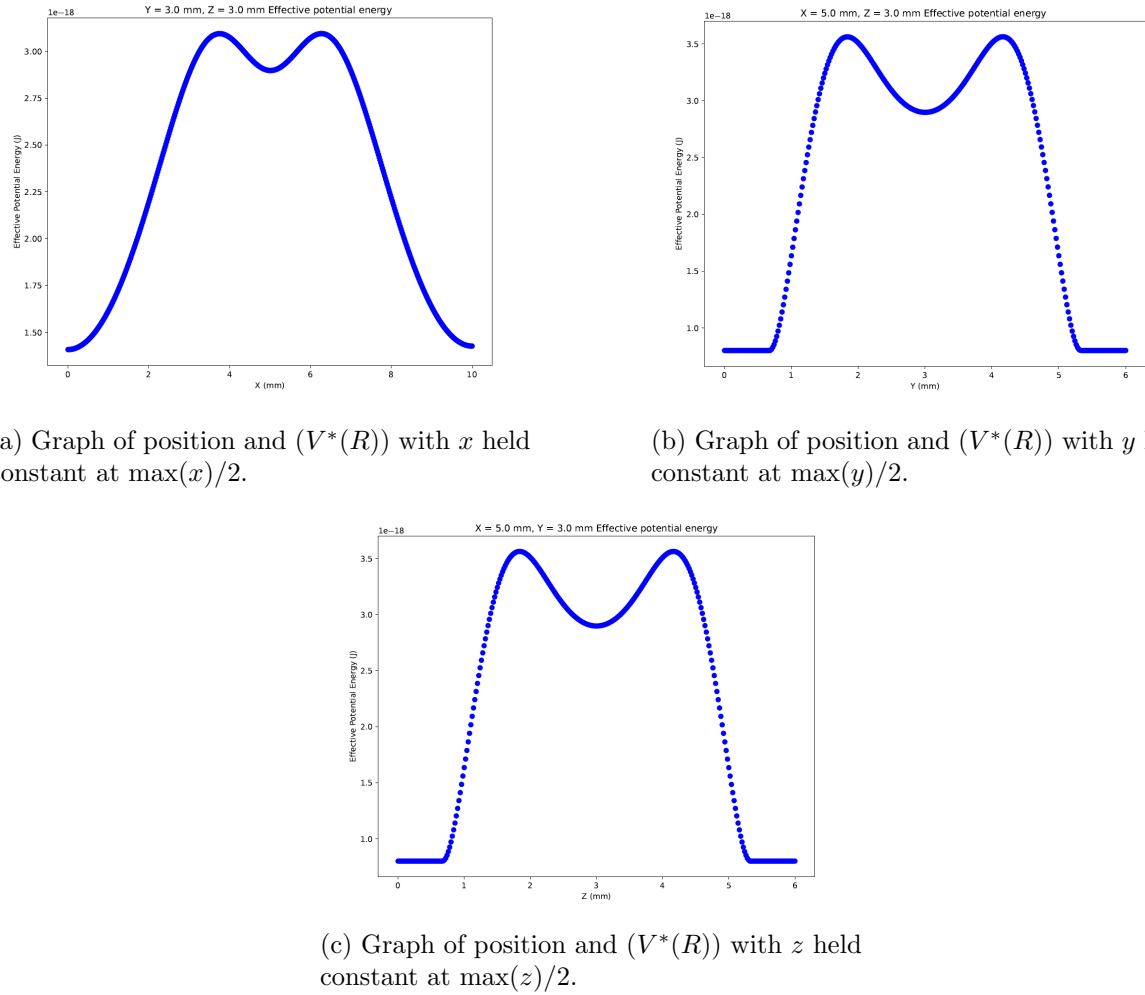
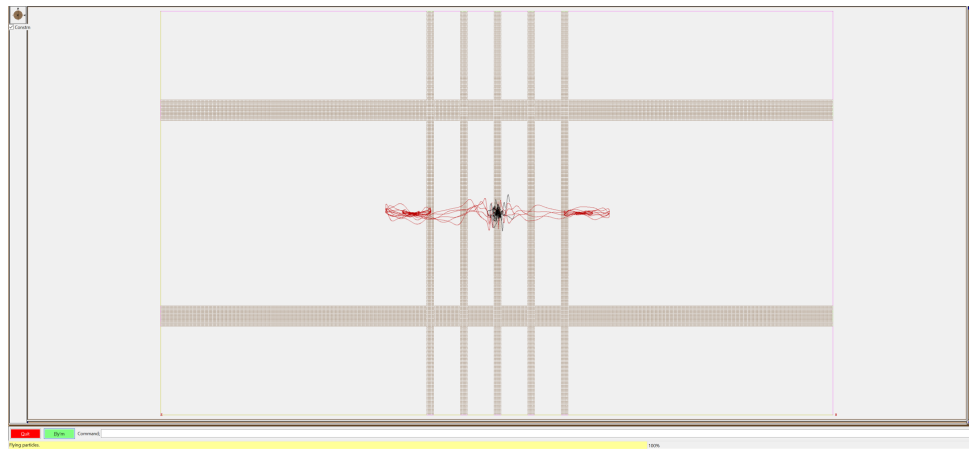
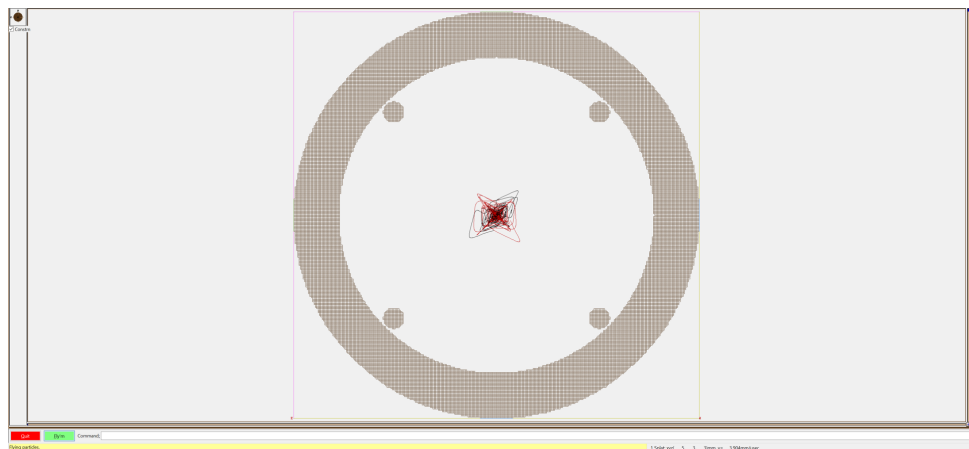


Figure 82: Graph of position and effective potential energy ( $V^*(R)$ ).

As indicated by the effective potential energy graphs above, both positive and negative ions can be trapped in the axial and radial directions due to the sufficient trap depths (refer to Section 8.3.4 for more detailed information). Specifically, positive ions are trapped at the midpoint ( $x = 5.0$  mm), while negative ions are trapped at positions  $x = 3.72$  mm and  $x = 6.28$  mm. For a sketch of the ion trap design in the XY plane, see Figure 41.



(a) View of the simulation on the XY axis (in axial direction). The trajectories of  $^{40}\text{Ca}^+$  ions are depicted with black lines, while the trajectories of  $^{40}\text{Ca}^-$  ions are shown with red lines.



(b) View of the simulation on the ZY axis (in radial direction). The trajectories of  $^{40}\text{Ca}^+$  ions are depicted with black lines, while the trajectories of  $^{40}\text{Ca}^-$  ions are shown with red lines.

Figure 83

As shown in Figure 83(a), the ion simulation was successful: positive ions were trapped at the midpoint ( $x = 5.0$  mm), while negative ions were trapped at symmetrical positions on either side. Observations in SIMION, where negative ion accumulation was examined using the mouse, indicated that they were trapped at approximately  $x = 3.72$  mm and  $x = 6.28$  mm. Furthermore, Figure 83(b) demonstrates successful radial trapping for both positive and negative ions. Consequently, the results from SIMION simulations are consistent with the effective potential energy graphs.

### 9.4.2 $U_{RF,max} = 300V$ and $U_{DC} = 10V$

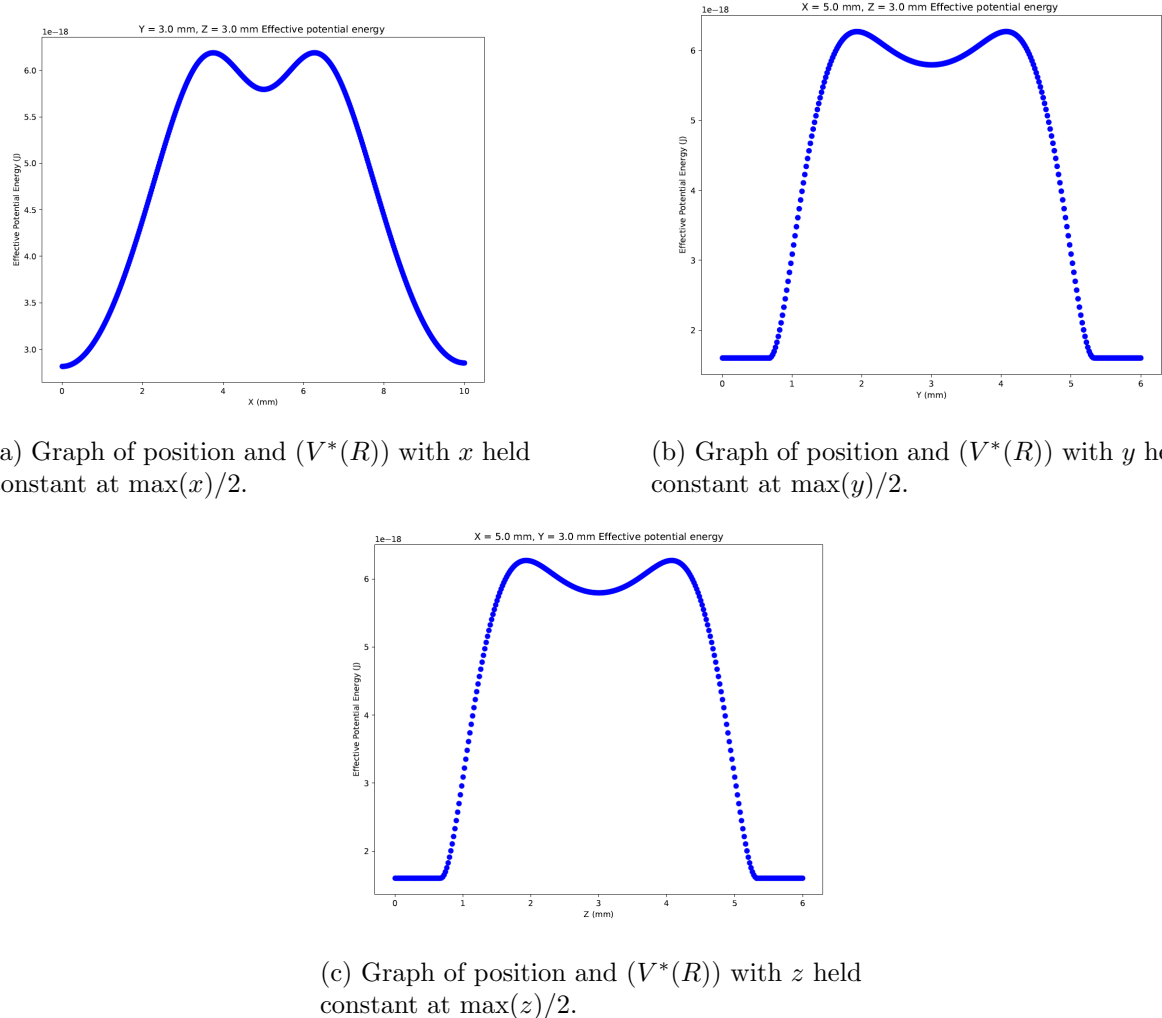
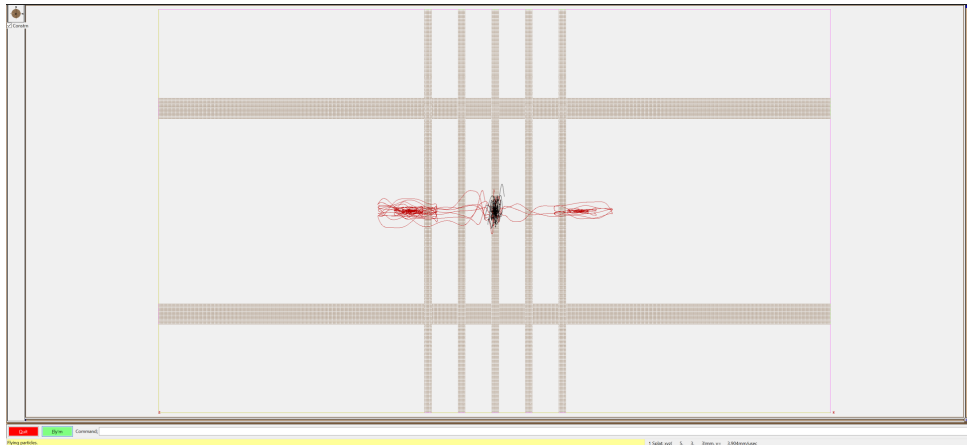
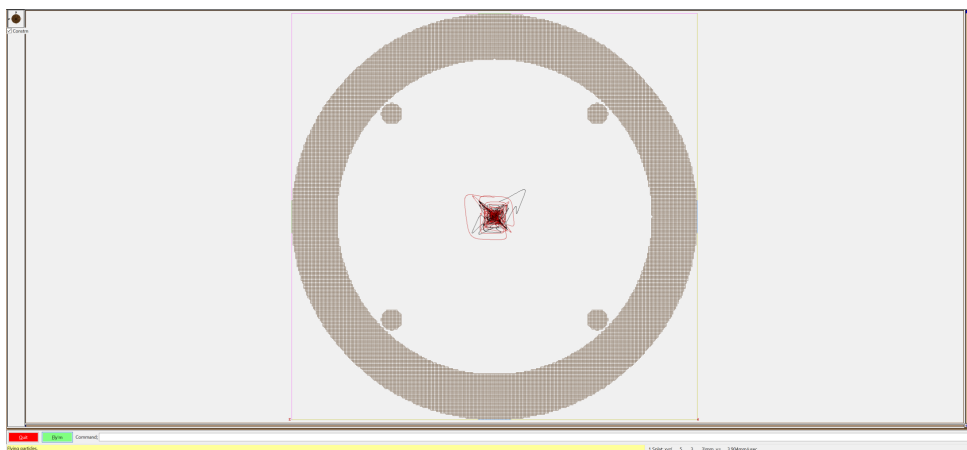


Figure 84: Graph of position and effective potential energy ( $V^*(R)$ ).

As indicated by the effective potential energy graphs above, both positive and negative ions can be trapped in the axial and radial directions due to the sufficient trap depths. Specifically, positive ions are trapped at the midpoint ( $x = 5.0$  mm), while negative ions are trapped at positions  $x = 3.72$  mm and  $x = 6.28$  mm.



(a) View of the simulation on the XY axis (in axial direction). The trajectories of  $^{40}\text{Ca}^+$  ions are depicted with black lines, while the trajectories of  $^{40}\text{Ca}^-$  ions are shown with red lines.



(b) View of the simulation on the ZY axis (in radial direction). The trajectories of  $^{40}\text{Ca}^+$  ions are depicted with black lines, while the trajectories of  $^{40}\text{Ca}^-$  ions are shown with red lines.

Figure 85

As shown in Figure 85(a), the ion simulation was successful: positive ions were trapped at the midpoint ( $x = 5.0$  mm), while negative ions were trapped at symmetrical positions on either side. Observations in SIMION, where negative ion accumulation was examined using the mouse, indicated that they were trapped at approximately  $x = 3.72$  mm and  $x = 6.28$  mm. Furthermore, Figure 85(b) demonstrates successful radial trapping for both positive and negative ions. Consequently, the results from SIMION simulations are consistent with the effective potential energy graphs.

### 9.4.3 $U_{RF,max} = 300V$ and $U_{DC} = 25V$

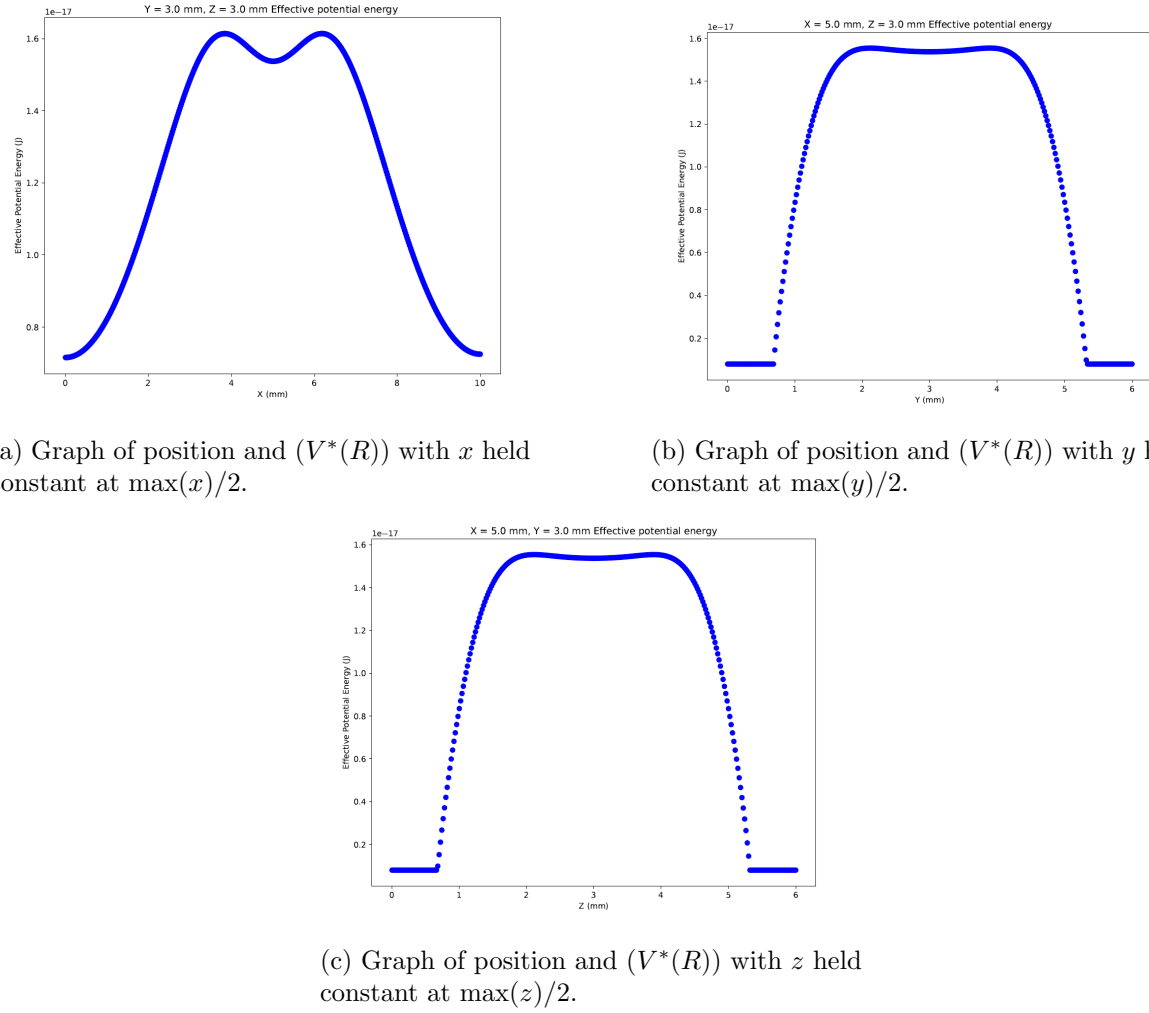
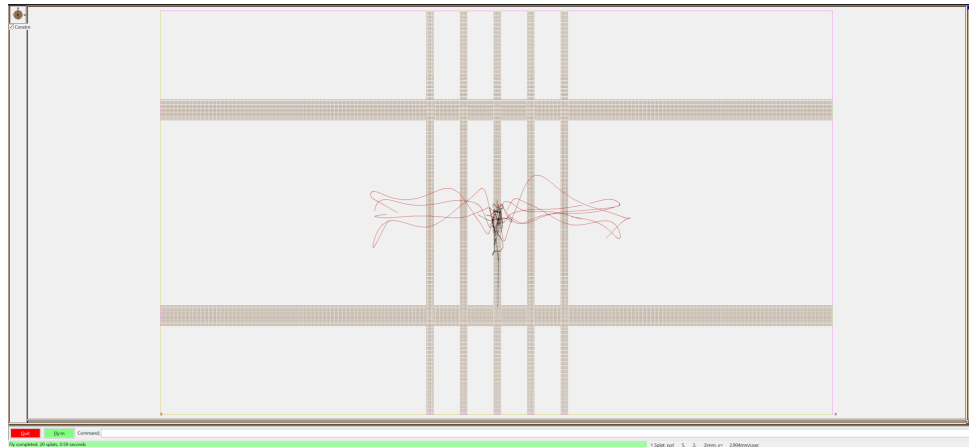
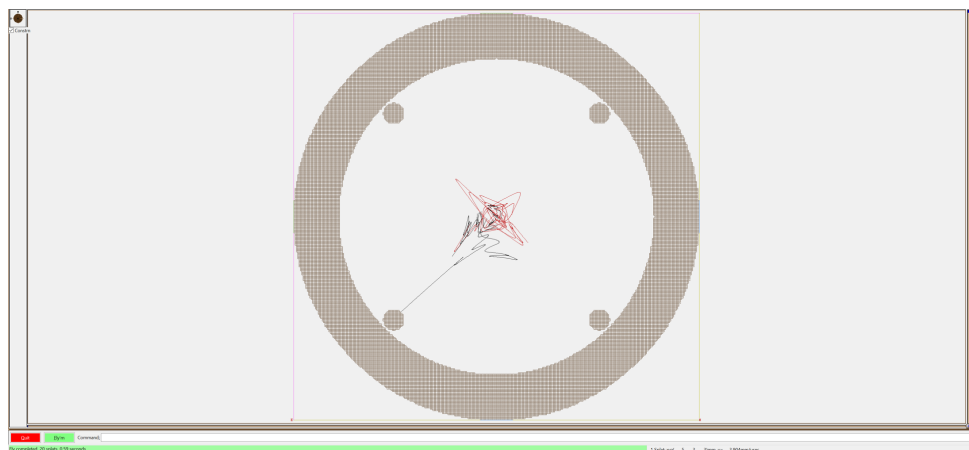


Figure 86: Graph of position and effective potential energy ( $V^*(R)$ ).

As can be seen from figures 86 (b) and 86 (c) above, it is not possible to trap positive ions in the radial direction since there is no trap depth for positive ions.



(a) View of the simulation on the XY axis (in axial direction). The trajectories of  $^{40}\text{Ca}^+$  ions are depicted with black lines, while the trajectories of  $^{40}\text{Ca}^-$  ions are shown with red lines.



(b) View of the simulation on the ZY axis (in radial direction). The trajectories of  $^{40}\text{Ca}^+$  ions are depicted with black lines, while the trajectories of  $^{40}\text{Ca}^-$  ions are shown with red lines.

Figure 87

As shown in Figure 87(a), ions could not be trapped in the SIMION simulation. Figure 87(b) clarifies the reason: the simulation stopped because positive ions failed to be trapped radially and subsequently collided with one of the RF electrodes. This outcome was anticipated based on the effective potential energy graphs, which indicated insufficient radial trap depth for positive ions. The results demonstrate a strong consistency between the effective potential energy graphs and the SIMION simulations.

## 10 Conclusion

In this internship, effective potential energy calculations for ion traps were performed using mathematical approaches and electric field and potential data obtained from the SIMION program. Then, 3D contour plots and 2D graphs of the effective potential energy were plotted to interpret ion behavior. The longitudinal and radial frequencies of the ions were calculated numerically from these graphs and compared with theoretical results. It was determined that the numerical results obtained from the effective potential energy graphs were very close to the theoretical results.

After confirming the correctness of the method, a trap design was developed to capture both positive and negative ions by interpreting the effective potential energy graphs. The effective potential energy graphs were then used again to optimize this trap by examining the trap depths and the distance between the trapped regions of positive and negative ions. A trap capable of trapping both positive and negative ions in separate but close regions was designed, with details provided in Section 8.

This trap was subsequently used in SIMION simulations, and the results were compared with the effective potential energy graphs. It was confirmed that both positive and negative ions were trapped in the expected locations, demonstrating the accuracy of the approach applied throughout the project.

The two primary objectives of my project—analyzing ion behavior through effective potential energy calculations and designing an ion trap capable of confining both positive and negative ions in separate but adjacent regions—have been successfully accomplished. This design holds potential for future real-world ion trap experiments and may contribute to advancing our understanding of ion physics.

## Acknowledgments

During my internship, I had the invaluable opportunity to learn and utilize programs such as SIMION, LaTeX, and SolidWorks, which were previously unfamiliar to me. Over the course of this three-month internship, I gained significant experience, enhanced my problem-solving abilities, and made substantial personal and professional growth.

I would like to thank Professor Katrin Erath Dulitz for providing me with this opportunity and for her valuable guidance and support throughout my internship. I also wish to thank my colleagues Beke Leonie Breitmeier and Sam White for their contributions.

## Appendix A

### A Components

#### A.1 The alternative design for three segmented linear Paul trap

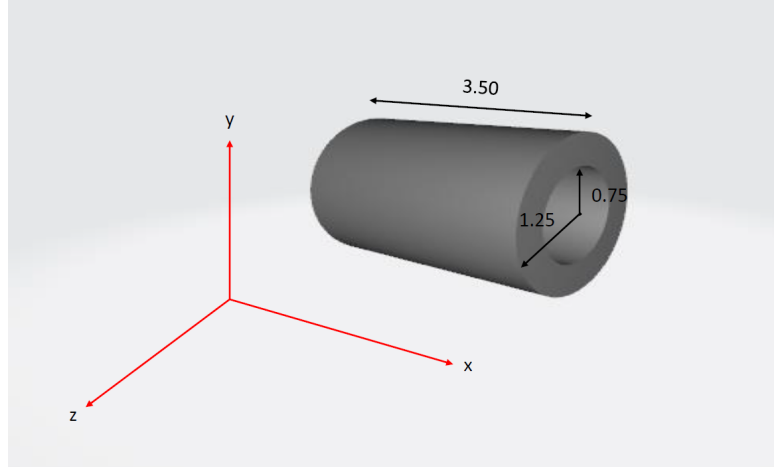


Figure A.1: SolidWorks 3D model of the DC electrode, developed for the assembly of the linear Paul trap according to the parameters in table 1.

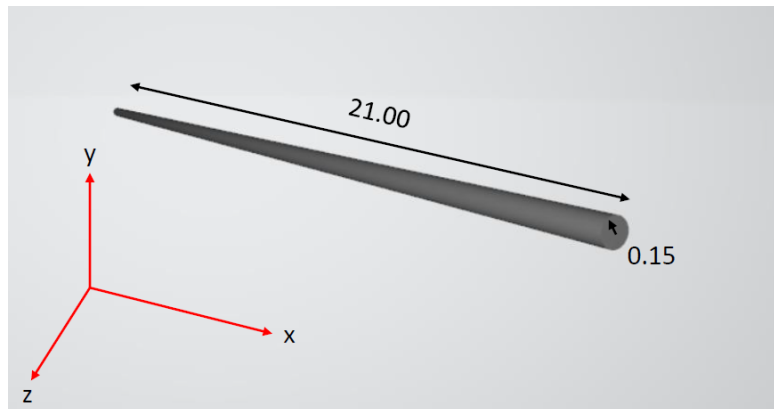


Figure A.2: SolidWorks 3D model of the RF electrode, developed for the assembly of the linear Paul trap according to the parameters in table 1.

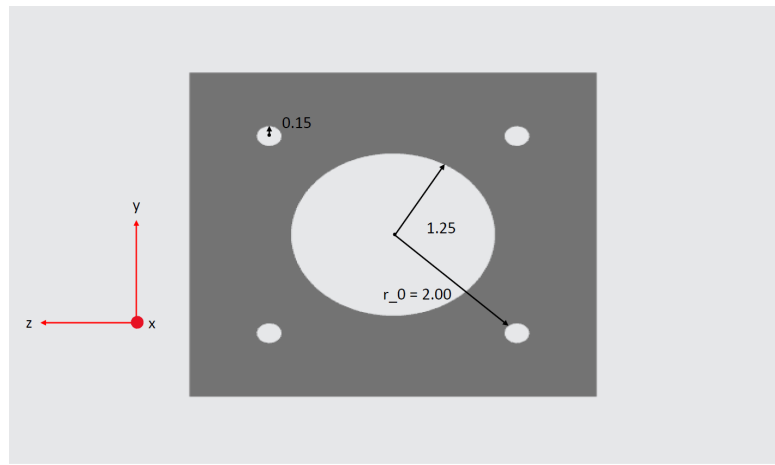


Figure A.3: SolidWorks 3D model of the holder, developed for the assembly of the linear Paul trap according to the parameters in table 1.

## A.2 The trap design for trapping both positive and negative ions simultaneously

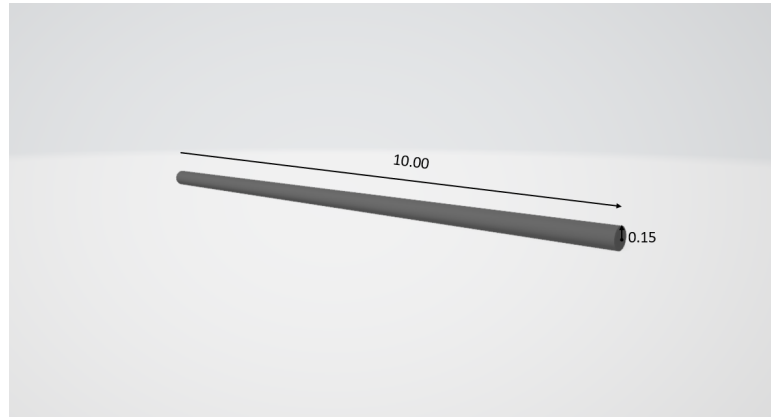


Figure A.4: SolidWorks 3D model of the RF electrode, developed for the assembly of the ion trap according to the parameters in table 7.

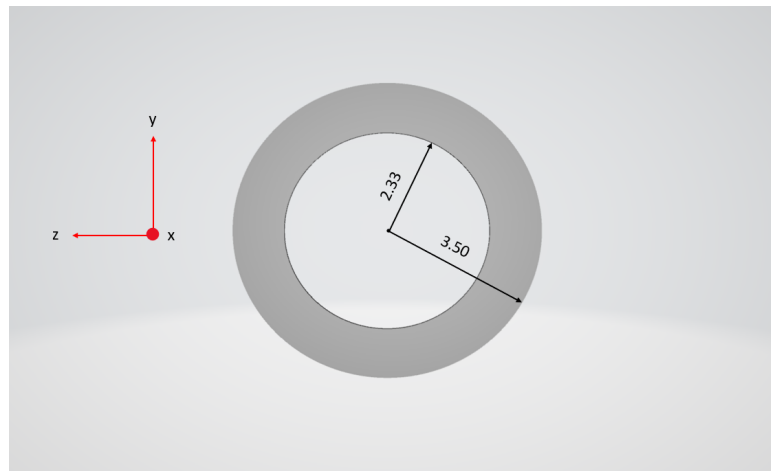


Figure A.5: SolidWorks 3D model of the DC electrode (washer), developed for the assembly of the ion trap according to the parameters in table 7.

## Appendix B

### B Codes

#### B.1 Lua code

```
1  --[[  
2    SIMION Lua workbench program for octupole simulation.  
3    This oscillates octupole rod potentials  
4    (and also updates PE display periodically).  
5  
6    D.Manura-2007-09  
7    (c) 2007 Scientific Instrument Services, Inc. (Licensed under SIMION  
8     8.0)  
9  --]]  
10 simion.workbench_program()  
11  
12 -- Variables adjustable during flight:  
13  
14 adjustable pe_update_each_usec      = 0.05    -- potential energy  
   display                                -- update period (microsec  
                                             )  
                                             -- (for display purposes  
                                             only)  
15  
16  
17 -- Variables adjustable only at beginning of flight:  
18 adjustable _linear_damping           = 1  
19 adjustable effective_radius_mm       = 2.0     -- half the minimum  
   distance between  
                                             -- opposite rods (mm)  
20 adjustable phase_angle_deg          = 0       -- entry phase angle of ion (deg)  
21  
22 adjustable _frequency_hz            = 3.85E6  --6.8E6 --3.85E6 -- RF  
   frequency (Hz)  
23  
24 adjustable _rfvolts = 300 --tonumber(os.getenv("SIMION_RFVOLTS")) --  
   RF voltage for octupole  
25 adjustable _dcvolts = 10 --tonumber(os.getenv("SIMION_DCVOLTS")) --  
   DC voltage for octupole;  
26  
27                                         -- typically zero for RF-only octupoles  
28 adjustable max_time = 10000000000    -- microseconds  
29  
30  
31 -- internal variables  
32 local last_pe_update = 0.0 -- last potential energy surface update time  
   (usec)  
33  
34  
35 -- SIMION segment called by SIMION to set adjustable electrode voltages  
36 -- in the current potential array instance.  
37 -- NOTE: this is called frequently, multiple times per time-step (by  
38 -- Runge-Kutta), so performance concerns here can be important.  
39  
40 function segment.fast_adjust()  
41  
42   local omega = _frequency_hz * ( 1E-6 * 2 * math.pi)
```

```

43 local theta1 = phase_angle_deg * (math.pi / 180)
44 local tempvolts = sin(ion_time_of_flight * omega) * _rfvolts
45 local _dc = _dcvolts
46
47 adj_elect01 = - tempvolts
48 adj_elect02 = tempvolts
49 adj_elect03 = - tempvolts
50 adj_elect04 = tempvolts
51 adj_elect05 = 16 * _dc
52 adj_elect06 = - 2 * _dc
53 adj_elect07 = _dc
54 adj_elect08 = - 2 * _dc
55 adj_elect09 = 16 * _dc
56
57 end
58
59 -- See also the README.html for how memory usage might be further
60 -- reduced by 1/3 or 2/3 by sharing electrode solution arrays.
61
62 -- SIMION segment called by SIMION after every time-step.
63 local is_initialized
64 function segment.other_actions()
65 if ion_splat ~= 0 then
66 --print(_rfvolts, _dcvolts, ion_splat, ion_number)
67 f = assert(io.open("neu.txt", "a"))
68 f:write(_rfvolts, " ")
69 f:write(_dcvolts, " ")
70 f:write(ion_splat, " ")
71 f:write(ion_number, " ")
72 f:write(ion_charge, " ")
73 f:write(ion_ax_mm, " ")
74 f:write(ion_ay_mm, " ")
75 f:write(ion_az_mm, " ")
76 f:write(speed_to_ke(math.sqrt(ion_vx_mm^2 + ion_vy_mm^2 + ion_vz_mm
    ^2), ion_mass), " ")
77 f:write(ion_time_of_flight, " ")
78 f:write("\n")
79 f:close()
80 max_time = 0
81 elseif ion_time_of_flight >= max_time then
82 --print(_rfvolts, _dcvolts, ion_splat, ion_number)
83 f = assert(io.open("neu.txt", "a"))
84 f:write(_rfvolts, " ")
85 f:write(_dcvolts, " ")
86 f:write(ion_splat, " ")
87 f:write(ion_number, " ")
88 f:write(ion_charge, " ")
89 f:write(ion_ax_mm, " ")
90 f:write(ion_ay_mm, " ")
91 f:write(ion_az_mm, " ")
92 f:write(speed_to_ke(math.sqrt(ion_vx_mm^2 + ion_vy_mm^2 + ion_vz_mm
    ^2), ion_mass), " ")
93 f:write(ion_time_of_flight, " ")
94 f:write("\n")
95 f:close()
96     ion_splat = -1
97 end
98

```

```

99
100    -- Update potential energy surface display periodically.
101    -- The performance overhead of this in non-PE views is only a few
102    -- percent.
103    -- NOTE: the value inside abs(...) can be negative when a new ion is
104    -- flown.
105    if abs(ion_time_of_flight - last_pe_update) >= pe_update_each_usec
106        then
107            last_pe_update = ion_time_of_flight
108            sim_update_pe_surface = 1      -- Request a PE surface display update
109
110
111    end
112
113    end
114    function segment.tstep_adjust()
115        -- Keep time step size <= X usec.
116        ion_time_step = min(ion_time_step, 0.1) -- X usec
117    end
118
119    function segment.accel_adjust()
120        if ion_time_step == 0   then return end -- skip if zero time step
121        if _linear_damping == 0 then return end -- skip if damping set to
122            zero
123
124        -- Compute correction factor.
125        _linear_damping = abs(_linear_damping)           -- force damping
126            factor positive
127        local tterm = ion_time_step * _linear_damping   -- time constant
128        local factor = (1 - exp(-tterm)) / tterm         -- correction factor
129
130        ion_ax_mm = factor * (ion_ax_mm - ion_vx_mm * _linear_damping)
131        ion_ay_mm = factor * (ion_ay_mm - ion_vy_mm * _linear_damping)
132        ion_az_mm = factor * (ion_az_mm - ion_vz_mm * _linear_damping)
133
134    end

```

## References

- [1] LLC. Adaptas Solutions. *SIMION 2020 Supplemental Documentation*. <https://simion.com/info/>.
- [2] B.L. Breitmeier. *Simulation of the simultaneous trapping of positively and negatively charged ions in a linear quadrupole trap*. Bachelor thesis, Innsbruck University, Austria, 2023.
- [3] K. Geistlinger, M. Fischer, S. Spieler, L. Remmers, F. Duensing, F. Dahlmann, E. Endres, and R. Wester. *A sub-4 Kelvin radio frequency linear multipole wire trap*. Rev. Sci. Instrum. 92, 023204 (2021); doi: 10.1063/5.0040866.
- [4] A. Calvin, S. Eierman, Z. Peng, M. Brzeczek, S. Kresch, E. Lane, L. Satterthwaite, and D. Patterson. Nondestructive inelastic recoil spectroscopy of a single molecular ion: A versatile tool toward precision action spectroscopy. Phys. Rev. A **108**, 062819 (2023). doi:10.1103/PhysRevA.108.062819.
- [5] A.D. Gingell. *Applications of Coulomb crystals in cold chemistry*. PhD thesis, Oxford University, UK, 2010.
- [6] H. G. Dehmelt, "Radiofrequency Spectroscopy of Stored Ions I: Storage," *Advances in Atomic and Molecular Physics*, vol. 3, pp. 53-72, 1968. doi:10.1016/S0065-2199(08)60170-0.
- [7] J. P. Stacey. *Stabilization and Control In a Linear Ion Trap*. PhD thesis, Oxford University, UK, 2003.
- [8] M. Drewsen and A. Bröner, Phys. Rev. A, 62, 045401 (2000).
- [9] Stability Chart (<https://www.mathworks.com/matlabcentral/fileexchange/35355-stability-chart>), MATLAB Central File Exchange.
- [10] H. X. Li, Y. Zhang, S. G. He, and X. Tong, "Determination of the geometric parameters  $\kappa_z$  and  $\kappa_r$  of a linear Paul trap," Chin. J. Phys. **60**, 61–67 (2019). doi: 10.1016/j.cjph.2019.03.017.
- [11] A. Fyrillas, *Simulations of sympathetic cooling of an anion with a cation*, Internship Report, ETH Zurich, May-August 2020.